FORSCHUNGSZENTRUM ROSSENDORF
Mitglied der Wissenschaftsgemeinschaft Gottfried Wilhelm Leibniz

WISSENSCHAFTLICH-TECHNISCHE BERICHTE
FZR-366
Februar 2003
ISSN 1437-322X

Jan Džugan

Crack initiation determination for Charpy size specimens

Herausgeber:
Forschungszentrum Rossendorf e.V.
Postfach 51 01 19
D-01314 Dresden
Telefon +49 351 26 00
Telefax +49 351 2 69 04 61
http://www.fz-rossendorf.de/

Als Manuskript gedruckt

FORSCHUNGSZENTRUM ROSSENDORF
WISSENSCHAFTLICH-TECHNISCHE BERICHTE
FZR-366
Februar 2003

Jan Džugan

Crack initiation determination for Charpy size specimens

Content:

Abstract

An investigation in the field of the crack initiation determination for Charpy size specimens was carried out. An extensive literature survey of published methods for the crack initiation was performed. Methods based on the stretch zone width measurement, blunting line, multiple gauge measurement, electric potential drop, compliance changing rate, acoustic emission, ultrasonic method and magnetic emission are discussed in the theoretical part of the report. Analytical methods for the critical J-integral evaluation were also taken into account, as well as the expressions for the J-integral calculation. On the basis of the theoretical survey suitable measurement methods were chosen and applied in the experimental programme to several different materials. Namely blunting line related methods, multiple gauge methods, electric potential drop and compliance changing rate methods were used. The initiation J-integrals were evaluated with use of wide range of evaluation procedures and compared together in order to find a reliable method for the crack initiation determination. There was not found a universal method for the crack initiation determination. The performance of the methods was varying in dependence on the investigated material, so the results enable to choose perspective method for considered case.

1 Introduction

Fracture mechanics has attained great attention in establishing ultimate load limitations and assessing the safe-life for a large number of engineering structures of multifarious types. One of the most used fracture mechanics limitation for monotonic loading is defined by the onset of crack growth (crack initiation). Unfortunately, there have not yet been methods to measure a real material parameter characterizing the load limitation against crack initiation in every case.

The problem is solved using the fracture toughness parameter K_{Ic} under the condition of the linear-elastic fracture mechanics. Its application is, however, limited to brittle fracture behaviour and its measurements need heavy sections that are costly, inconvenient and often not available.

With increasing size of the plastic zone in the structure a J-integral based fracture toughness parameter become increasingly more appropriate because this criterion describes the energetic situation of the crack surroundings better than stress-related characterization with K values.

Critical material parameters measured on the base of the J-integral at the onset of crack growth are derived from very different approaches. The master curve concept according to ASTM E 1921-02 [1] uses K_{Jc} determined from the J-integral at the onset of instable fracture of the specimen (cleavage). A small contribution of preceded stable crack growth is permissible. A statistical brittle fracture model is involved and, in this way, the specimen thickness considered. Therefore, fracture mechanics parameter can be determined using Charpy size specimens. The approach is applicable up to the lower transition temperature region. The ESIS P2-92 [2] recommendation allows even larger ductile crack growth until spontaneous fracture but rejects a correction of different specimen thickness. In consequence the parameter clearly shows an influence of the thickness.

For a structure failure under large-scale yielding these approaches are inappropriate. In this case the J-integral at maximal load is determined rather by the test geometry and the loading conditions than by the material toughness. Various national and international standards recommend the determination of the crack extension resistance J_{Ic} near the onset of stable crack extension as an engineering estimate of stable crack extension [3, 4]. Herein the stable crack resistance curve (R-curve) is developed and a single point on the R-curve by means of a prescribed but random-selected procedure characterizes J_{Ic} value. These methods require specimen dimensions that must satisfy specific criteria for determination of valid J_{Ic} values. As a rule, Charpy size bend specimens do not meet the standard-size requirements when applied at tempered low alloy steel of high toughness and medium strength. Furthermore, the R-curve depends on specimen type and size and, thus, the R-curve related the material does not only determine critical J value.

Only the definition of a J_i value, which has a direct relation to the physical event of crack initiation in the material volume, seems to be a real size-independent material parameter. For that many methods have been proposed. They try to correlate the change of a physical or geometrical parameter directly to the crack initiation process or the onset of stable crack growth. As the most appropriate methods the measurement of the stretch zone width (SZW) has been established. Unfortunately, this methods needs high experimental effort, is time consuming and subjective. Therefore the development of alternative methods is still of recent interest.

The report will give a brief survey over the situation in this field. The aim is to look for a reliable and efficient way of J_i determination on Charpy size specimens, which shows the potential for a successful application for a broad range of strength-toughness properties.

In the first theoretical part (chapters 2 to 11) the report summarizes suitable techniques proposed in the literature. Furthermore analytical single specimen methods necessary for J-R curve evaluation in cases when the crack length monitoring method is not available (chapter 10) are briefly discussed and an overview of the J-integral calculations is given (chapter 11). The second, experimental part (chapter 12) presents experimental results regarding the efficiency of multiple-gauge measuring methods and potential drop methods.

2 Stretch Zone Width Measurement

In the course of loading of a precracked specimen a stretch zone at the crack tip forms under elastic-plastic conditions due to strain concentration. When the stretch zone width (SZW) attains the critical value, physical crack initiation starts and the crack growths further in cleavage or ductile manner. From the measurement of SZW, Fig. 2-1, prior to crack initiation, critical initiation value of J-integral can be evaluated. The critical value of SZW depends on the stress-strain state of the crack tip and the properties of the material [5].

The SZW assessment is based on the fact, that subsequent to blunting the SZW is fully developed and is maintained as crack growth continues [6]. The measurement is performed subsequently after specimen full rupture usually with use of scanning electron microscope (SEM). In cases when the borders of stretch zone are not clearly distinguishable, or even interrupted by cleavage fracture areas, the SZW cannot be determined.

According to present recommendations in publications [2, 7], SZW should be measured at 9 equally distributed points over specimen thickness. In each single point the measurement is to be performed at least five times and then the average value can be used further.

The measurements are rather complicated due to subjectivity of SZW determination. Round robin on SZW measurement was performed in Germany and relatively high scatter of about 35% and deviation from the average value in the range ±50 % was reported [7, 8, 9]. There was not found a big difference between values measured by experienced and green people.

To decrease scatter of SZW values it is recommended to measure both specimen halves [10, 11]. Additionally, it was found that the SZW varies across the crack front; maximum is near the middle and minimum near to edges. Side grooves decrease clearly the difference of SZW between middle section and the edges of the specimen. Both these steps could decrease uncertainty of the measurement.

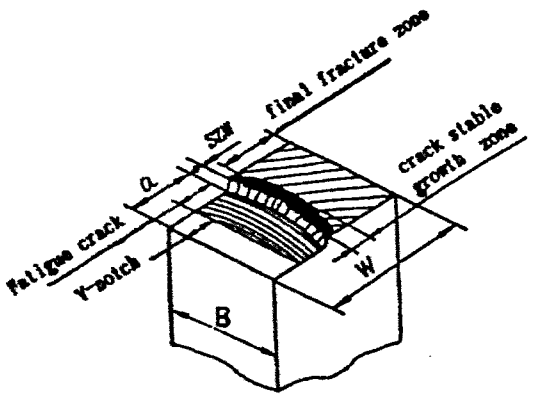

Fig. 2-1. Formation of SZW on fracture surface [12]

Measured SZW values are used for J_i determination. In order to evaluate critical value of J_i , J – Δa relation is constructed. Parallel line to J axis at Δa = average SZW_i is plotted and best fit curve is fitted to the J-crack extension (Δa) data. The intersection point between best fit curve and SZW_i line represent J_i critical value, Fig 2-2a).

Kobayashi [13, 14] used slightly different method using fact that SZW below critical value SZW_i increases linearly with J–integral value and beyond SZW_i value the SZW is independent of J-integral. Several specimens were tested, loaded at different levels below expected crack initiation load. Another set of specimens was subsequently loaded above the crack initiation load and then SZW for all specimens was measured. J - SZW plot was constructed, Fig. 2-2b), and the blunting line based on specimens loaded below critical load was inserted. Average value of SZW was calculated for specimens loaded above critical value and plotted as iso-SZW line into J-SZW plot. The intersection between the blunting line and best fit curve defines the critical value of SZW and subsequently J_i value.

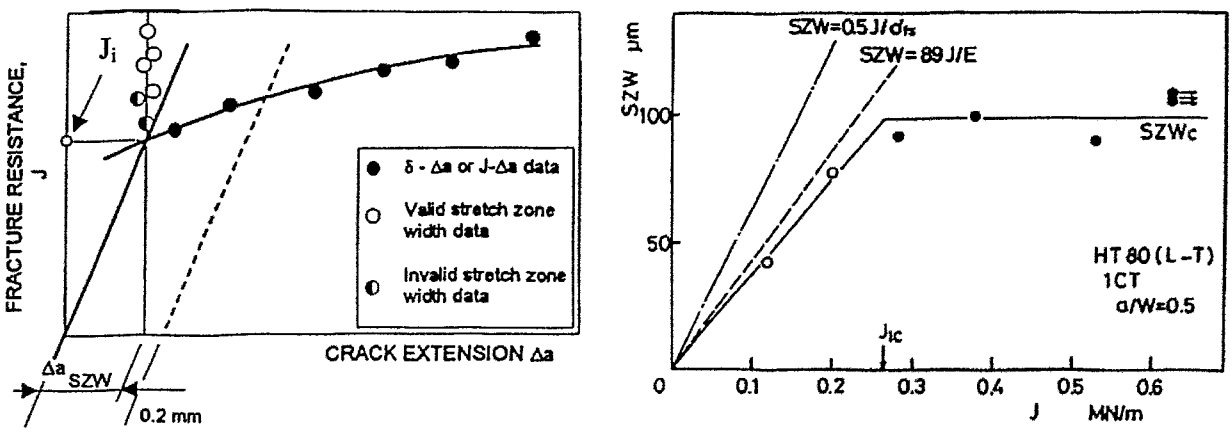

Fig. 1-2 a) SZW_i determination according to ISO[15] b) SZW_i determination procedure used by Kobayashi [13].

Further formulas were also developed using the SZW_i for evaluation of critical crack opening displacement (COD) [16] or J_i without J-R curve construction.

For evaluation of dynamic J_{id} tests following equation was found [12]:

$$J_{id} = K \bullet \sqrt{2}\sigma_{yd} \bullet SZW_c, \tag{2-1}$$

where K is the constrain factor concerning the stress strain state of a crack tip, specimen geometry and size, as well as the strain hardening characteristics of material. K can be estimated by:

$$K = \frac{1}{0{,}54 \bullet (1+n)} \frac{2}{\sqrt{3}} \left[(1+\nu) \bullet (1+n) \frac{\sigma_{yd}}{n \bullet E} \right]^{-n} \tag{2-2}$$

$$\sigma_{yd} = \frac{2{,}85 \bullet F_y \bullet W}{B \bullet (W-a)^2}, \tag{2-3}$$

where σ_{yd} is dynamic yield strength of material, ν is Poisson constant, n is strain hardening coefficient, F_y is force at yield stress, W, B and a are specimen width, thickness and crack length.

3 Blunting line derived crack initiation toughness

So called blunting line represents crack advance before the sharp tearing crack appears. The blunting line is used in J-R curve construction to determine J_{Ic}. The model for blunting comes from a construction in which the crack tip is assumed to be of a semicircular shape. The radius of the circle is the apparent crack advance due to blunting, Δa_B, and the diameter is the crack tip displacement. The first suggested blunting line expression, Eq. 3-1, is still used. It is implemented into J_{Ic} fracture toughness method ASTM E1820 [4].

$$J = M \bullet \sigma_Y \bullet \Delta a_B \tag{3-1}$$

$$\sigma_Y = \frac{\sigma_y + \sigma_u}{2} \tag{3-2}$$

M is blunting coefficient, Δa_B is crack extension within blunting region, σ_y is yield stress and σ_u is ultimate tensile strength. Recommended value of M is 2 according to ASTM 1820 [4].

In several publications can be found application of Eq. 3-1 to some real cases [17- 21]. In most cases disagreement between measured blunting line by SZW or by any other single specimen method and values obtained with use of ASTM blunting line was found. Usually, value 2 of blunting line coefficient underestimates real material behaviour. In some materials of low and intermediate strength, the intersection point of the assumed blunting line and R-curve does not exist [13]. Published values of coefficient M are in the range from 2.2 to 4 [18, 19, 21, 22].

Recent studies have also opened question whether σ_Y is really the most appropriate parameter for blunting line description. Landes [20] compared the change of parameter M for different materials in relation with various strength-related parameters. Namely, yield stress σ_y, effective yield strength σ_Y and ultimate tensile strength σ_u were considered. The analysis revealed that the σ_y -related procedure results in M values between 4 and 13. The σ_Y-using procedure exhibited narrower range of M values from 3,5 to 6. The smallest variation of blunting line parameter with material was documented for σ_u -based evaluation. In this case M for all materials was within 3,5 and 4. When average value of M is considered, then following expression can be obtained:

$$J = 3{,}75 \bullet \sigma_u \bullet \Delta a \tag{3-3}$$

This form of blunting line formula can be found in ESIS and ISO recommendations [2, 15].

From above mentioned facts it can be concluded that the accuracy of J_{Ic} determination with use of blunting line formula Eq. 3-1 or 3-3 depends on the material whether it follows these blunting lines or not. Since this method does not provide consistent values and the accuracy changes with the tested material it is not very reliable for precise crack initiation determination, it can be only used for rough estimation.

Another way of blunting line determination is numerical procedure proposed by Schwalbe [23] using blunting line coefficient d_n^* and E-modulus. This procedure was later used by Heerens et al. [8] and Landes [20]. The procedure was also recently included into ESIS recommendation [2].

The procedure was developed on the basis of SZW measurement and the relations between stretch width zone, stretch width height and the crack tip opening. These relations led to following expression for blunting line:

$$\Delta a_B = 0{,}4 \bullet d_n^* \frac{J}{E} \tag{3-4}$$

where d_n^* is a coefficient depending on yield stress and strain hardening exponent. To determine d_n^* both an analytical or a graphical procedure can be used [2, 20].

The analytical solution consists of following steps:

- Strain hardening coefficient *n* determination:

$$\frac{\sigma_y}{\sigma_u} = \frac{1}{1+\varepsilon_y}\left(\frac{2{,}718}{n}\ln(1+\varepsilon_y)\right)^n \tag{3-5}$$

where

$$\varepsilon_y = \frac{\sigma_y}{E} + 0{,}002 \tag{3-6}$$

Coefficient *n* can be determined with use of these relationships with application of iteration calculation procedure.

- Reference stress calculation:

$$\sigma_0 = \sigma_y \bullet 10^t \tag{3-7}$$

where

$$t = \frac{n}{n+1}\log\left(E\frac{\varepsilon_y}{\sigma_y}\right) \tag{3-8}$$

- Finally d_n^* can be evaluated with use of following relationship:

$$d_n^* = \left[\left(\frac{\sigma_0}{E}\right)^{n-1}\right] D_n \tag{3-9}$$

where

$$D_n = 0{,}787 + 1{,}554n - 2{,}45n^2 + 16{,}952n^3 - 38{,}206n^4 + 33{,}13n^5 \tag{3-10}$$

Both analytical procedure and graphical solution [2] are rather complicated and time consuming. Procedure can be simplified if following assumptions are considered:

- σ_y/E ratio is in the range 0,001 - 0,013
- σ_y/σ_u ratio is in the range 0,3 – 0,95.

These ranges would cover the most of engineering materials. With pre-mentioned simplifications and transformation of blunting line expression to similar form like ASTM expression we can finally obtain formula for blunting line used in ESIS documents according to Eq. 3-3, [20].

4 Multiple Gauge Methods

4.1 Double Clip Gauge Method

Double clip gauge method (DCGM) for crack initiation determination is based on the concept of rotational factor. The method needs only two clip gauges attached to the specimen.

According to the slip line field analysis on the perfectly plastic rigid body, the specimen rotates around the centre of rotation after yielding point. The distance between the centre of rotation and the crack tip can be written as follows:

$$a = r \bullet (W - a_0) \tag{4-1}$$

where W specimen width

a_0 initial fatigue crack length

r rotational factor.

Let V_1 and V_2 be the distance between crack surfaces on the load line, at the positions according to Fig. 4-1.

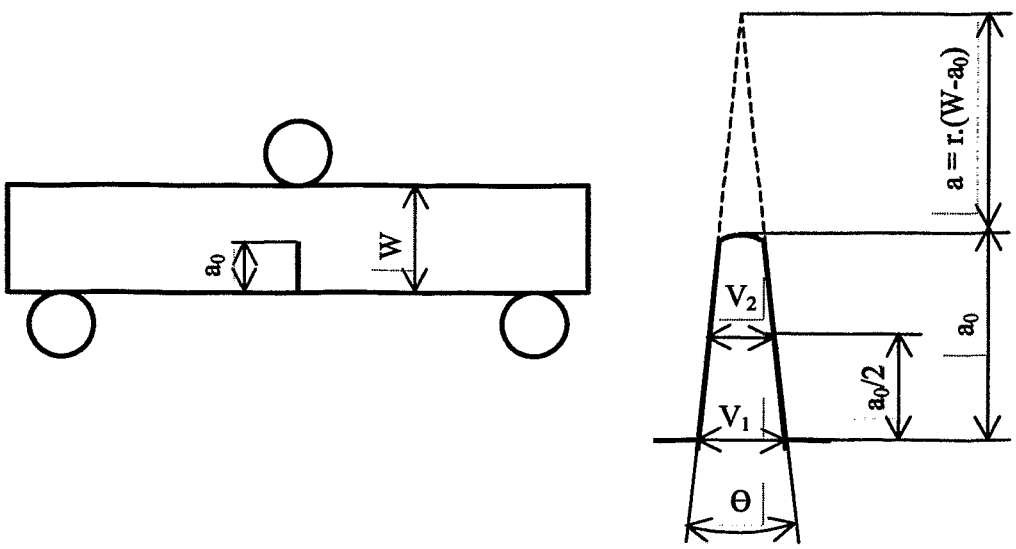

Fig. 4-1. Three point bend specimen for DCGM

The relationship between V_1 and V_2 can be described as follows:

$$V_1 = (a_0 + a)\Theta \tag{4-2}$$

$$V_2 = (\frac{1}{2}a_0 + a)\Theta \tag{4-3}$$

Θ is the angle between the crack surfaces. Taking derivative of V_2 with respect to V_1 one obtains:

$$\frac{dV_2}{dV_1} = \frac{(\frac{1}{2}a_0 + a)d\Theta + \Theta da}{(a_0 + a)d\Theta + \Theta da} \tag{4-4}$$

The changes in dV_2/dV_1 because of crack tip blunting, the ductile crack initiation and the crack growth are considered as stages I, II, III, Fig. 4-2. The transition between region I and II corresponds to the general yielding and the transition between region II and III is related to the initiation of ductile crack. In stage I, the crack tip blunts off, therefore the centre of rotation moves away from the crack tip. When the specimen is generally yielded, stage II, a is constant since the specimen rotates itself around the centre of rotation. Thus dV_2/dV_1 is constant value until the ductile crack initiates. After ductile crack initiation, stage III, the centre of rotation moves forward again.

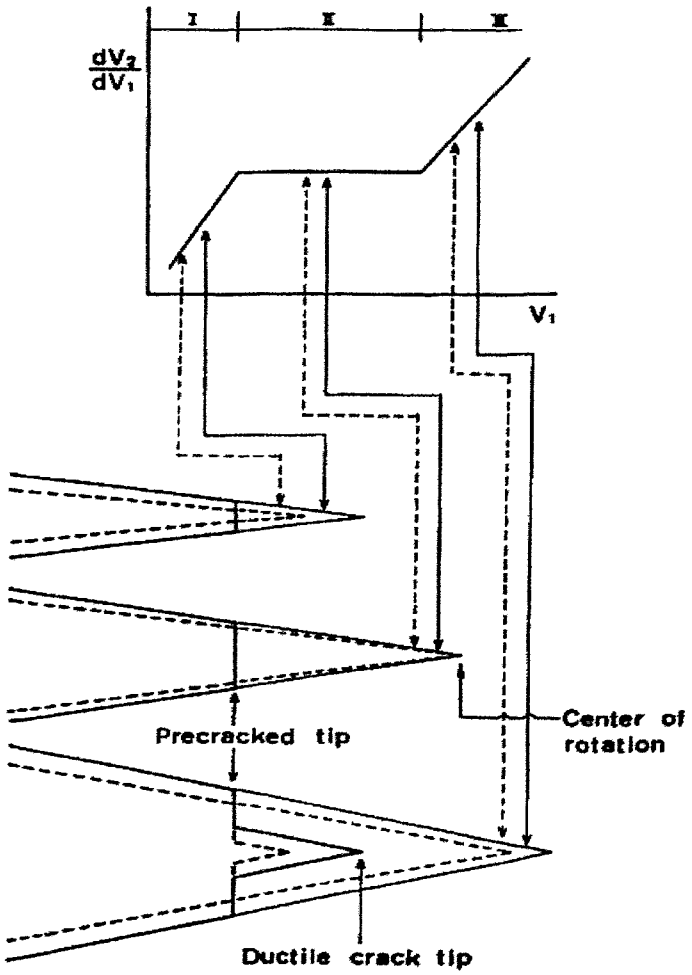

Fig. 4-2. Stages of crack growth [24]

The ductile initiation is defined as the location where dV_2/dV_1 begins to increase from the constant value [24- 26].

It was found by Kagawa [24] that this method provides good reproducibility and accuracy for J_{IC} determination for material with tensile strength above 500 MPa. When steels of tensile strength of about 400 MPa were tested, the obvious plateau was not obtained. Microfractograpic investigation revealed that there are many dimples in stretch zone, which means that the ductile crack was initiated at the crack tip in the process of blunting. According to Rintamaa [9] this method for static fracture resistance tests provides consistent results with the ASTM $J_{0,15}$ procedure.

4.2 Double Displacement Ratio Method

Double displacement ratio method (DDR) is similar to previous DCG method, but instead of two attached clip gauges, *COD* and striker displacement data are used [9, 27, 28]. An analytical basis for detection of crack initiation by the DDR method is the hinge model, Fig. 4-3.

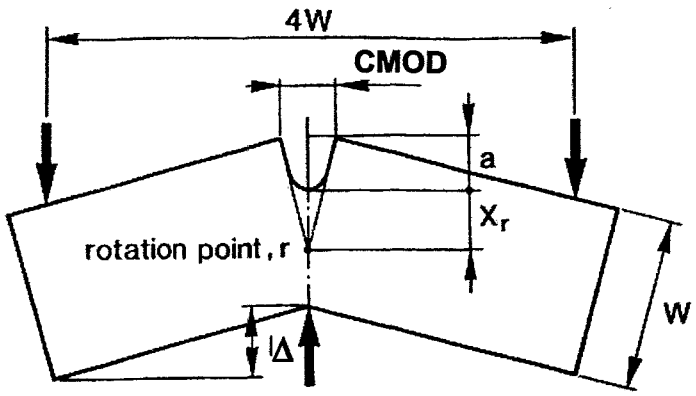

Fig. 4-3. DDR method [9].

Crack mouth opening displacement (CMOD) can be expressed as:

$$CMOD = r \bullet (1 - \frac{a}{W}) \bullet \Delta_{pl} + \frac{a}{W} \bullet \Delta_{pl} \qquad (4\text{-}5)$$

where Δ_{pl} is plastic deflection of the specimen. Differentiation and rearrangement of this formula leads to expression:

$$\frac{dCMOD}{d\Delta_{pl}} = \frac{dr}{d\Delta_{pl}} \bullet \left(1 - \frac{a}{W}\right) \bullet \Delta_{pl} + d \bullet \left(\frac{a}{W}\right) \bullet (1 - r) \bullet \frac{\Delta_{pl}}{d\Delta_{pl}} + r \bullet \left(1 - \frac{a}{W}\right) + \frac{a}{W} \qquad (4\text{-}6)$$

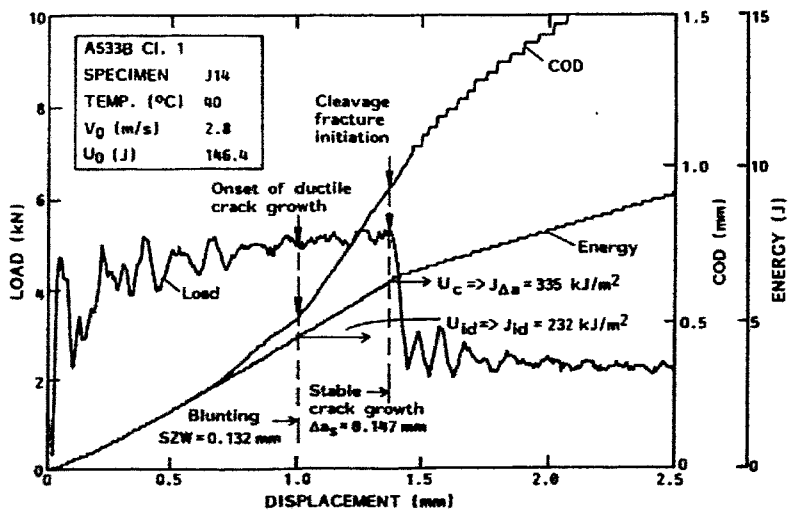

Fig. 4-4. DDR evaluation [9]

The ratio of plastic *dCMOD* and deflection $d\Delta_{pl}$ is termed here as double displacement ratio, DDR, which can be evaluated during different phases of specimen loading. The evaluation of DDR method could be the same as previously described DCG method. Also deviation from the line in COD versus displacement plot could be considered as the crack initiation, Fig.4-4.

The results of DDR method were compared with J_i^{SZW} crack initiation values obtained from stretch width zone measurement. The average values J_i^{SZW}, used due to high scatter of SZW values, exhibited good agreement with J_i^{DDR} obtained by presented method [9].

DDR method was used by Anderson el al. [27] for the crack initiation determination. They detected initiation as sudden drop in the first derivative, Fig. 4-5, which is characteristic

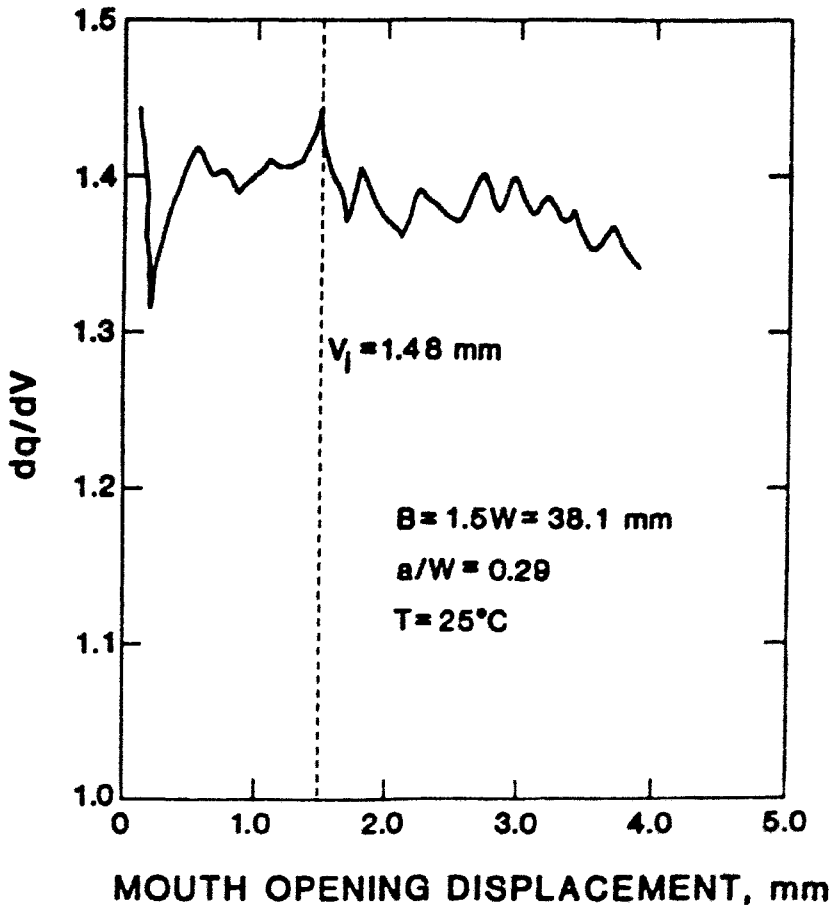

Fig. 4-5. Crack initiation determination by DDR method [27]

behaviour when tearing occurs. Observations of fracture surfaces of the specimens before and immediately following the onset of tearing indicate that the sharp drop in the first derivative coincides with incipient tearing. Figs. 4-5. represent typical plot of the first derivative from the fracture test. The spike in the curve, which was taken as the point of incipient tearing, is slightly more pronounced than the other spikes. The initiation point could be easily ill defined by this method, because of uncertainty which spike corresponds with the crack initiation, so relatively large scatter could be expected.

4.3 Strain Gauge Near to Crack Tip Method

During the loading of an elastic-plastic structure containing the crack, deformation field around the crack tip forms. The size of this field reaches maximum value in the moment of the crack initiation and then moves together with the crack advance. The moment of deformation field translation, defining the crack initiation, can be detected by the change of strain rate increase in near crack tip area. To detect the crack initiation event, strain gages, etched or glued lattice can be applied [29- 32].

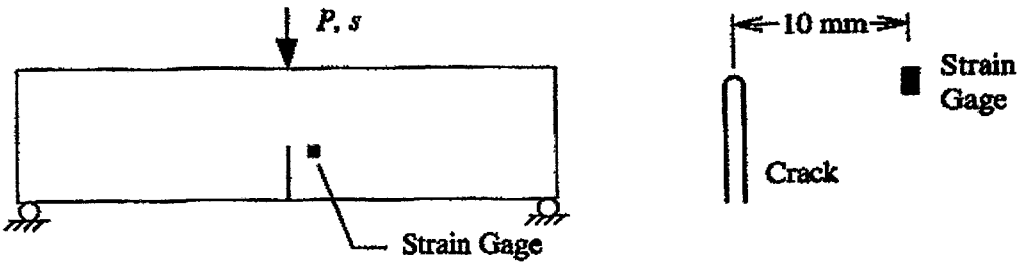

Fig. 4-6. Specimen instrumentation [29]

Strain gauge instrumentation was employed to identify the fracture initiation event during deformation of the precracked specimen subjected to three point bend loading [29], Fig. 4-6. The change in specimen compliance was reflected as a change in the rate at which strain signal increases, for the typical record of test see Fig. 4-7. This method was verified by high speed photography which was used for independent measurement of crack tip opening displacement [29].

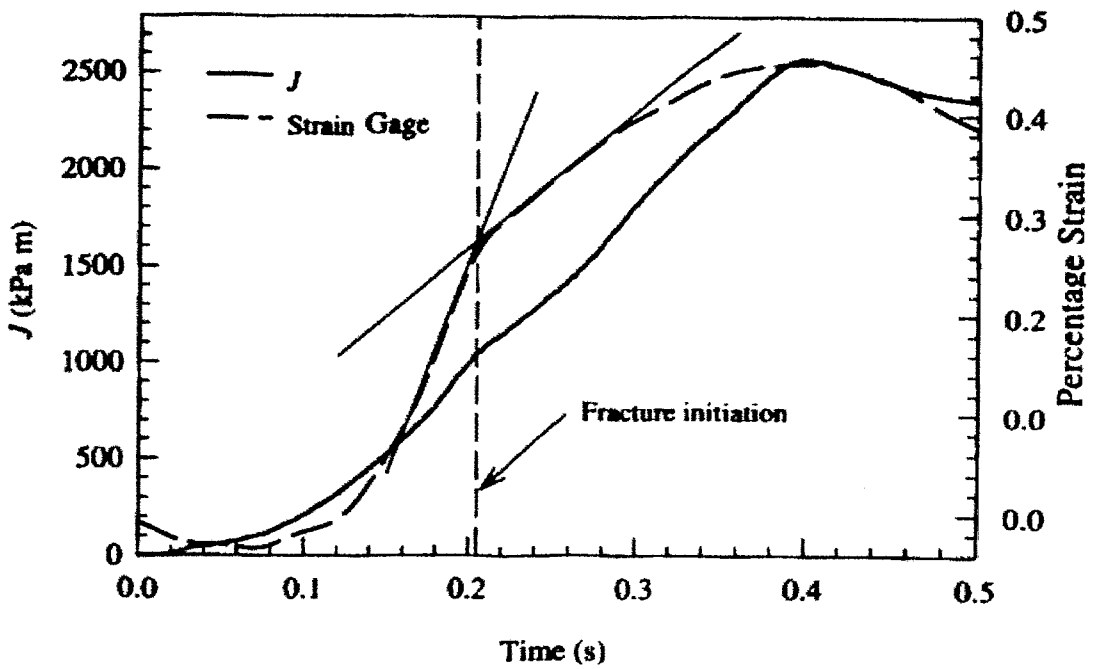

Fig. 4-7. Evaluation of the near to crack tip gauge measurement [29].

5 Potential Drop Methods

5.1 Standard Methods

The Potential Drop (PD) method is based on a change of the electrical resistance with the change of the specimen cross section area. For a constant current flow, the electric potential or voltage difference across the crack plane will increase with increasing crack size due to modification of the electrical field and associated perturbation of the current steamlines. This method is applicable for any electric conductive material in wide range of testing environments.

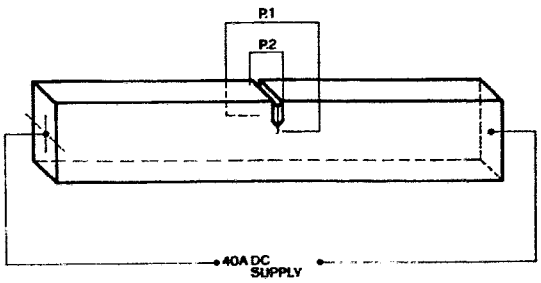

Fig. 5-1. Specimen instrumentation for DCPD measurement [33].

There are two basic variations of potential drop method, alternated current method and direct current method. In case of the Alternated Current Potential Drop (ACPD) method, only a layer near the metal surface carries the current. This effect is known as "skin effect" and results in high effective resistance. In case of Direct Current Potential Drop (DCPD) method the current density through the specimen thickness is almost constant. On the one hand, to attain the same sensitivity for both methods, much higher current must be used for DCPD application than for the ACPD (high current could cause specimen heating). On the other hand, "the skin" effect associated with ACPD cause relatively local measurement and thus, presents a distinct disadvantage in J-R curve testing, where the average crack extension over specimen thickness is required [39]. Potential drop method is used for quasi static loading condition as well as for the dynamic ones [22, 34-38].

The measurement with use of the potential drop is affected by many factors, the most important are: current level, current input/output location, potential drop measuring locations and frequency in case of ACPD. To attain the highest sensitivity the measuring points should be as close to the crack plane as possible, but at the same time the reproducibilty decreases, optimal distance has to be found [39]. Example of the specimen electric connection for the DCPD method is in Fig. 5-1.

The crack length measurement by both ACPD as well as DCPD method is using the relation of the crack length to the potential change in the crack extension region, Figs. 5-2 and 5-3. The calibration curve should be determined for each tested material to provide reliable results. Considered relation between the crack length and potential drop is linear [40, 41]. On contrary to previous statement, Bernard [33] reported non linear relationship between potential drop and the crack extension, which prevented him from using this method. Formulas for the crack length calculation can be found in [2, 15, 42, 43].

As it was mentioned above, the change of the potential value is expected to be associated with the crack extension but there are additional sources of the electrical resistance change. Those are: deformation, void growth and change of electro-mechanical behaviour of the material. The deformation, especially plastic deformation of the specimen could cause relatively large change of resistance, without the crack advance. Additionally, there is crack tip blunting associated also with plastic deformation. Void growth due to the high local

deformation in process zone ahead of the crack results in change of electrical resistance of this material volume as well [39, 44]. Finally, there is also change of the electrical resistance due to magnetostriction effect. All these effects have a crucial impact on the crack initiation detection.

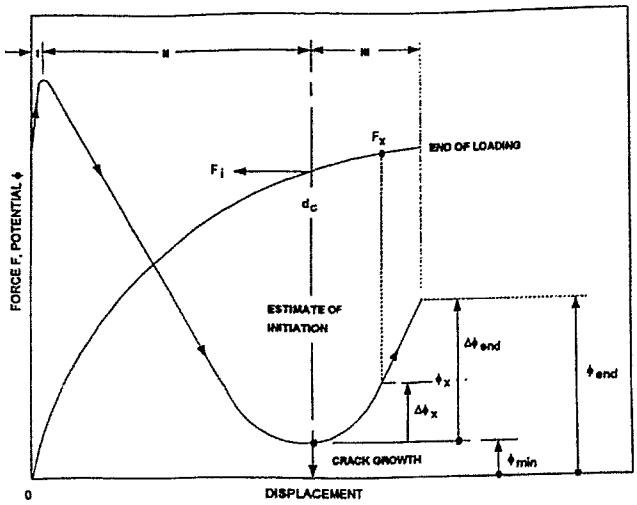

Fig. 5-2. Typical record of ACPD test [15].

The crack initiation is supposed to be represented as a minimum of the potential – crack extension trace by ACPD method, or as a sudden change of the slope of the potential – crack extension record for the DCPD method [2, 15]. The minimum on the ACPD traces has not been satisfactorily explained. It is supposed that the initial resistance growth is connected with separation of fatigued surfaces, the second stage is caused by inverse magnetostrictive effect and the final impedance increase is due to the crack extension [44]. Furthermore, it was found that the minimum detected by ACPD method is not a constant of a material, but depends on the current frequency. Wallin [45] reported the shift of the minimum towards lower values with increasing current frequency.

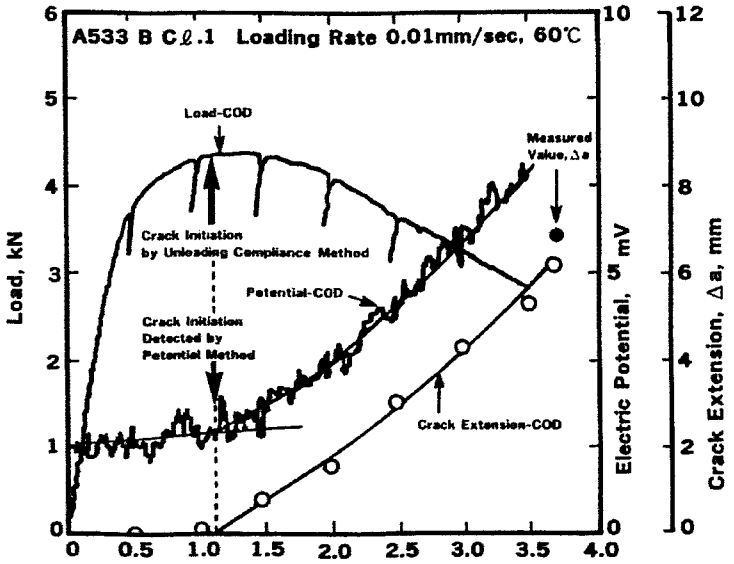

Fig 5-3. Record of DCPD [46]

The sensitivity to determine the crack extension and so crack initiation was determined by Reiff and Ernst [47] as 0,1 mm, below this crack extension, the electric potential is not effectively influenced.

5.2 *Induced Current Focusing Potential Drop and Remotely Induced Current Potential Drop Method*

Induced Current Focusing Potential Drop (ICFPD) and Remotely Induced Current Potential Drop Method (RICPD) are variants of ACPD method. They differ mainly from a conventional current potential drop in that, that the ICFPD and RICPD techniques take advantages of electromagnetic induction to provide a specimen with an alternating current, while for a conventional ACPD technique, the alternated current is directly supplied to the specimen through current terminals.

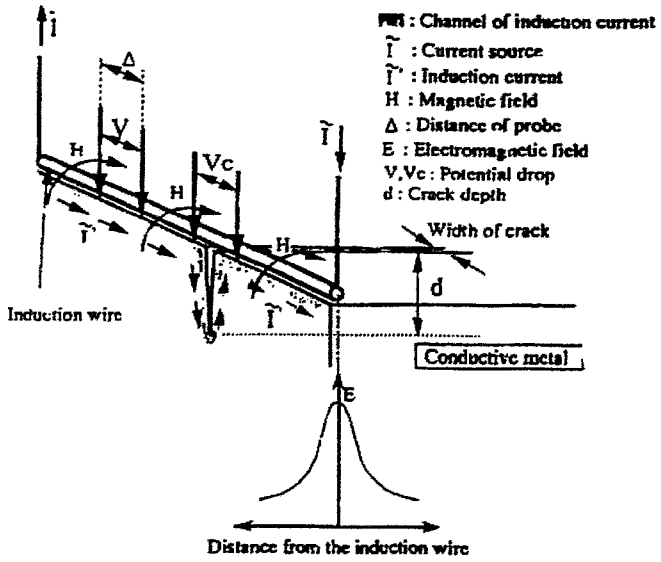

Fig. 5-4. ICFPD method scheme [48]

The principle of the ICFPD technique is schematically illustrated in Fig. 5-4 and testing set up is depicted in Fig. 5-5. Conductive straight wire is placed on a piece of solid metal, which has a surface crack. The wire is insulated from the metal piece. A current that flows along the straight wire induces magnetic field, which follows the right hand screw law. The magnetic field intensity is inversely proportional to the distance to the wire. When an alternating current is supplied to the wire, an induced alternating current flows in the metal

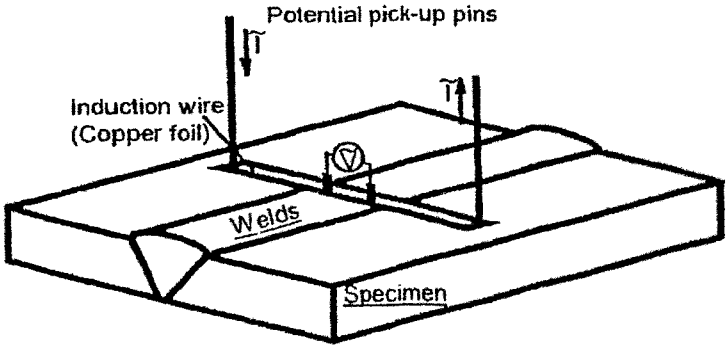

Fig. 5-5. Testing set up for ICFPD technique [49]

piece following Lorenz's law. A pair of metal needles is used to pick up the potential drop. If crack exists, it makes the current path longer and then potential drop increases. The induced current is inversely proportional to the distance to the wire, that is, the induced current density has a strong distribution in horizontal direction. In addition to the unique characteristic of electromagnetic induction, the induced current has also the general nature of an alternated current. Namely the alternated current tends to flow near the surface of a metal piece, which is well known as a skin effect. The skin depth is a function of permeability, conductivity and frequency [48].

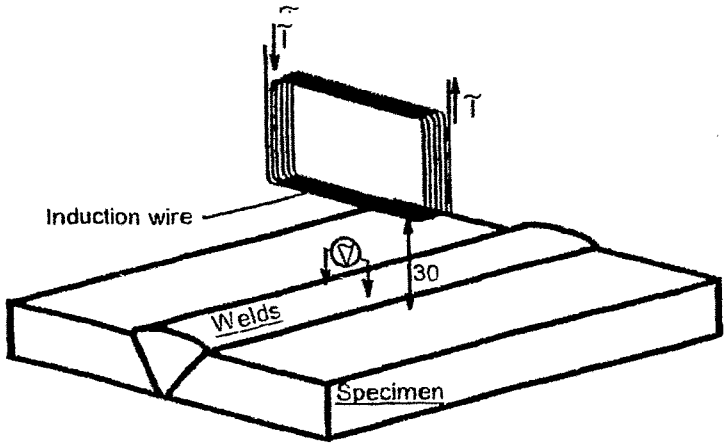

Fig. 5-6. Testing set up for RICPD technique [49]

Hence, the use of an induced current can focus a current in the vicinity of the induction wire and that characteristic of the induction current technique results in the advantages of the ICFPD technique compared to a conventional ACPD technique both in sensitivity and in availability, as described below:

- Current can be focused at desired local area.
- A big electrical source is not necessary regardless of the specimen size.
- Measurement work is quicker and easier because there is no need to have current terminals.

In case of RICPD technique, the basic principle is the same, but instead of pick up pins, pick up coil is used. The current flowing through the material creates a magnetic field that induces current in the pick up coil. The intensity of magnetic field is influenced by microstructure, irregularities and cracks and thus enables to evaluate crack lengths from the measured voltage. This method also resolves the main problem of ICFPD technique, necessary good electric contact between pick up pins and the specimen. For both current input and pick up, remotely placed probes are used which dramatically simplifies the measurement procedure, Fig. 5-6.

It was found by the authors [48] that the ICFPD method provides higher accuracy then conventional ACPD method for crack size prediction. When ICFPD and RICPD are compared following conclusions were drawn out [49]:

- RICPD has lower scattering by 35-50 %
- Sensitivity of RICPD is higher.

These methods have not been yet used for the crack initiation detection, but they close relation to already used ACPD and DCPD methods might make them possible successors of them due to simplified measurement methodology and probable higher sensitivity.

6 Compliance Changing Rate Method

This method is very simple without any additional requirements for equipment, only force and deflection is necessary. It can be used for quasi-static tests as well as for dynamic tests. Especially in case of dynamic ones, the simplicity makes this method very convenient.

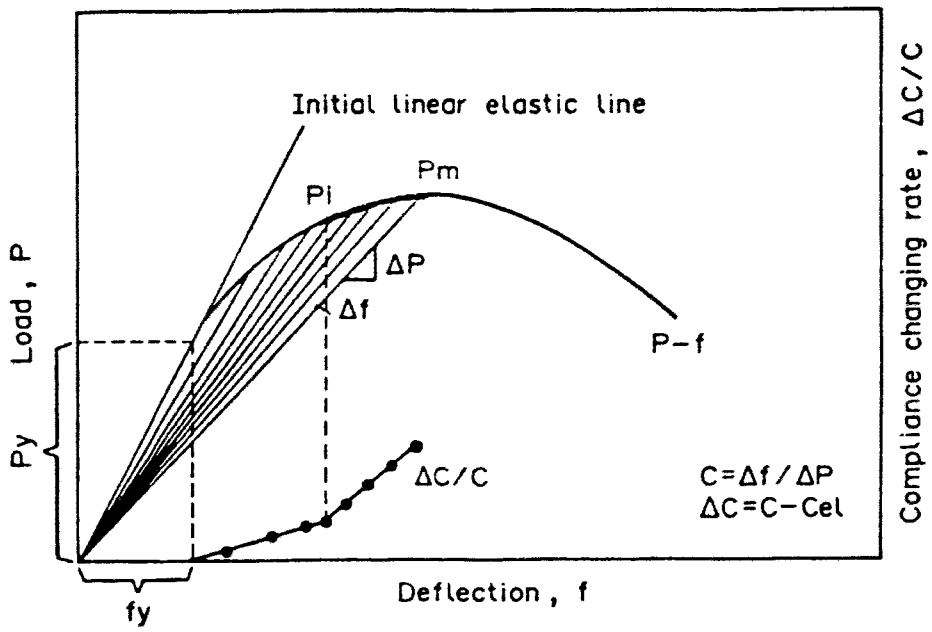

Fig. 6-1 Crack initiation determination with use of Compliance Changing Rate method [16]

The compliance changing rate as it was defined by Kobayashi [50] is evaluated from load-deflection curve, Fig. 6-1. It is calculated as:

$$\frac{\Delta C}{C} = \frac{C - C_{el}}{C_{el}} \tag{6.1}$$

C is assumed linear compliance from original point to any point on the load-deflection curve and C_{el} is initial compliance that is determined assuming linear elastic loading until yield point. The abrupt change in compliance changing rate defines the crack initiation point.

CCR method was firstly applied for dynamic test by Kobayashi et al. [50], who was later followed by Tosal et al.[51], Chen et al.[16], Shanmugam el al.[52], and Zhang et al. [5]. Tseng et al. [53] also used this method for quasi-static tests on Al-alloys. The experiences with this method are contradictory. While Kobayashi [50, 53] and Shanmugam [52] found this method reliable, Tosal [51] Chen [16] and Zhang [12] obtained approximately 10% lower values in comparison with the other methods. Moreover, Tosal [51] and Zhang [5] found very big scatter when this method was applied, making it rather unreliable.

7 Acoustic Emission

Sudden release of elastic energy from localized sources within a material or structure is connected with acoustic emission (AE) and can be detected by an appropriate sensor. Almost all damage processes in materials are accompanied by AE. Typical examples are plastic deformation, in particular near the yield stress, instable brittle fracture or crack growth. The AE methods have repeatedly been used for crack initiation detection for both quasi-static testing and dynamic testing [55-60]. The AE activity is measured by counts of burst-type emissions, Fig. 7-1, 7-2, or averaged signal intensity of continuous-type emission and reprocessed regarding the distribution of peak amplitudes, the signal duration, the emitted energy, Fig. 7-3, etc.

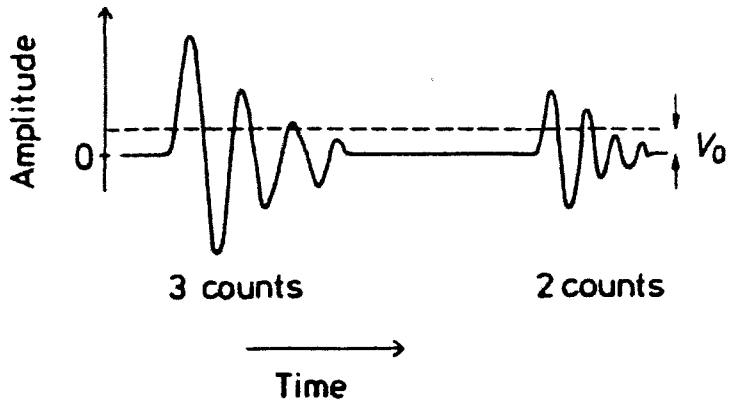

Fig. 7-1. Typical acoustic signal bursts; V_0 is the counter threshold [61]

In principle, there are some crucial characteristics which the application of the method for crack initiation detection impede:

- AE is generated within the specimen and monitored by a sensor located anywhere on the surface. The received signal is influenced by the wave propagation in the specimen, reflection and mode transformation at the boundaries, the contact conditions of the sensor and the transducer/ instrumentation response (bandwidth, threshold, resonance frequency etc.). Thus, the received signals do not really depict the original signal generated by the source.
- There are many sources of AE during the loading process of the mechanical test. The phenomena superimpose and it is complicated to separate the different effects. Moreover, disturbing signals, as the hammer impact in the Charpy test, can tend to be appreciably greater in magnitude than the real signal characterizing crack initiation.
- AE amplitude depends on the rate of the elastic energy release. A continuous process with slow energy release rate does not become recognizable by AE. This means that AE has a high sensitivity to instable brittle crack growth but is rather insensitive to slow crack growth processes in ductile materials.

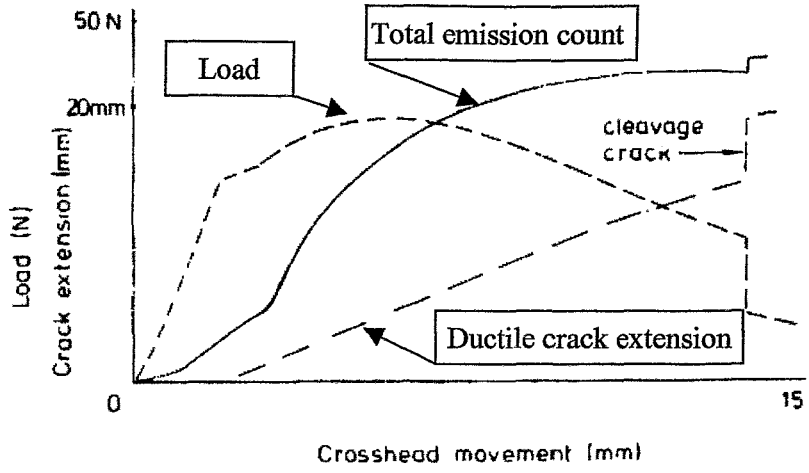

Fig. 7-2. Record of acoustic emission for quasy-static testing [57].

AE is the result of a complex series of processes and has not been understood completely. Thus, the application of the AE method has preferentially evolved in an empirical manner. There are no physical-based models that attribute AE to the micromechanical process of ductile crack initiation.

The crack initiation is presently detected as an inflection point on AE record. It was found that AE analysis enables to separate various emission kinds and to determine crack initiation [17, 62]. The accuracy of the AE defined crack initiation was compared with stretch zone width based initiation and error within range –2 to +8 % was found [26]. Another results of comparison of the AE defined initiation with SZW defined one could be found in [56, 58-60], but no systematic trend is obtained. In some cases the initiation points are similar [59], but in others are values notably lower [58] or higher [59] than SZW defined initiation. More details on AE method can be found in Richter's report [56].

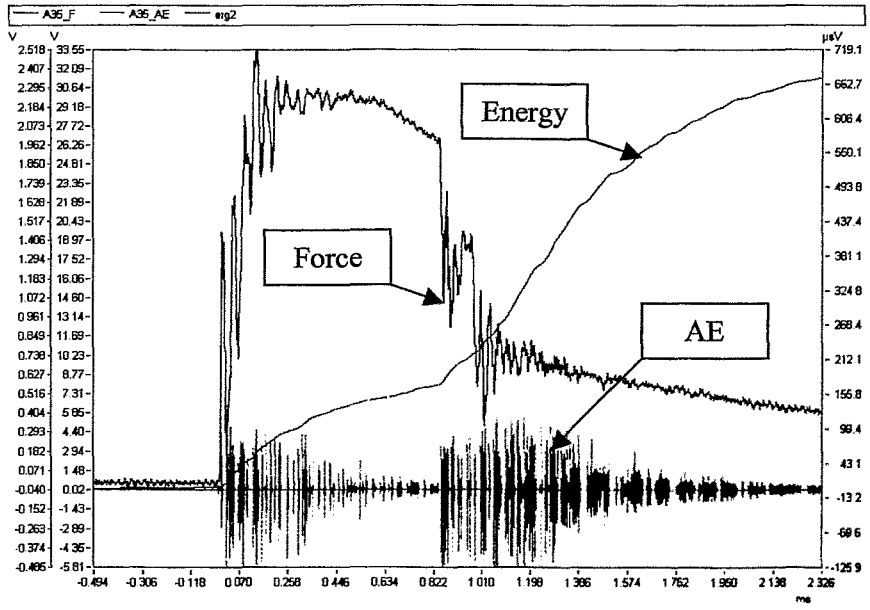

Fig. 7-3. Record of dynamic impact test

It is obvious that before the AE method can be used for detecting stable crack initiation in high-tough steels a great deal of additional research is required.

8 Ultrasonic Method

The ultrasonic method (US) is another method used in fracture mechanics tests for the crack lengths evaluation. The method has not been yet well established nowadays and effort is paid to development of US technique for fracture mechanics testing purposes. The principle of US method is modification of the ultrasonic waves travelling trough the specimen on every interface boundary due to abrupt change in acoustic impedance. Such an interface boundary is the crack also and thus, the crack length as well as the crack initiation could be evaluated.

Ultrasonic waves propagating in materials could be of two basic kinds: compressional (longitudinal) and shear (transverse). All materials transmit longitudinal wave, while the share wave could travel trough solids only. The presence of the surface also allows propagation of the other vibration modes. The most common is probably the Rayleigh (surface). This wave mode is bound to the specimen surface and for this reason they will follow surface through very tight bends, all around the rectangular block or around the crack tip for instance. Any elastic wave may cause the initiation of wave of another mode but only in the situation where there is abrupt change in acoustic impedance, i.e. at material interfaces.

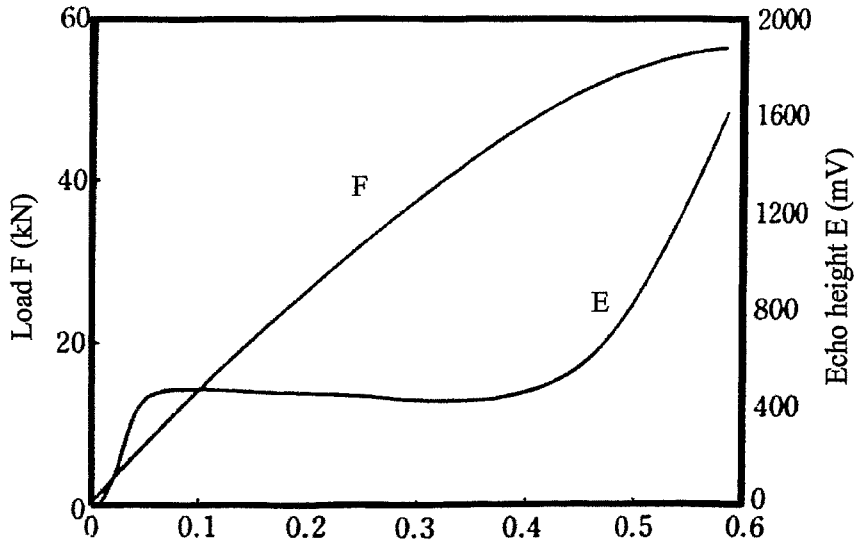

Fig. 8-1. Signal record using normal probe set up [63].

The resolution of any wave is, roughly taken, comparable to its wavelength. To attain the resolution of about 1 mm the elastic waves frequency should be in megahertz range. The upper limit for the frequency is the material attenuation. In many materials the higher frequency range is accompanied by a distinct increase of the elastic waves attenuation. Thus the compromise between resolution and attenuation should be found.

The basis for the crack detection is the abrupt change of acoustic impedance between bulk material and the filling of the crack. The main difference between a crack and a material boundary is that now there are two abrupt changes in acoustic impedance in close juxtaposition. The interaction of ultrasound with a crack results in the reflection, diffraction and scattering. Reflection is mainly caused by interaction with the crack surface. Diffraction takes place at the crack tip and scattering is connected with the crack face as well as with the crack tip.

Formerly used ultrasonic methods like "Pulse echo", "Pitch and catch" and "Obscuration" were just able to detect the flaw, but for precise size evaluation they were insufficient. The "Obscuration" method was applied by Loibnegger [64], while angle beam transducers were used by Kalkhof [65] for the crack initiation evaluation but not convincing results were attained. Reflection method was used by Hirano and Yasunaka [63, 66, 67]. Hirano used "Top-on" and "End-on" method (probe above crack plane and probe behind the crack tip, respectively) with normal probes (NP). That instrumentation enabled him to measure relatively accurately the crack extension, but the crack initiation was not determined.

Further US methodic development brought US holography and focussed transducers. Yasunaka used point focussing normal probe (PFNP) together with "Top-on" normal probe [63]. Both probes were operating in the reflection mode. The PFNP exhibited much higher sensitivity in comparison to the NP. Example of the typical record obtained with use of that

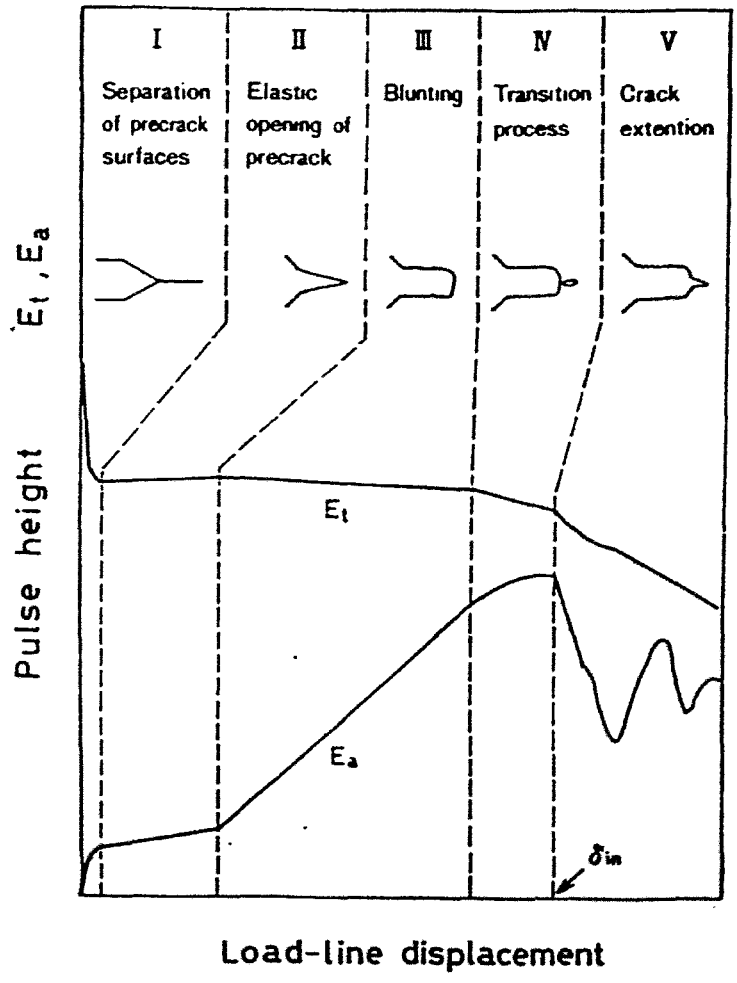

Fig. 8-2. Test stages with use of the point focusing normal probe; E_t – transmission pulse height (NP), E_a – reflection pulse height (PFAP) [67]

set up is in Fig. 8-1. Three observed separate regions are supposed to be related to following processes. The first echo increase is connected with opening of the crack surfaces being in contact in unloaded state. In the second range the crack tip blunting takes place; the shape of this range is strongly influenced by the probe position. The third range (second increase of the echo height) presents crack growth. The results obtained from these tests were confronted with SZW values. Ultrasonic initiation values notably underestimated the crack initiation

values in comparison with the SZW measurement results. On the basis of previous experiment the experimental set up was changed [67]. Two NP probes are used, one probe above the crack, the second probe below the crack plane operating in transmission mode. Additionally applied was point focussing angle probe (PFAP) of reflection magnitude of 40°. Schematic drawing of obtained record is in Fig. 8-2. Sudden changes of the course of both E_t and E_a curves are clearly visible. They are attributed to the onset of the crack initiation. Comparison of ultrasonic crack initiation values with initiation values obtained from J-R curve (intersection of blunting line with fit curve - line was used in this case) exhibited good agreement. This method yields promising results, but for its application to Charpy size specimens further modifications have to be applied considering the problematic of three point bend specimens testing.

The most recently reported technique is Time Of Flight Diffraction Technique (TOFD) [68, 69]. Two probes are placed on opposite sides of the crack, but on the same specimen surface, Fig. 8-3. Flawless structures would provide two pulses: surface (lateral) and second back wall echo. In presence of the crack (coming from surface) additional echo appears due to sound diffraction at the crack tip. From the change of the echo delays, the crack length can be evaluated.

Experimental studies showed that the diffracted energy is emitted over very wide angular range. Moreover it appears that the amplitude of the diffracted pulse in not a strong function of the angle between transducer and the crack. These observations are important because no special relationship has to be achieved between location and angle of the transducer and the crack. Additionally the amplitude of the diffracted echoes is sufficient for reliable detection [69].

Bergmann [68] used this method for the crack length evaluation at Charpy size specimens and subsequently the crack initiation was also evaluated. Very good agreement was found in case of the crack length measurement, but the crack initiation determination brought ambiguous results. Comparison of the crack initiation values with values obtained from SZW measurement revealed relatively big scatter and common trend could not be found. The resolution limits are perhaps reached for Charpy size specimens.

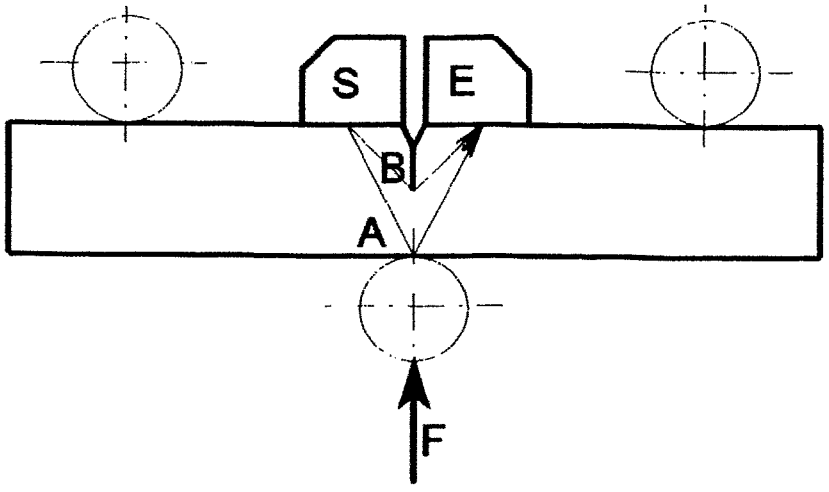

Fig. 8-3. Experimental set up for TOFD technique [68]

9 Magnetic Emission Method

Mechanical events taking place during the material deformation cause alternation of the material magnetic structure that outwardly appears as a rise of magnetic emission (ME) signals. The analyse of detected signal can one enable to distinguish actual processes. The method is applicable to all ferromagnetic materials.

Magnetic signals are generated when the magnetic structure of the ferromagnetic material is rearranged. This can be caused, for example, by external field magnetization. Barkhausen discovered that even with a continuously rising magnetization field the magnetization curve is discontinuous. It consists of a small steps called "Barkhausen jumps" and the generation of each step is accompanied by a rapid change of external magnetic field.

The magnetic domains in ferromagnetic materials are spontaneously magnetized to saturation. Size and orientation follow the energy minimizing principle. If the internal energy was changed by an external magnetic field, mechanical impact, or by material separation, the domains would seek the new state of minimum energy. Changes in the energy balance are instantly followed by rapid changes of the external magnetic field and are therefore detectable.

Event accompanying the material separation may exhibit an effect caused by a drastic change in the permeability. The magnetic permeability of air or vacuum is of several orders lower than permeability of ferromagnetic material. Therefore, if void or crack growth appears alternation of magnetic field is detected.

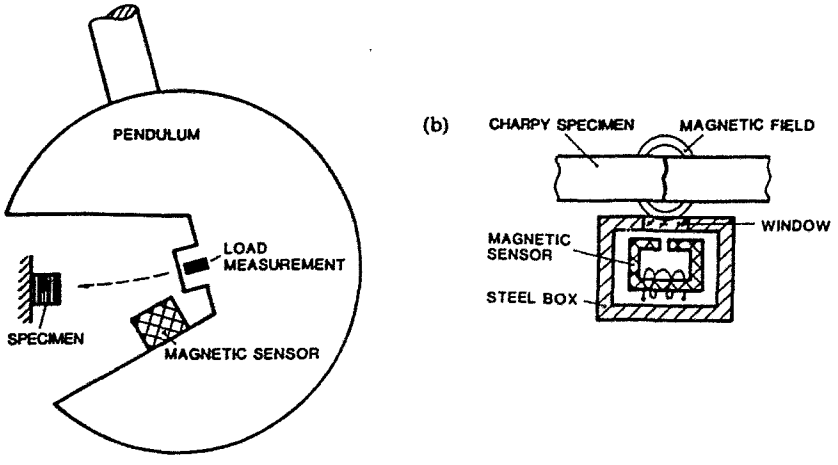

Fig. 9-1 Experimental set up for magnetic emission method [70].

The ME method could be applied to quasi static as well as dynamic loading. The sensor for the magnetic events detection is an electric coil placed near to the notch and connected to an oscilloscope. Due to wide range of recorded signal amplitudes use of the logarithmic amplifier could assure the coverage of the whole interesting range. An example of the testing set up is given in Fig. 9-1. Typical record of ME of dynamically loaded ductile material is shown in Fig. 9-2. Three different regions in the ME trace can be observed. The first one is connected with impact of the tup on the specimen surface, induced pressure wave transverses the specimen. The second region is close to the force maximum indicating the onset of stable crack growth. The last one is connected with the load drop and cleavage fracture step followed by ductile rupture of the resting specimen ligament [70- 73].

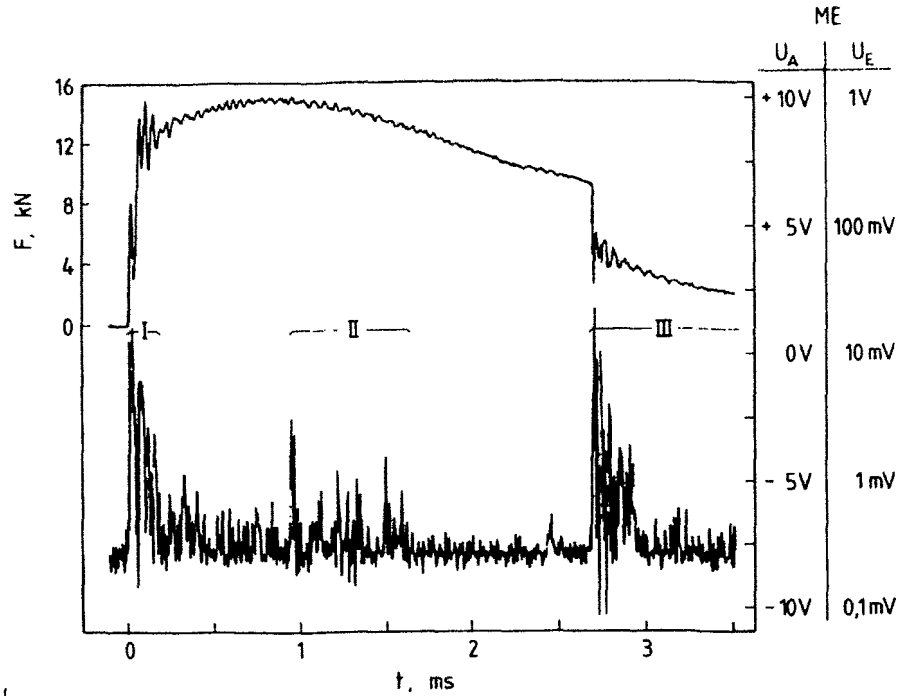

Fig. 9-2 Magnetic emission record [70]

Magnetic emission method was used by Lenkey [74, 75] to determine crack initiation. To improve the precision of the crack initiation, a new method of ME evaluation developed. Magnetic field history is used, i.e. the integrated ME signal:

$$MF(t) = \int_{\tau=0}^{t} ME(\tau)d\tau \qquad (9\text{-}1)$$

This method enabled clearer detection of the onset of the crack initiation by discontinuity in the curve slope, Fig. 9-3.

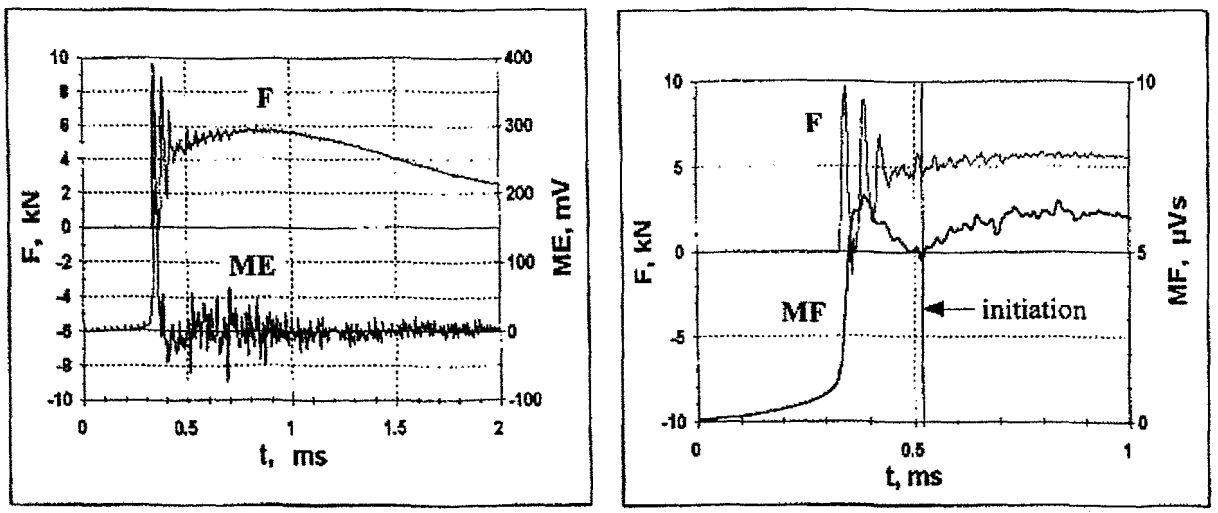

Fig. 9-3. ME crack initiation determination [74]

10 Key Curve and Related Methods

Up to now it was expected that the testing method allows crack length monitoring and by further analyse of the crack monitoring method, or with use of some other method the crack initiation point would be determined. Having crack initiation point and J-R curve, J_i can be easily evaluated. However the J-R curve is not always available because the crack length monitoring methods are time consuming, requiring special equipment or are not applicable for considered case. Then another methods for J-R curve evaluation have to be applied together with appropriate analysis for the crack initiation detection. The main method for J-R curve construction is the key curve method from which many other methods have been derived.

Key curve was educed from dimensional analysis of the dependence of the load on the crack length and displacement using deformation theory of plasticity. Complete J-R curve can be constructed only with use of load-displacement record. The plasticity in a cracked specimen is confined to the remaining ligament at the crack section and the load displacement relationship has the form [76-79]:

$$\frac{P \bullet W}{B \bullet b^2} = F\left(\frac{\Delta}{W}, \frac{a}{W}, \frac{L}{W}, \frac{B}{W}, material\right) \tag{10-1}$$

where P is applied force, Δ is total load-line displacement, a is crack length, b is uncracked ligament, B is specimen thickness and W is specimen width.

It was proved that identical key curves could be obtained for deeply cracked specimens of various crack lengths [25, 76]. For these specimens with use of Eq. 10-1 simplified expression for the J integral and crack length calculation could be used:

$$dJ = \frac{2 \bullet b}{W} F \bullet d\Delta + \left[-\frac{2}{W} \int F \bullet d\Delta \right] \tag{10-2}$$

$$da = \frac{\frac{b^2}{W^2} \frac{\partial F \bullet d\Delta}{\partial\left(\frac{\Delta}{W}\right)} - dP}{\frac{2b}{W} F} \tag{10-3}$$

The key curve function F was obtained from the specimens with blunted notches, so the obtained load-displacement curve is not affected by the crack growth [25]. This has proved to be a complicated procedure, even more, only valid for the considered temperature and test rate. Additionally, the presence of blunt notches modified the shape of the load-displacement record and so it was hardly possible to develop J-R curves of desired extent. To reduce this work and to develop general methodology, analytical curve for three point bend specimen was proposed [79]:

$$F = \frac{P \bullet W}{B \bullet b^2} = k \bullet \left(\frac{\Delta_{PL}}{W} \right)^N \tag{10-4}$$

where Δ_{PL} is plastic component of load-line displacement and k, N are fitting coefficients dependent on material, temperature, test rate... . According to the theory the plastic displacement should be used in key curve method, however Wallin [81] reported better results with use of total load-line displacement. Parameters k and N are determined with use of a stable crack extension point, Fig.10-1. For the crack initiation point the coefficient k is

determined and subsequently the N is evaluated so that the final crack length evaluated according to key curve method is identical with measured one [25, 78].

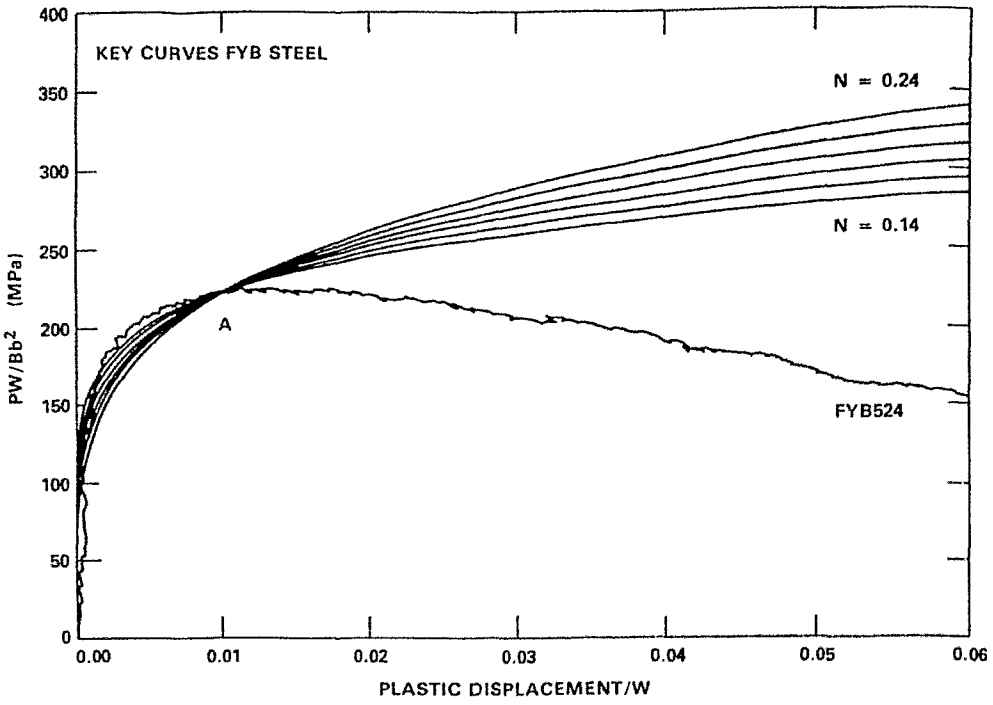

Fig. 10-1. Key curve, fitting of parameters k and N [25].

Key curve method as proposed by Ernst et al. [77, 82] was successfully applied to quasi-static loading as well as to dynamic loading conditions [76-79, 83, 84]. There was also approach to establish the key curve using only directly measured specimen data with use of an iterative key curve method [85].

Another single specimen method recently standardized in ASTM 1820 [4] is the so-called normalization method (NM). It is derived from the key curve. A unique curve exists for the considered material but instead of using of a universal one, individual normalized curve for each specimen is used. Normalization method is based on a principle of variables separation [4, 86- 90]. The load is expressed with use of the crack length and the load line displacement, Eq. 10-5.

$$P = G\left(\frac{a}{W}\right) \bullet H\left(\frac{\Delta_{pl}}{W}\right) \tag{10-5}$$

where a is crack length, W is specimen width and v_{pl} is plastic load line displacement.

The Eq. 10-5 can be rearranged and written is another way defining normalized load, Eq.10-6.

$$P_N = \frac{P}{G\left(\frac{a}{W}\right)} = H\left(\frac{\Delta_{pl}}{W}\right) \tag{10-6}$$

Function H can be graphically defined by a plot P_N versus Δ_{pl}/W , Fig. 10-2. Function G can be defined by power law function, Eq. 10-7.

$$G\left(\frac{a}{W}\right) = W \bullet B\left(\frac{b}{W}\right)^{\eta} \qquad (10\text{-}7)$$

The value of coefficient η is 1.94 for SENB specimen according to [87] and for dynamic three point bend test was found value of 2,08 [88] which is close in both cases to theoretical value of 2 for deeply cracked specimen subjected to pure bending.

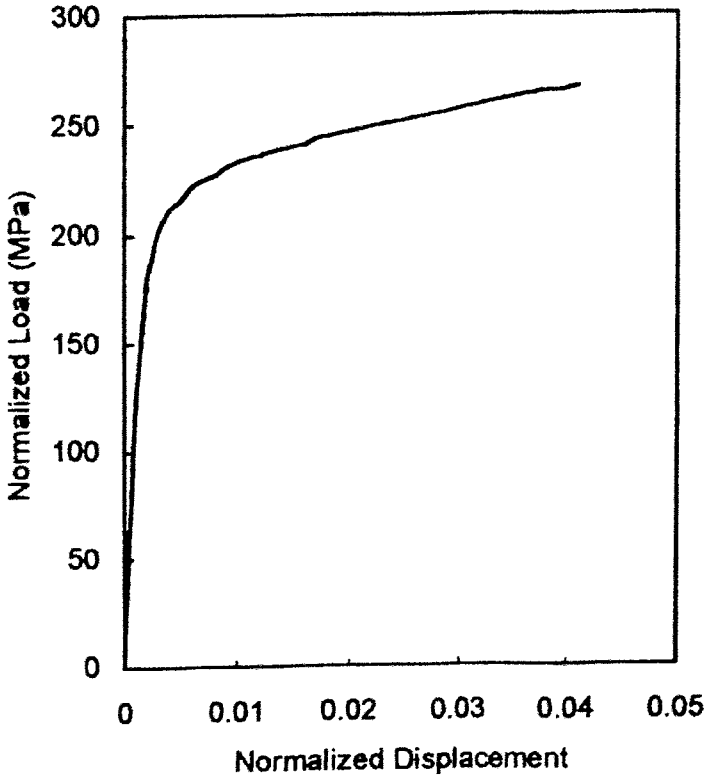

Fig. 10-2. Normalized load versus normalized displacement [87]

Another proposed way of the P_N function solution is the so-called LMN function, Eq. 10-7.

$$P_N = \frac{L + M \bullet \left(\frac{\Delta_{pl}}{W}\right)}{N + \left(\frac{\Delta_{pl}}{W}\right)} \bullet \left(\frac{\Delta_{pl}}{W}\right) \qquad (10\text{-}7)$$

For the LMN calibration curve three calibration points are needed, where the first is the physically measured crack length. The second calibration point is taken from a set of points obtained from forced blunting calibration and the third, intermediate calibration point is not based on a crack length [87].

Further method using the force – load line displacement trace is the load ratio method (LRM). In this case the assumption that the crack begins to extent after the force maximum is used. The crack extension is inferred from the assumption that the ratio of the load to the square of the length remains the same [84, 89].

There are many variations of the numerical single specimen methods [81, 87, 89, 91, 92, 94, 95,]. The LRM was, for example, modified by Byun [91] who proposed an iterative version of this method. In this modification, variables of the exponential functions are

changing until agreement with measured data is attained. With use of obtained parameters crack lengths could be subsequently calculated.

All these methods provide relatively simple and cheap way to obtain J-R curve from the testing of a single specimen. Their main disadvantage is that they use some assumptions which are not generally valid, e.g. the crack initiates at maximum force. Thus determined crack initiation values can be strongly influenced by the evaluation procedure making it difficult to compare the results obtained according to different methods.

11 J-integral calculation

One of the factors affecting the determination of J-integral initiation value is also evaluation procedure for the J-integral calculation. To analyse the influence of J-integral evaluation, recommended formulas were investigated and possible sources of errors were detected.

Formulas for the J-integral calculation are recommended in existing standards. There are two basic modification of the calculation, considering constant crack length and allowing for the crack growth. According to ASTM 1820 [4], following formula for stationary crack is recommended:

$$J = \frac{K^2(1-\nu^2)}{E} + \left[\frac{2.A_{pl}}{b_0.B_N}\right] \qquad (11\text{-}1)$$

where K is stress intensity factor, ν is Poisson constant, E is Young modulus, A_{pl} is plastic work under load-load line displacement curve, b_0 is initial specimen ligament and B_N is the specimen net thickness.
For the growing crack, crack extension Δa correction is added:

$$J = \frac{K^2(1-\nu^2)}{E} + \left[\frac{2.A_{pl}}{b_0.B_N}\right] \bullet \left[1 - \frac{\Delta a}{b_0}\right] \qquad (11\text{-}2)$$

Procedure for fracture behaviour evaluation proposed by ESIS group [2] uses slightly different form. The J-integral in this procedure is not divided into elastic and plastic one, but the J- value is directly calculated from total work under load-load line displacement record U, Fig. 11-1 b). Eq. 11-3 is ESIS calculation formula considering growing crack.

$$J = \left[\frac{2.U}{b_0.B_N}\right] \bullet \left[1 - \frac{\Delta a}{2 \bullet b_0}\right] \qquad (11\text{-}3)$$

The determination of A_{pl} according to ASTM [4] is slightly different for the basic method and for the J-R curve measurement. In case of the first one, parallel line to the initial slope, Fig. 11-1 a), is used for the calculation. In case of J-R curve measurement actual compliance at the test end is expected to be known and so the real plastic energy absorbed by the specimen during bending is known. This is possible in case of quasi-static tests, but for the dynamic tests the unloading line is not so accurately measured and so the original slope is used for A_{pl} determination.

Comparison of the J-R curves evaluated with use of above-mentioned formulas was performed in order to assess comparability of the values obtained by slightly different evaluation procedures. As a basic data for the comparison, data from the three point bend testing of Charpy size specimen applying single specimen unloading compliance method were used.

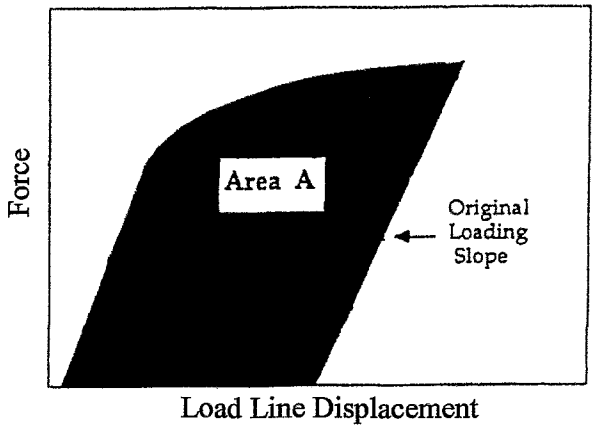

Fig. 11-1 a) Work determination according to ASTM basic procedure [4].

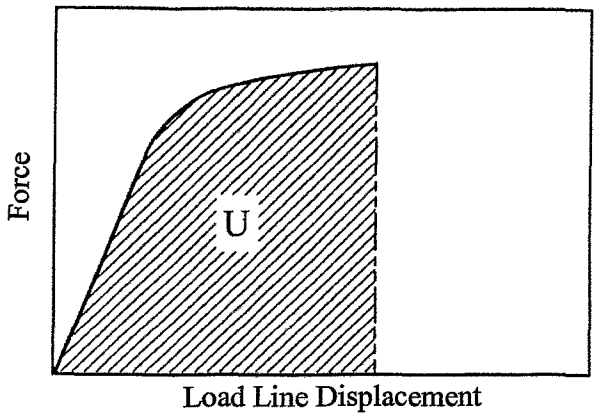

b) Work determination according to ESIS method[2].

In the first step, evaluation according to multiple specimen method was performed. After each unloading overall J-integral was calculated with use of the initial ligament. The J-R curves for stationary crack, Eq. 11-1, and corrected for the crack growth, Eq. 11-2, were determined (*J-stationary crack*, respective *J-growing crack* in Fig. 11-2). The J-R curve was also calculated on the basis of the ESIS procedure with crack growth correction, Eq. 11-3 (*J-ESIS* in Fig. 11-2).

In the second step, the single specimen calculation was performed and the influence of the energy calculation was observed. After each unloading sequence appropriate increase of the J-integral was quantified with use of actual ligament. Plastic energies with use of parallel line to original slope according to Fig. 11-1a, and with use of actual unloading line were evaluated (*J-parallel to initial part*, respective *J-UC* in Fig. 11-2).

The reason for performing calculation according to single specimen and multiple specimen method was to compare the results of these methods obtained on the same data set. According to recommendations in standards or in the literature [4, 96]. The Eq. 11-1 is valid only for stationary crack. The results of the present analyse shows that the curves in the initial part of the J-R curve where the crack initiation takes place are almost identical, Fig. 11-2. Thus, simpler Eq. 11-1 provides results of acceptable accuracy.

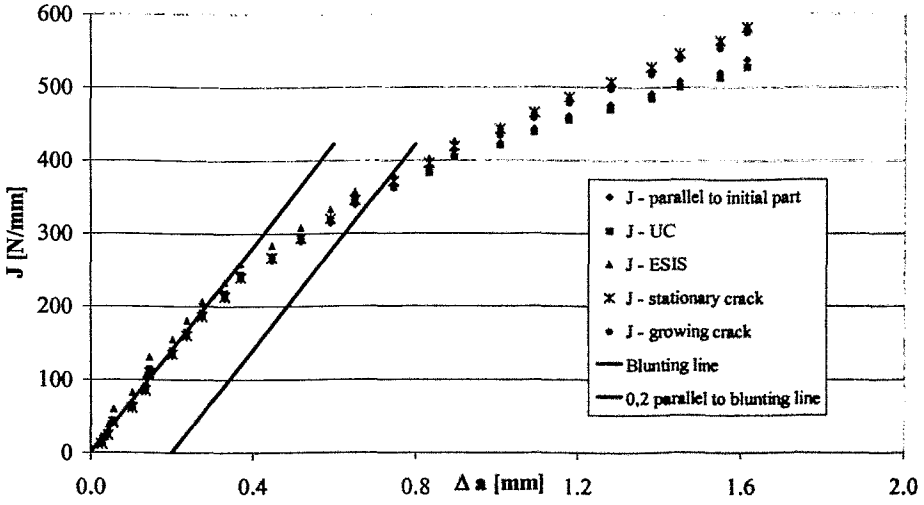

Fig. 11-2. Comparison of J-R curves

Principally, there is difference in energy used for the J-integral calculation according to ASTM [4] basic and J-R curve method and the ESIS [2] procedure for J-calculation, but practically the difference in the results is almost negligible. The ESIS simplified procedure for J-calculation using only total energy provides values in agreement with the results obtained with use of more complicated evaluation formulas. In fact, there is bigger difference coming from the used testing procedure, if single or multiple specimen method is used, Fig. 11-2.

Wallin et al. [12] were also observing the differences between various expressions for the J-integral calculation. According to their findings, noticeable difference between the used formulas started at higher crack extension, yielding almost identical results in the initial part of the J-R curve. These conclusions are in agreement with previous comparison giving a hint that for the crack initiation determination, standard formulas can be used without significant influence on the resulting values.

12 Experimental part

The aim of experimental work is to provide some information about the applicability of previously listed method to our testing facilities. Since special equipment necessary for most of pre-mentioned method, except of AE installed at Charpy impact pendulum, was not available, the tests were focused on multiple-gauge and potential drop methods. Present tests were performed under quasi-static loading.

12.1 Multiple clip gauge based methods

The experimental testing was focused on multiple gauge measurement techniques, namely Double Clip Gauge Method, chapter 4.1, Double Displacement Ratio Method, chapter 4.2, and method described in chapter 4.3 using strain gauge near to crack tip. Subsequently, further methods for the evaluation were applied utilizing standard measured data.

Additionally for the verification of the results obtained from those methods, stretch zone width measurement was performed with use of SEM.

12.1.1 Experimental material

The main purpose of experiment was to supply data for ductile crack initiation evaluation and thus, ductile material at considered (23°C) testing temperature was used. The material was a rolled plate from heat resistant 10CrMo9-10 steel. The material was austenitized at 950°C, cooled in oil and tempered. To obtain different strength-toughness relation different tempering temperatures were applied: 640°C/2h (code E), 720°C/2h (code F) and 760°C/2h (code G). Material chemical composition and basic mechanical properties can be found in Tab. 12-1 and 12-2.

Tab. 12.1 Chemical composition of 10Cr Mo 9-10 steel

	Weight %								
Material	C	Si	P	S	Mn	Cr	Ni	Cu	Mo
10 CrMo 9 10	0.14	0.32	0.007	0.021	0.504	2.31	0.106	0.155	0.99

Tab. 12-2. Material properties

Material	E [GPa]	$R_{p0.2}$ [MPa]	R_m [MPa]	A [%]	Z [%]
E4	207	634	728	18,6	79,0
G3	198	389	511	35,6	80,7
F2	201	446	565	27,7	80,1

12.1.2 Testing

Tests were performed on MTS 250 kN servohydraulic testing machine with laser scanner used as a crack opening gauge. All tests were carried out at room temperature on pre-cracked Charpy V specimens with 20 % side-grooves. Unloading compliance technique was applied to obtain J-R curve which will be used for J_i determination on the basis of crack initiation point determined by different methods. In order to obtain precise information about the beginning of the crack initiation, smaller load displacement step between single unloading cycles 0.015 mm was used, instead of usually used 0.05mm.

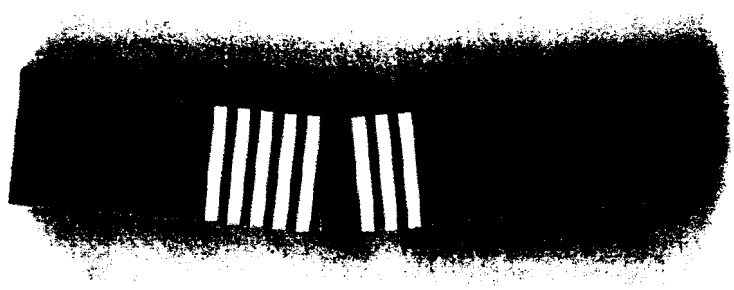

Fig. 12-1 Specimen D2 for Double Clip Gauge method measurement

For the measurement with the scanner a grid must be created on the specimen surface. In order to obtain sharp contrast between specimen surface and strips assuring accurate measurement, self adhesive strips were applied on the specimen surface.

For strain measurement, MTS clip gauge for crack mouth opening displacement and Laser scanner for strain measurement in the range between crack tip and crack mouths was used. For laser scanner two measuring positions were used, firstly in the middle between the crack tip and crack mouth and secondly at the crack tip position. At the crack tip position, laser scanner was used for the measurement of elastic fields according to the method described in chapter 4.3.

Testing set up was checked by tests on two dummy specimens, D1and D2. On the basis of these test further experiments were carried out. D1 was strip coated so, that three strips were on one half of the specimen with 1mm distance apart and 1mm from the crack plane and the second half so, that the first strip was exactly in crack plane, then there was 3 mm gap and then 5 strips with 1mm offset were applied. The wide range covered by strips was used to determine the field in which interesting processes are taking place. Specimen D2 was coated as displayed in Fig. 12-1.

12.1.3 Experimental results

Totally 8 specimens were tested, four with laser scanner at crack tip position and four in the middle between crack tip and crack mouth.

Double clip gauge method according to the procedure described in the chapter 4.1 was applied on the specimens with laser scanner positioned between the crack tip and crack mouth, Figs. 12-2, 12-4. Elastic field around the crack tip at different distances was evaluated, for the tests when the laser scanner was placed at the crack tip according to procedure 4.3. The strains between the strips are displayed in Figs. 12-3 and 12-5.

Crack initiation was determined for all specimens with use of more evaluation procedures using strain, displacement and force data and their combination. Namely, following procedures were applied: Double Clip Gauge Method (DCGM), Figs. 12-2, 12-4, 12-14 and 12-15, Double Displacement Ratio (DDR), Fig. 12-9, Strain Gauge Near to Crack Tip Method (SGNCT), Figs. 12-3, 12-5 and Compliance Changing Rate Method (dC/C_{0MTS}) Fig. 12-11. There were used two modifications of the CCR method. The first one was thr method according to Kobayashi ($CCR_{Kobayashi}$), described in the chapter 6. The second one (CCR_{MTS}) is using specimen compliance actually measured from the unloadings instead of the linear compliance assumed in Kobayashi´s method.

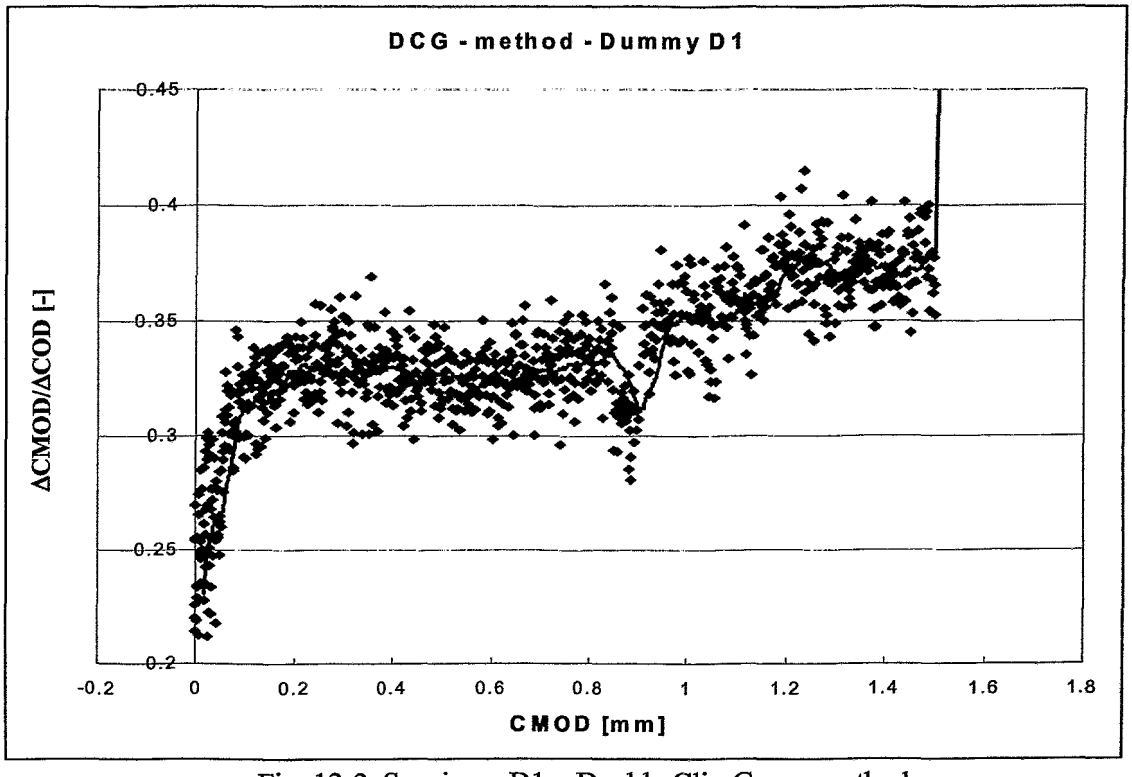

Fig. 12-2. Specimen D1 – Double Clip Gauge method

Subsequently, methods using derivations of measured values and their relations were also applied. As a crack initiation point, inflection point of considered parameters relationship in the force range between general yield point and maximum stress was supposed, Figs. 12-7, 12-8, 12-12 and 12-13, or intersection between elastic part linear fit and polynomical fit of the crack growing part, Fig. 12-10.

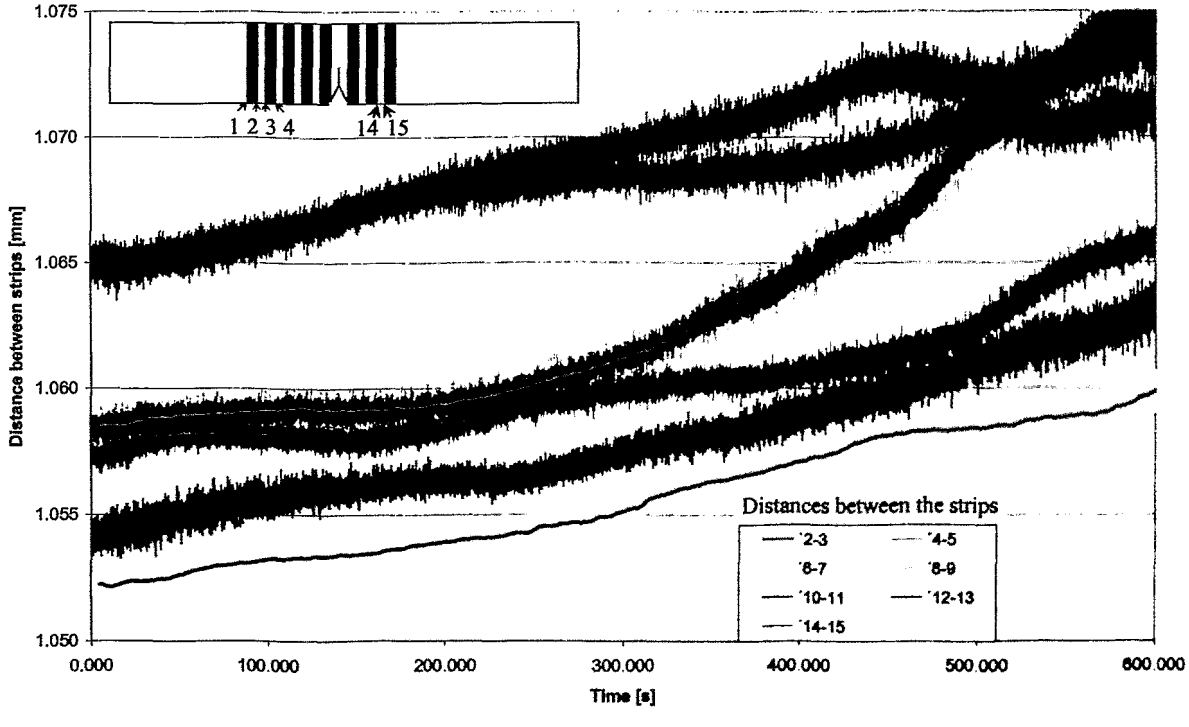

Fig. 12-3. Specimen D1 – Strain gauge near to crack tip method

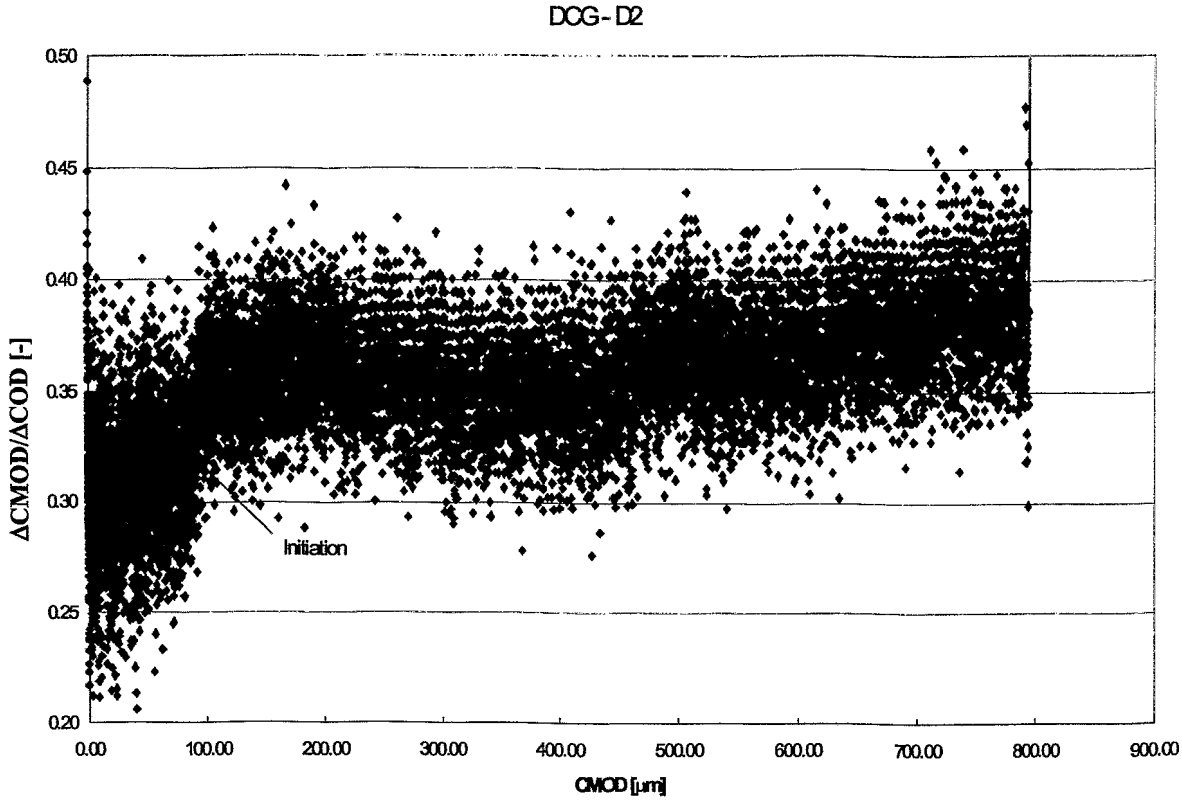

Fig. 12-4. Specimen D2 – Double Clip Gauge method

Stretch zone width (SZW) measurements were carried out. The crack initiation values evaluated on the basis of SZW were further considered a reference value for the comparison of the crack initiation values.

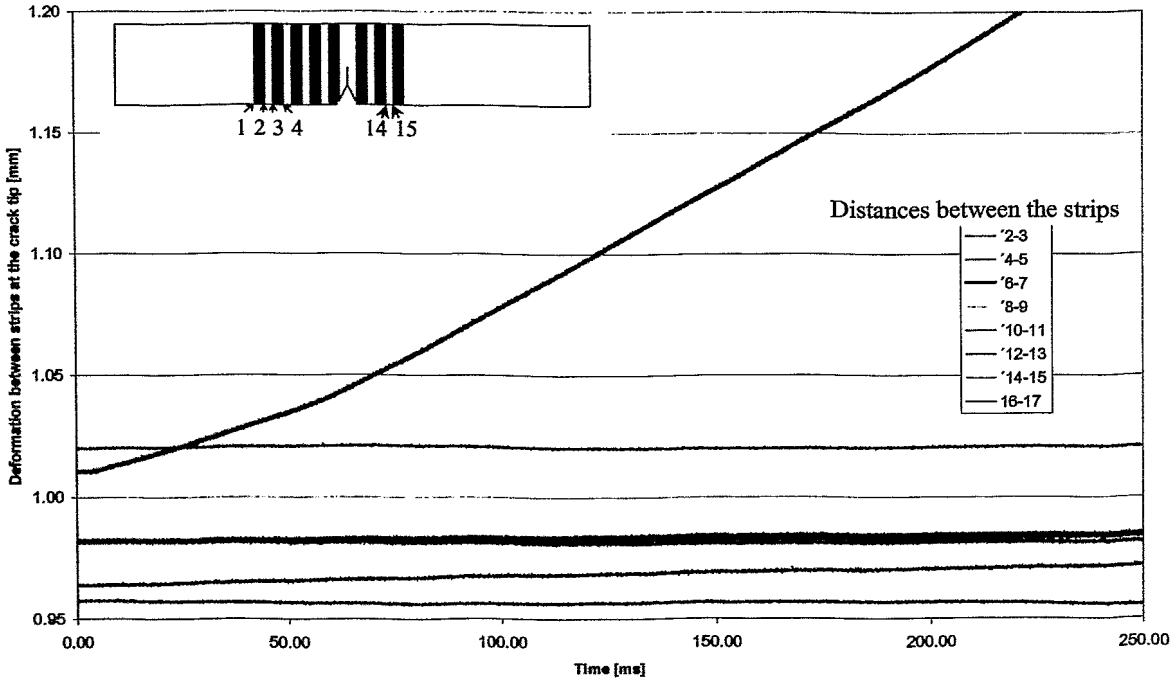

Fig. 12-5. Specimen D2 – Strain Gauge Near to Crack Tip method

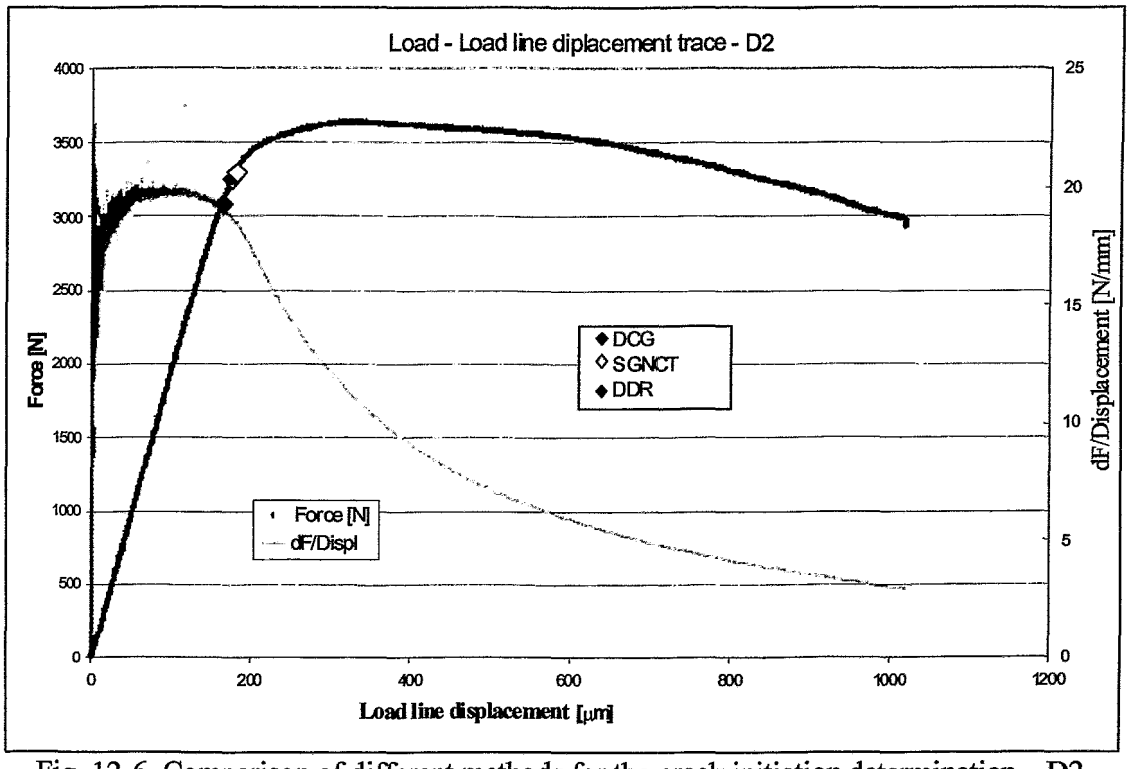

Fig. 12-6. Comparison of different methods for the crack initiation determination – D2

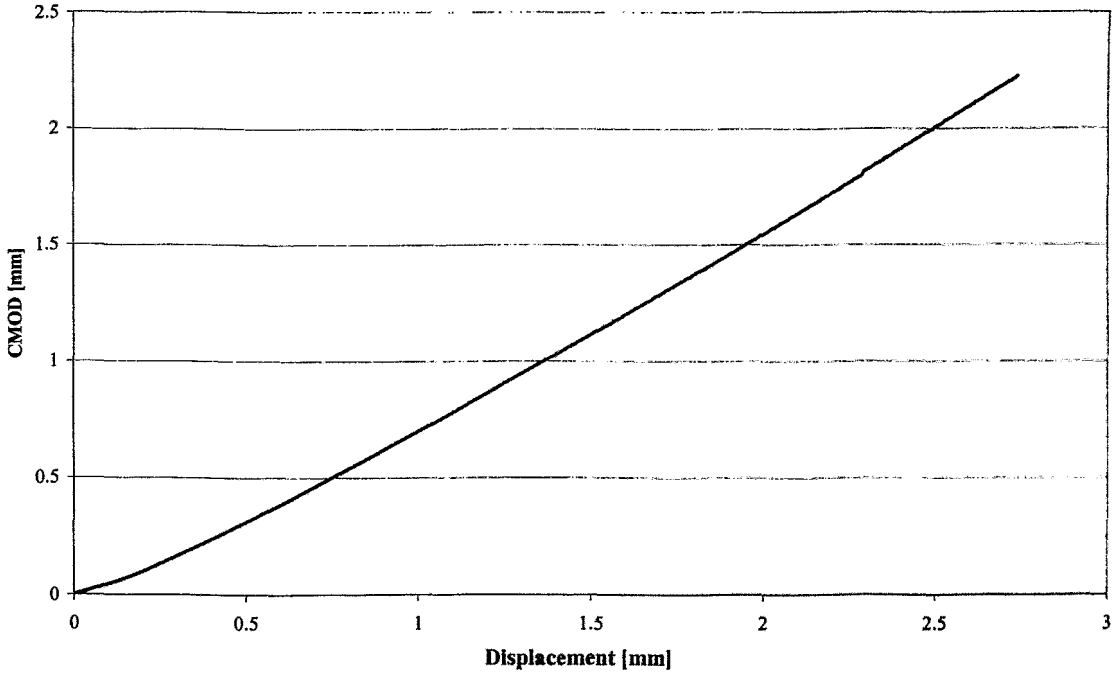

Fig. 12-7. Relation Crack Mouth Opening Displacement versus Load Line Displacement - E4_C2

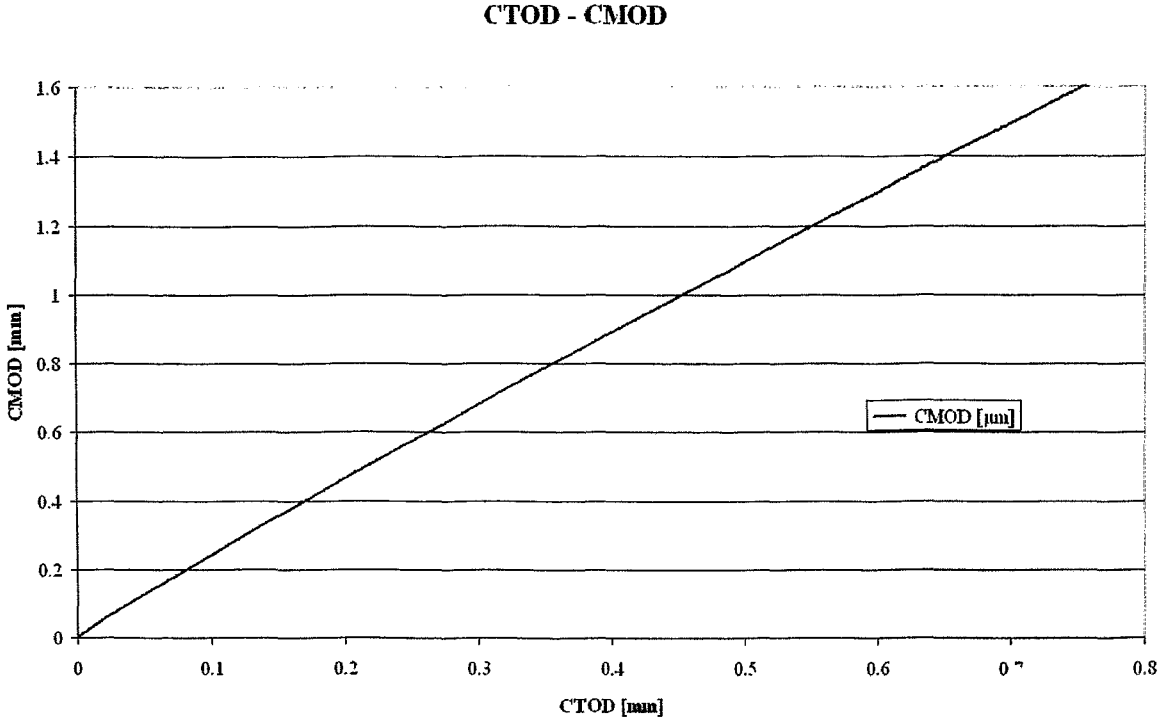

Fig. 12-8. Relation Crack Mouth opening displacement vs. Crack Tip Opening Displacement - E4_C2

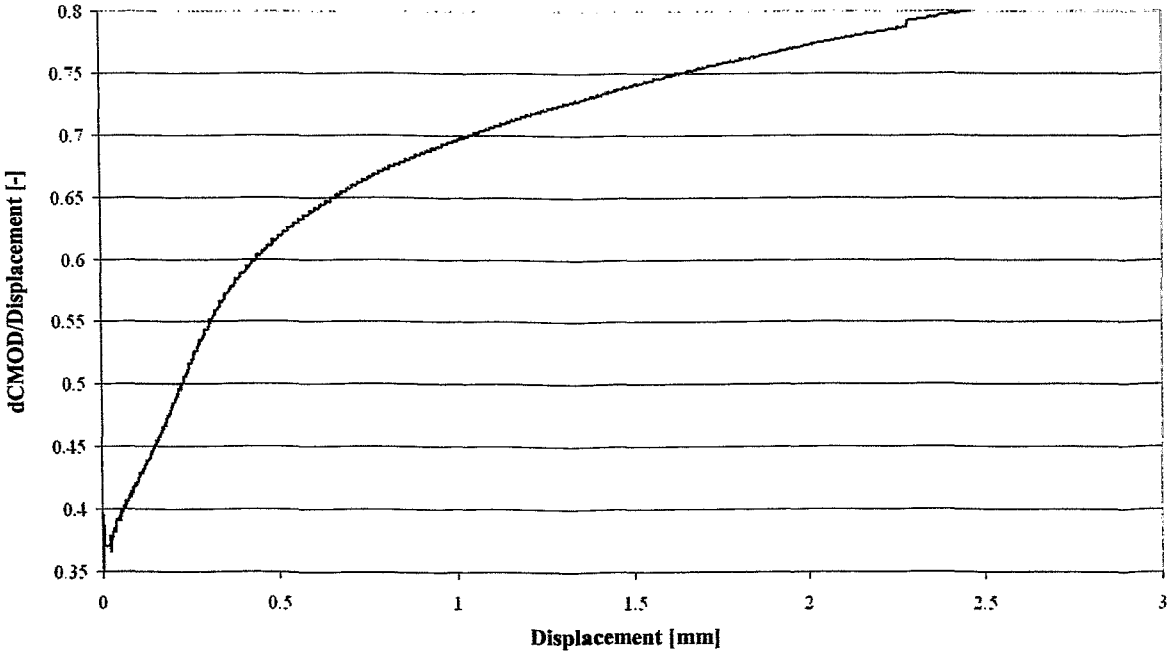

Fig. 12-9. Double Displacement Ration method - E4_C2

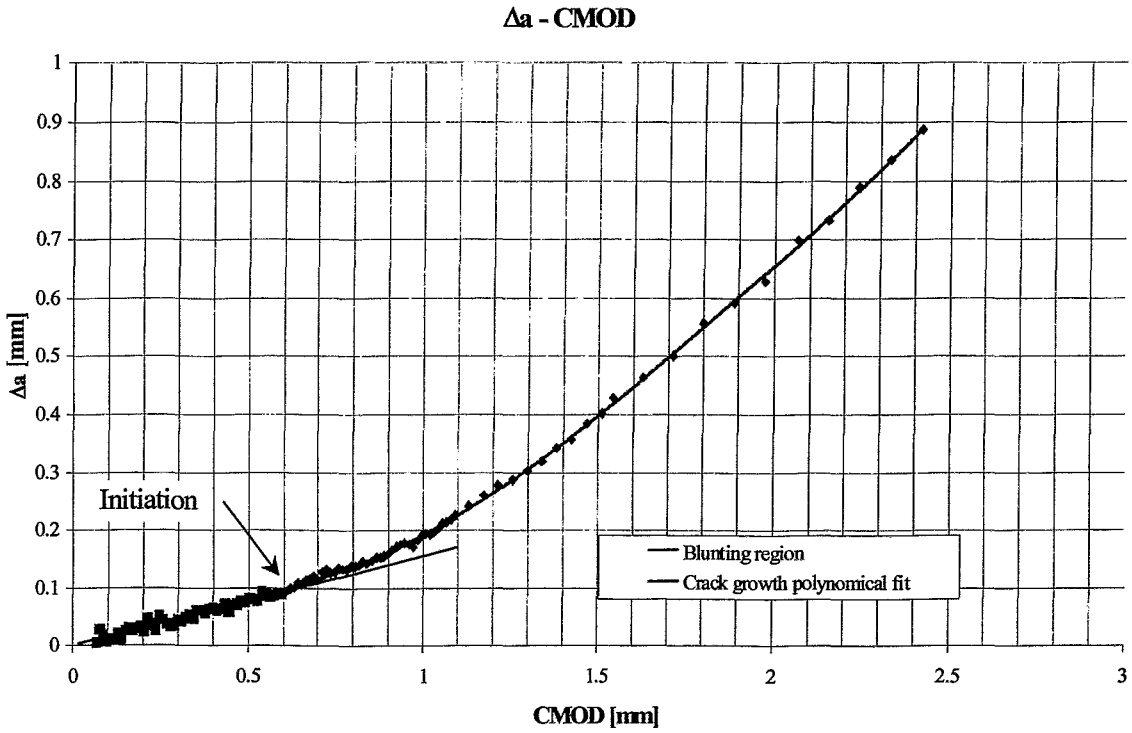

Fig. 12-10 Δa – CMOD relation for the crack initiation determination, specimen F2_C1

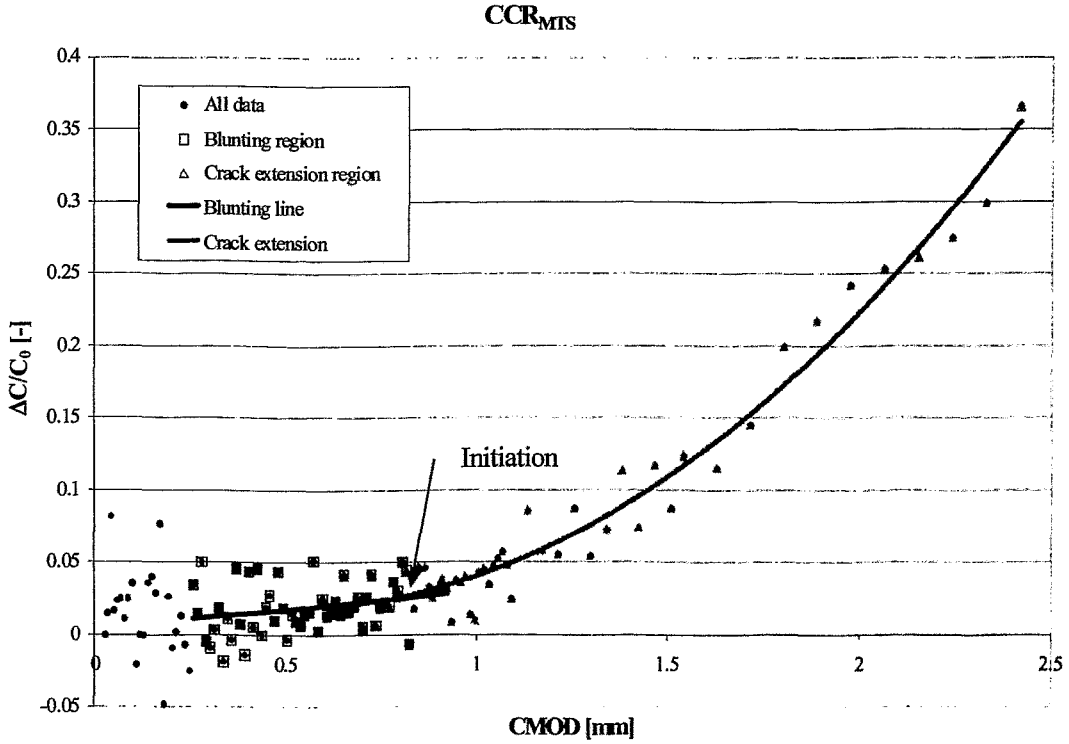

Fig. 12-11 CCR$_{MTS}$ crack initiation determination, specimen F2_C1

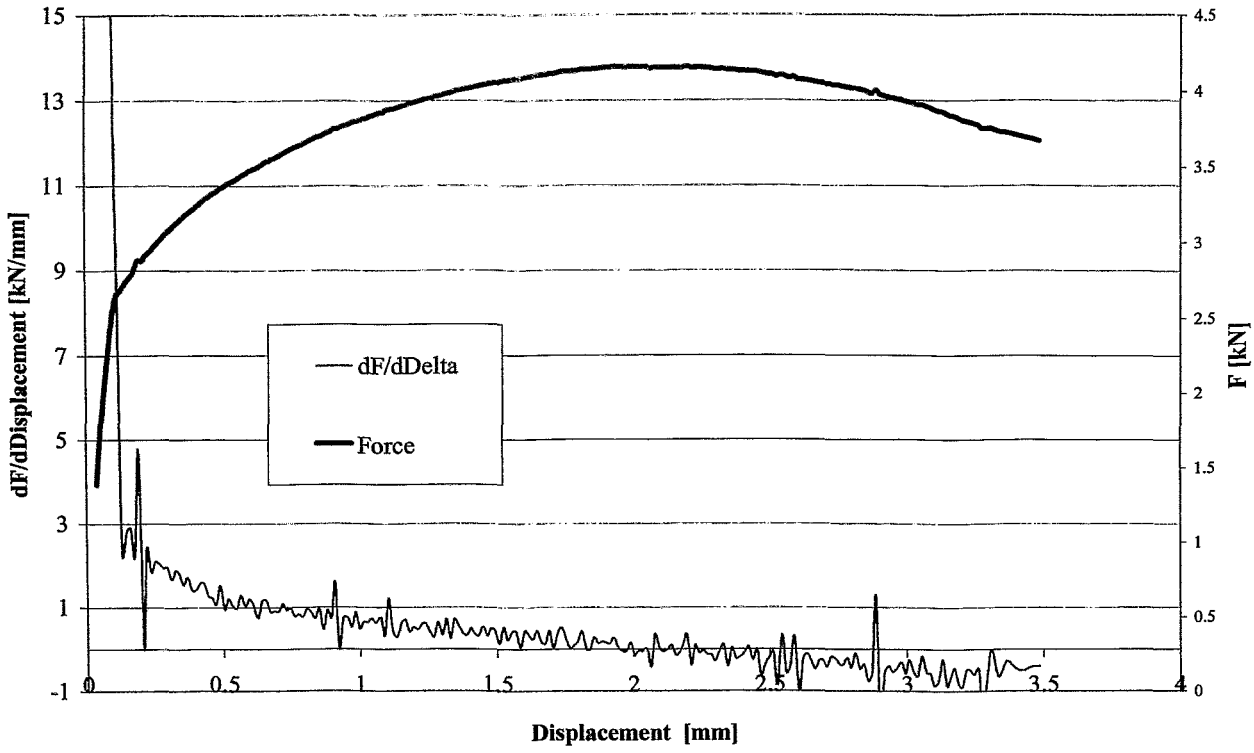

Fig. 12-12 Relation dF/dDisplacement versus displacement - G3_C2

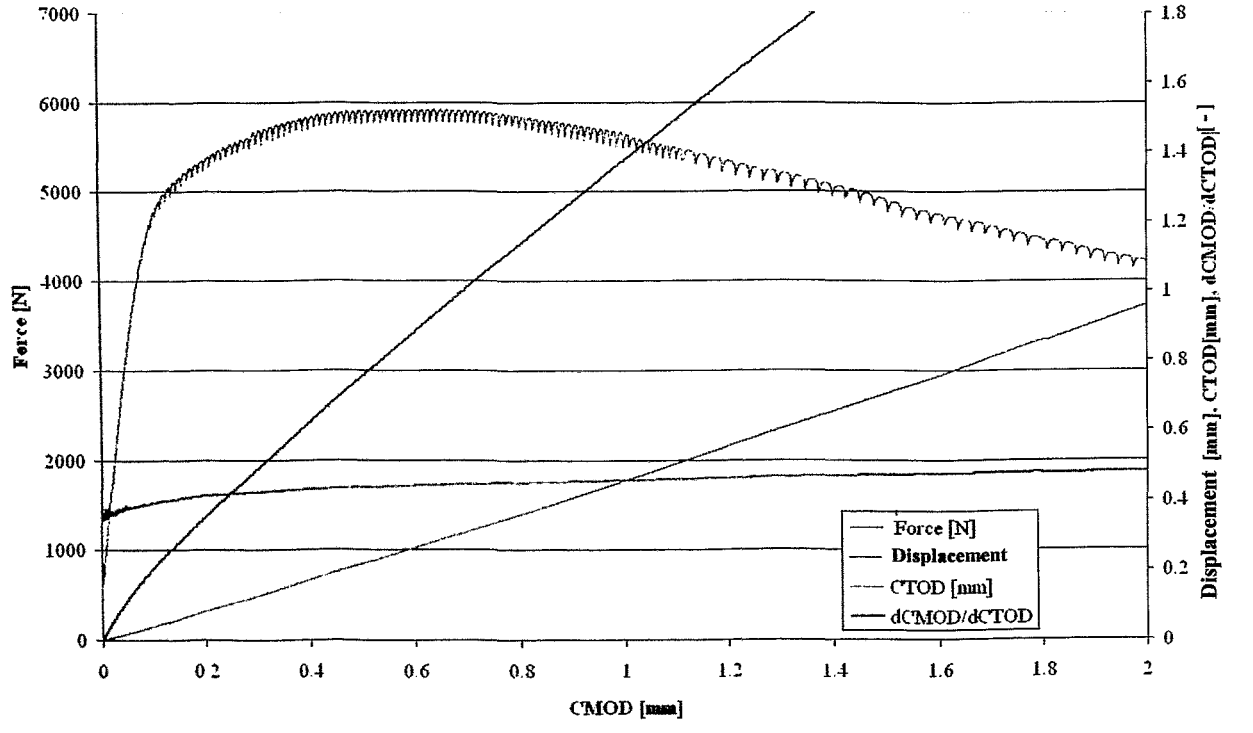

Fig. 12-13 Comparison of different relations for the crack initiation determination – E4_C2

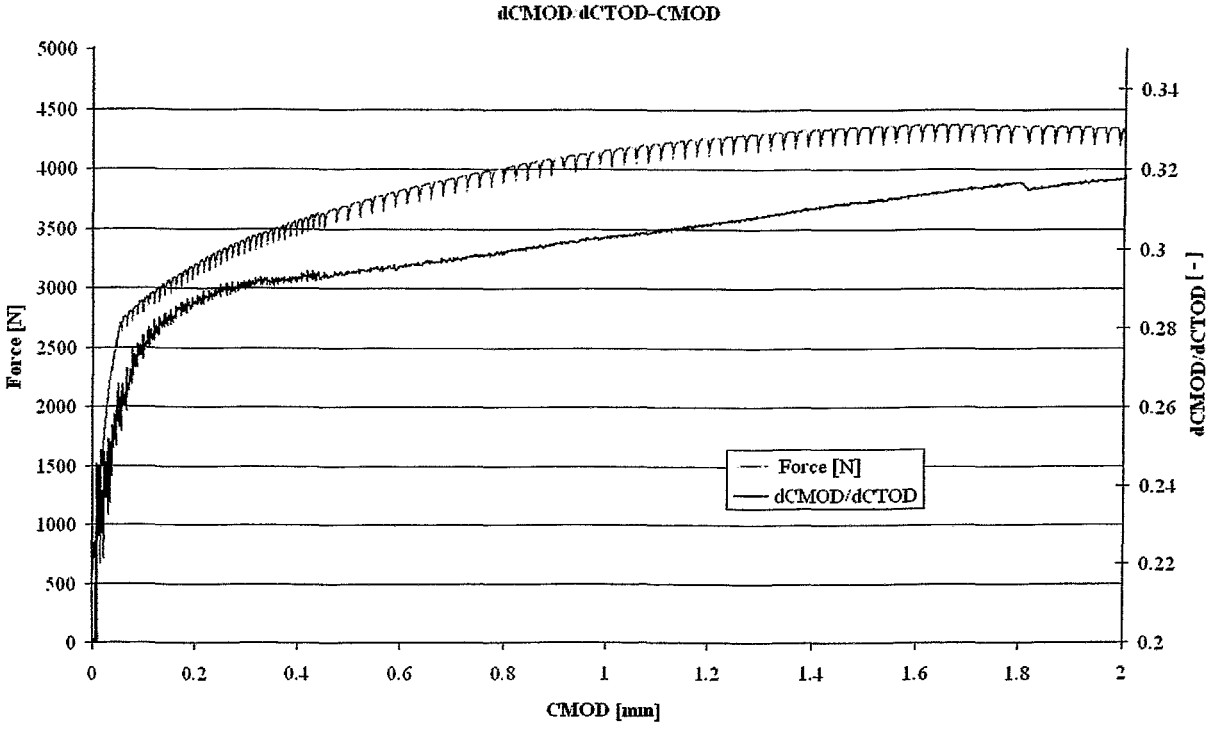

Fig. 12-14. Double Clip Gauge Method the crack initiation determination - G3_C1

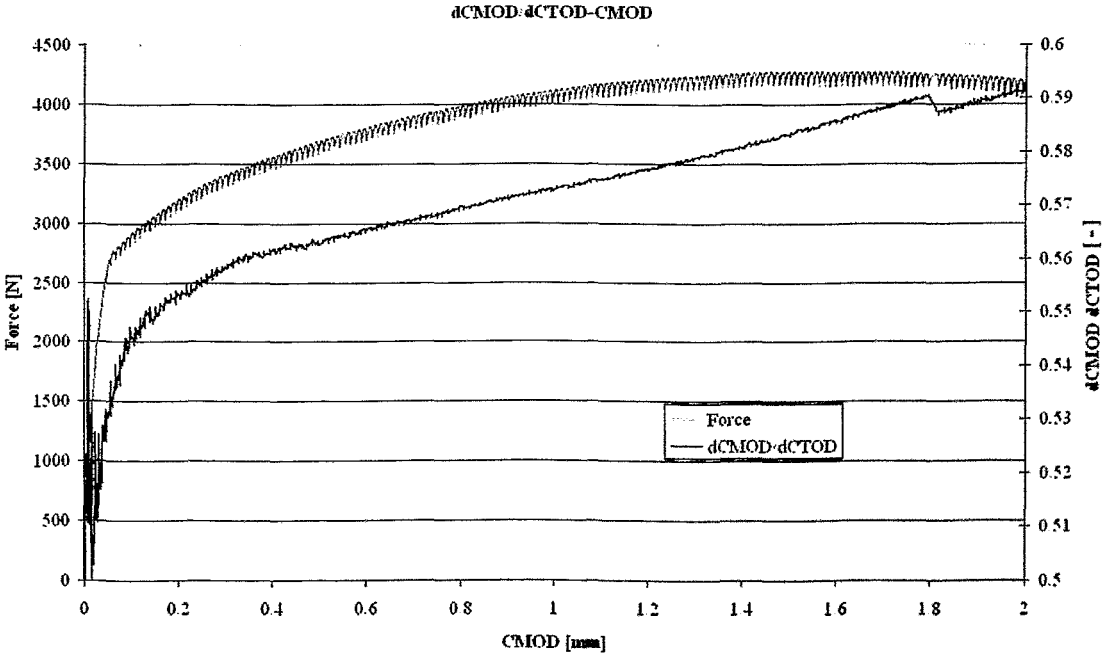

Fig. 12-15. Double Clip Gauge Method the crack initiation determination - G3_C2

Tab. 12-3. Results of crack initiation J_i value evaluation

Specimen	Δa_i^{DCGM} [μm]	$\Delta a_i^{\Delta a\text{-CMOD}}$ [μm]	$\Delta a_i^{CCR\ MTS}$ [μm]	$\Delta a_i^{CCR\ Kobayashi}$ [μm]	$\Delta a_i^{dF/dDispl}$ [μm]	SZW [μm]	J_i^{DCG} [kN/m]	$J_i^{\Delta a\text{-CMOD}}$ [kN/m]	$J_i^{CCR\ MTS}$ [kN/m]	$J_i^{CCR\ Kobayashi}$ [kN/m]	$J_i^{dF/dDispl}$ [kN/m]	J_i^{SZW} [kN/m]
E4_C2	187	86	171	145	199	83	212	119	136	147	161	117
E4_C3	128	96	227	174	253	72	157	118	145	156	182	89
E4_C4	118	100	168	174	199	96	149	123	124	138	158	120
E2_C1	105	93	131	174	219	102	179	166	72	209	114	177
E2_C2	90	100	152	168	230	104	145	159	79	197	114	163
E2_C3	71	87	195	151	304	93	131	165	69	194	111	171
G3_C1	52	121	161	171	377	150	104	295	74	305	202	358
G3_C2	56	132	155	177	328	147	102	296	42	270	189	309

12.1.4 Evaluation of the engineering crack initiation value

The engineering crack initiation values $J_{0,2bl}$ and $J_{0,2}$ were evaluated. The evaluation was done for all considered specimen to compare obtained various "initiation" values. The material properties necessary for the blunting line determination are in Tab. 12-2.

The results of the evaluation can be seen in Figs. 12-16 and 12-17. Critical J integral value was determined in accordance with standard ASTM [4], Eq. 4, ($J_{0,2Bl}$-ASTM). As the blunting line slope coefficient standard value 2 was used. ESIS procedure was also used and $J_{0,2Bl}$ ($J_{0,2Bl}$-ESIS) and $J_{0,2}$ ($J_{0,2}$-ESIS) were calculated. The $J_{0,2Bl}$ is calculated with use of the Eq. 6 and the determination of $J_{0,2}$ is comprehensible from Figs. 12-16 and 12-17. In the graphs also the results of further applied methods for the crack initiation can be found for comparison.

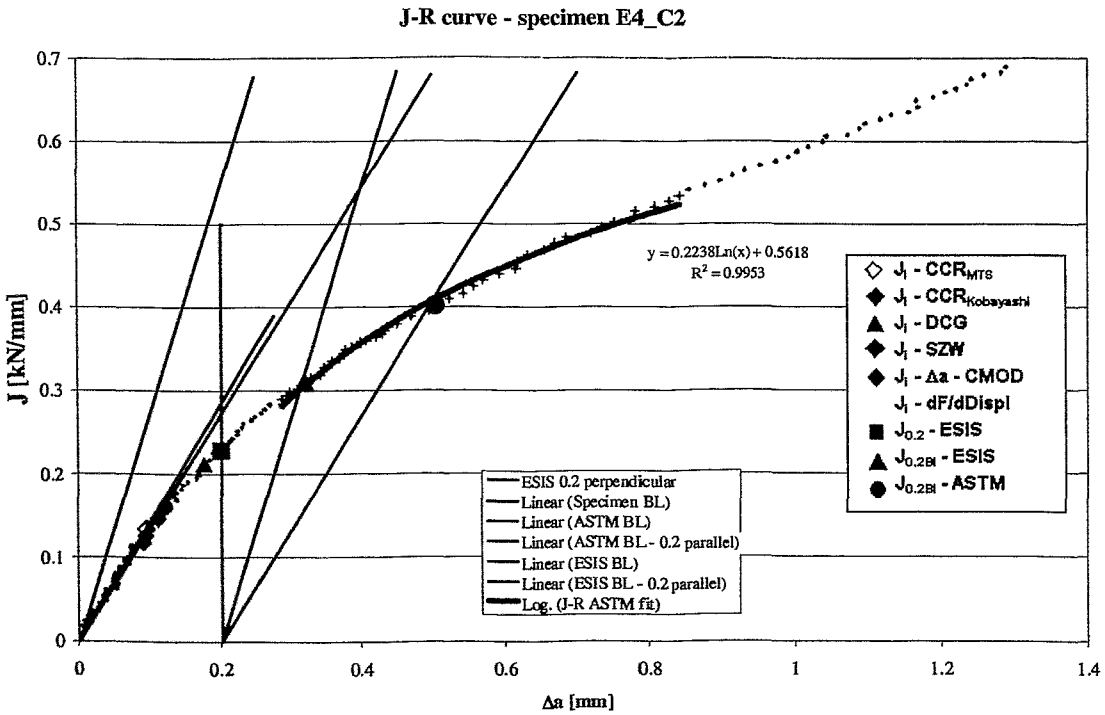

Fig. 12-16 Determination of the engineering crack initiation values, specimen E4_C2

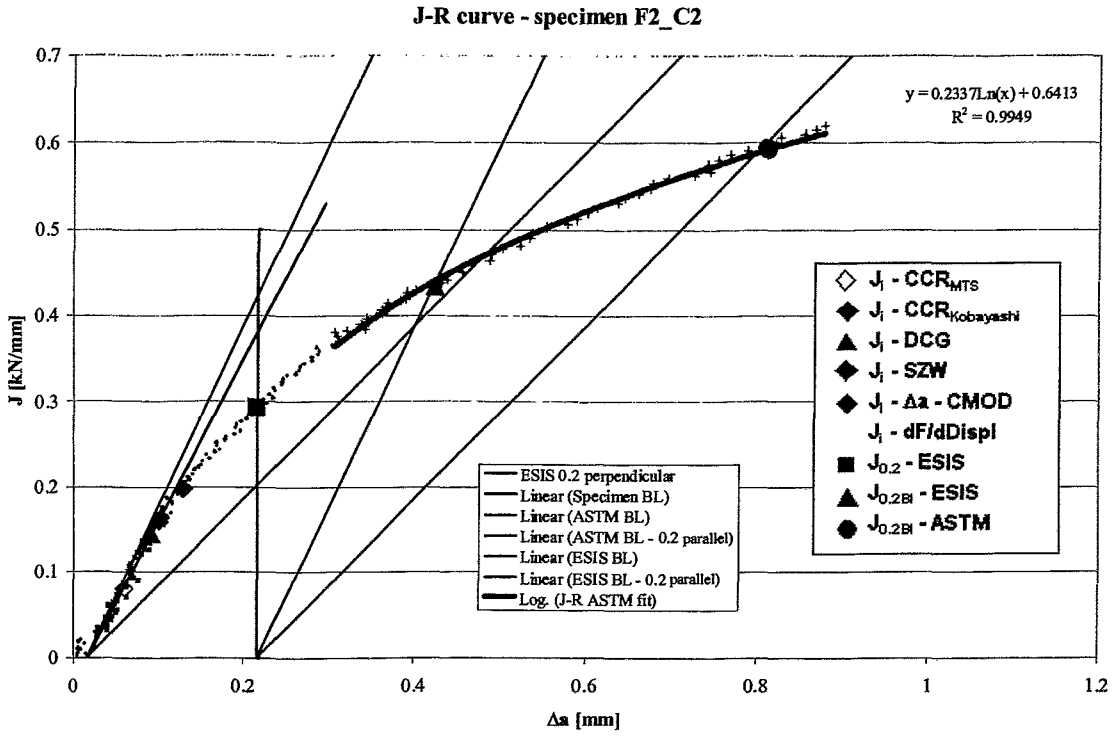

Fig. 12-17 Determination of the engineering crack initiation values, specimen F2_C2

Results in Tab. 12-3 are obtained during the testing under displacement controlled testing conditions, but the real structures are normally loaded under force controlled conditions. This means that the specimen which did not break during the testing in displacement control mode due to reaching displacement limit could easily break in the force control mode without exceeding the maximum force attained in displacement control mode. From the safety point of view it means that the critical value of the J-integral for the safety assessment must be below maximum force. To check this criterion, the corresponding forces to the J-integral values from Tab. 12-4 and Tab. 12-5, were determined and plotted into Force vs. CMOD graph., Fig. 12-18. Also "physical" crack initiation values obtained from previous evaluation summarized in Tab. 12-3 were included into the graph.

Tab. 12-4 Engineering crack initiation evaluation results

Specimen	$J_{0.2}$ [kN/mm]		
	ASTM 0.2 Blunting	ESIS 0.2 Blunting	ESIS 0.2 Perpendicular
E4_C2	0.394	0.310	0.229
E4_C3	0.400	0.317	0.240
E4_C4	0.384	0.299	0.230
F2_C1	0.588	0.425	0.300
F2_C2	0.595	0.445	0.295
F2_C3	0.580	0.450	0.310
G3_C1	---	0.621	0.430
G3_C2	---	0.600	0.398

Tab. 12-5 Forces corresponding with engineering J initiation values

Specimen	F_m [kN]	$F_{0.2}$ [kN]		
		ASTM 0.2 Blunting	ESIS 0.2 Blunting	ESIS 0.2 Perpendicular
E4_C2	5.897	5.270	5.600	5.757
E4_C3	5.896	5.220	5.580	5.750
E4_C4	5.649	5.045	5.346	5.500
F2_C1	4.903	3.850	4.500	4.740
F2_C2	4.930	3.890	4.480	4.790
F2_C3	4.739	3.900	4.330	4.580
G3_C1	4.369	---	3.900	4.220
G3_C2	4.288	---	3.797	4.148

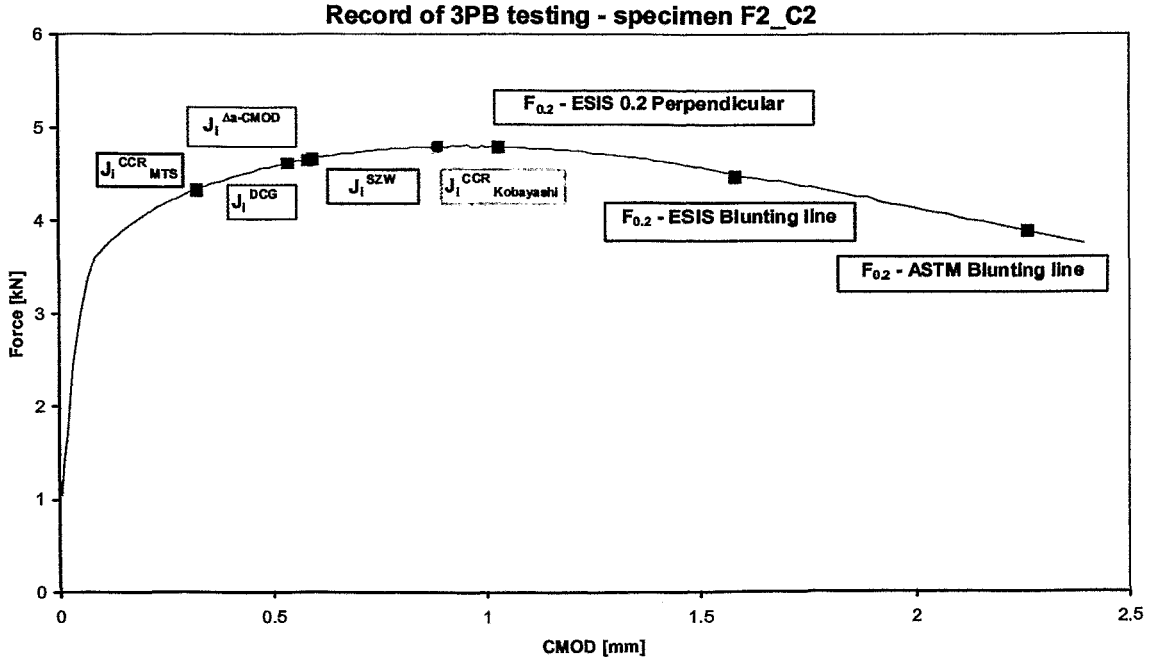

Fig. 12-18 Forces corresponding with J initiation values, specimen F2_C2.

Because in the most cases the recommended blunting lines did not follow the material behaviour, blunting line for each separate specimen was determined to provide guideline in which range are the real coefficients for the considered material. The data for the J-R curves evaluation were obtained by unloading compliance method, so sufficient data were available to determine blunting lines. The results of the blunting line coefficients determination is in Tab. 12-6.

Tab. 12-6 ASTM blunting line coefficients and blunting line slopes

Specimen	E4_C2	E4_C3	E4_C4	F2_C1	F2_C2	F2_C3	G3_C1	G3_C2
Blunting line coefficients [--]	2.06	2.00	1.88	3.52	3.78	3.72	6.26	5.81
Blunting line slope [MPa]	1401	1362	1280	1787	1919	1887	2818	2615

12.2 Potential drop related methods

Literature survey revealed a wide range of methods applicable or already applied for the crack growth and crack initiation measurement. Some of these methods were applied to verify they suitability for the application to crack initiation detection on Charpy size specimens. Following methods were used:

- Direct Current Potential Drop method (DCPD)
- Induced Current Focused Potential Drop method (ICFPD)
- Remotely Induced Current Potential Drop method (RICPD).

12.2.1 Experimental material and specimens

Potential drop measurements were run on three basic materials: SFA, A533B Cl. II and SUS 316L. The materials were selected so that wide range of construction steels was covered. SFA is standard carbon steel exhibiting stable crack extension at room temperature. A533B is a ferritic steel with high fracture toughness parameters and SUS 316L is an austenitic steel used in order to assess the methods applicability also for paramagnetic materials. The first one, SFA, is material of the train wheel set axle. The specimens were taken from the axle from two positions: axle centre – K and near to surface L, providing material with the same chemical composition but slightly different mechanical properties due to the mechanical treatment. The other two materials are usually used in nuclear pressure vessel design. Materials' chemical composition and basic mechanical properties can be found in Tab. 12-7, resp. Tab. 12-8.

Tab. 12-7 Chemical composition of tested materials

Material	Weight %								
	C	Si	P	S	Mn	Cr	Ni	Cu	Mo
SUS 316L	0.01	0.69	0.013	0.005	1.39	16.43	13.86	-------	2.18
A533B Cl II	0.21	0.29	0.007	0.014	1.45	0.03	0.65	0.03	0.5
SFA	0.38	0.26	0.010	0.006	0.78	---------	---------	---------	---------

Charpy size specimens were tested with use of DCPD technique. In order to obtain first experiences with ICFPD and RICPD method for the crack initiation determination during the fracture toughness tests, modified presently available probes were used. The probes' dimensions did not allow using such a small specimens as Charpy and thus bigger specimens had to be used. For these two methods three point bend specimens of 12,5x25 mm cross-section were used.

Tab. 12-8 Basic material properties of tested materials

Material	E [GPa]	$R_{p0.2}$ [MPa]	R_m [MPa]	A [%]	Z [%]
A533B Cl II	210	422	608	18.3	57.2
SUS 316L	192	229	512	56	---
SFA	204	363	608	32	---

12.2.2 Direct Current Potential Drop method (DCPD)

All specimens for PD techniques were tested with use of MTS 810 servo-mechanical testing system. DCPD tests were carried out utilizing Matelect DMC-1 DC Crack Growth Monitor. The DCM-1 utilises the pulsed DCPD technique. The advantage of pulsed DCPD technique over standard DCPD is that the current is supplied only for limited time in predefined intervals, which results in minimization of the specimen heating.

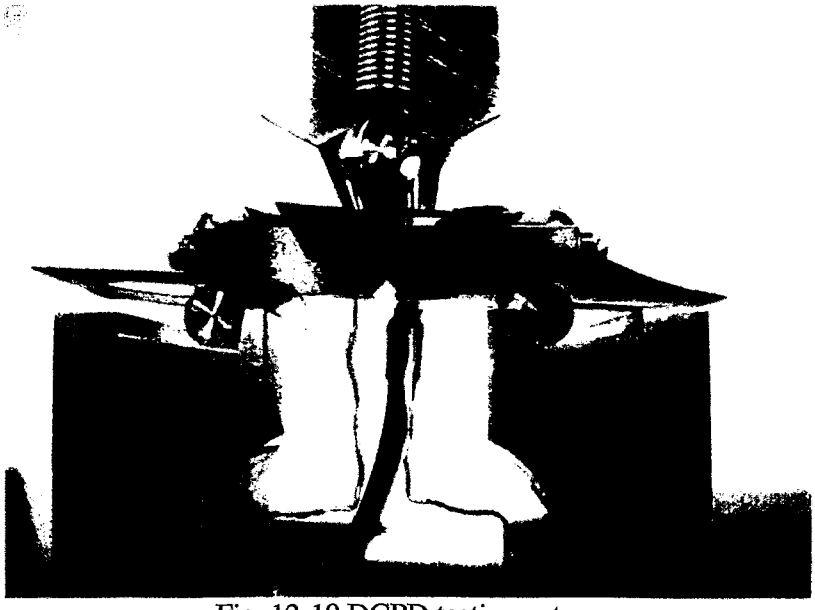

Fig. 12-19 DCPD testing set up

DCPD tests were performed in accordance with experiences and the recommendations in publications [32-38]. The current was supplied into the specimen at the end faces where the supply terminals were screw fastened. Pick up wires were spot welded at the front face of the specimen, Fig. 12-19. The specimen was electrically insulated from the testing system by zircon coated sheets.

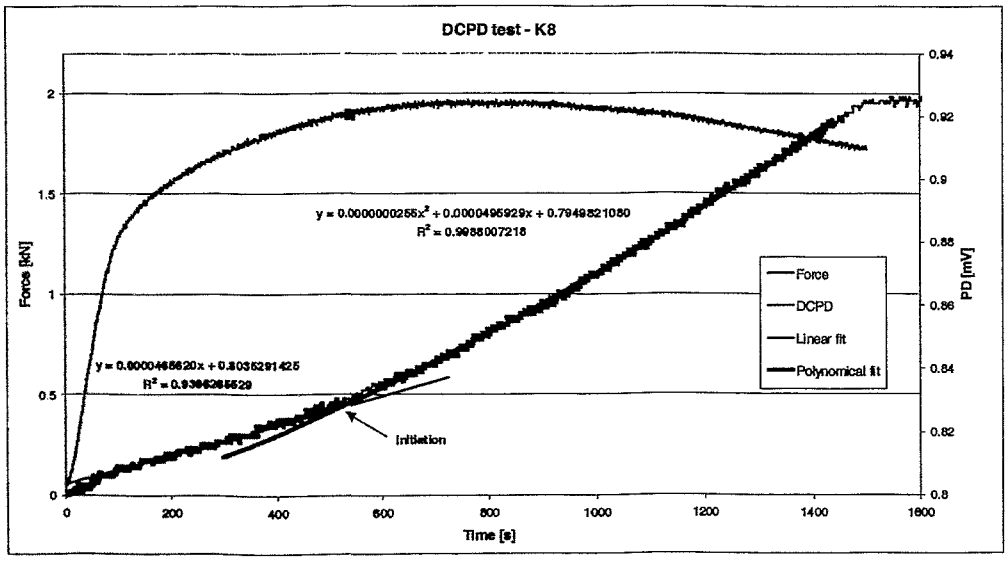

Fig. 12-20 DCPD test record

The main target of these tests was to find out whether there is observable some sudden change in the record course that might be associated with the crack initiation within expected range: between the end of elastic part and before the maximal force in Force-Displacement trace.

Parameters for these tests were based on the laboratory experiences: current 2A, sampling frequency 2s and gain 4000. Example of obtained test records can be found in Fig. 12-20.

12.2.3 Induced Current Focused Potential Drop (ICFPD) Remotely Induced Current Potential Drop method (RICPD)

These methods have been used up to now only for the crack detection during the non-destructive testing and thus their applicability for fracture toughness tests had to be proved and additionally suitable testing set up and test parameters had to be found out.

ICFPD and RICPD tests were performed with use of Matelect CGM-5R Crack Growth Monitor. The CGM-5R is an ACPD crack growth monitor that offers the user frequencies up to a maximum of 100kHz with a continuously variable excitation current of zero to 2A.

At the first stage existing probes with a small modifications were used, Fig. 12-21. The probes size did not allow their application to the Charpy size specimen and so specimens of 12,5x25x120 mm were used.

ICFPD probes were made according to scheme in Fig. 5-5., but because the specimen bends in our case, the probe had to consist of two parts and positioned on the opposite sides of the crack/notch. As an induction wire supplying the current to the specimen, copper foil was used. The probes had to be made so that the induced current will flow in one direction, normally this is assured if single probe is used having one induction foil. When two probes with two induction foils are used "bridge wire" has to be used and care must be paid to its appropriate connection. In our case wire between the end of the first foil and the beginning of the other one was used. The length of this wire was kept minimal to minimize noise, but sufficient for flexible connection even at high deflections. As a pick up terminals, copper spring assisted pins were used. The probes were attached to the specimen by double side self adhesive tape as close to the notch edge as possible. The probes were subsequently secured by rubber bands preventing the probes detachment in the test course, Fig. 12-21.

RICPD measurement was carried out with the probes following the principle schema depicted in Fig. 5-6. The basic design is the same as in case of ICFPD probe, but instead of pick up pins coil is used for the potential change measurement, Fig. 12-22. The probe mounting is exactly the same as in previous case of ICFPD probe.

Very important factors for PD measurement are testing parameters. In order to find appropriate testing parameters, dummy specimens were tested with various parameters. The current was kept constant 2A according to previous experiences with non-destructive tests. The frequency has next to the current the highest influence on the sensitivity and so frequencies between 3 and 100 kHz were applied to the specimens. Gain was set as high as possible within operation range of used equipment.

These pre-test were carried out in pre-cracking mode with use of unloading compliance for the crack extension monitoring that might be eventually used for the calibration. Total crack extensions attained during these tests were about 4 mm, exceeding maximal expected crack extension during the subsequent tests so whole considered operation range was covered. Traces obtained from these tests were similar to published curves obtained with DCPD method; linear part in the beginning followed by a polynomical trend, Fig. 12-23. In case of ICFPD increasing trend was obtained while for RICPD was decreasing, but the shape of the curves was similar.

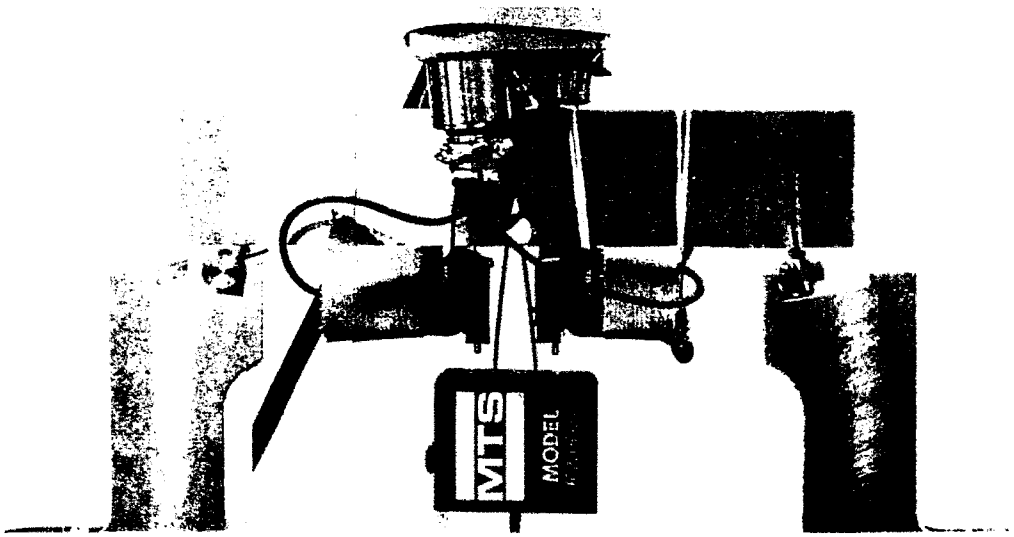

Fig. 12-21 ICFPD testing set up

When higher frequencies were applied, the sensitivity was higher, but at higher crack extension values the curve trend became gradually parallel to x-axis preventing crack length evaluation. On the basis of these pre-tests, frequencies between 3 and 10kHz were further used for testing.

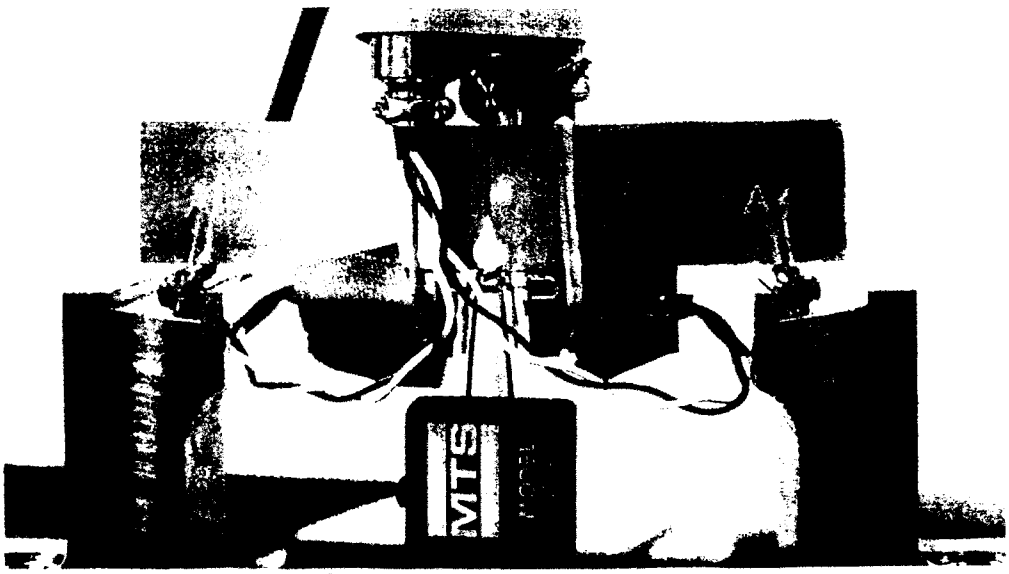

Fig. 12-22 RICPD testing set up

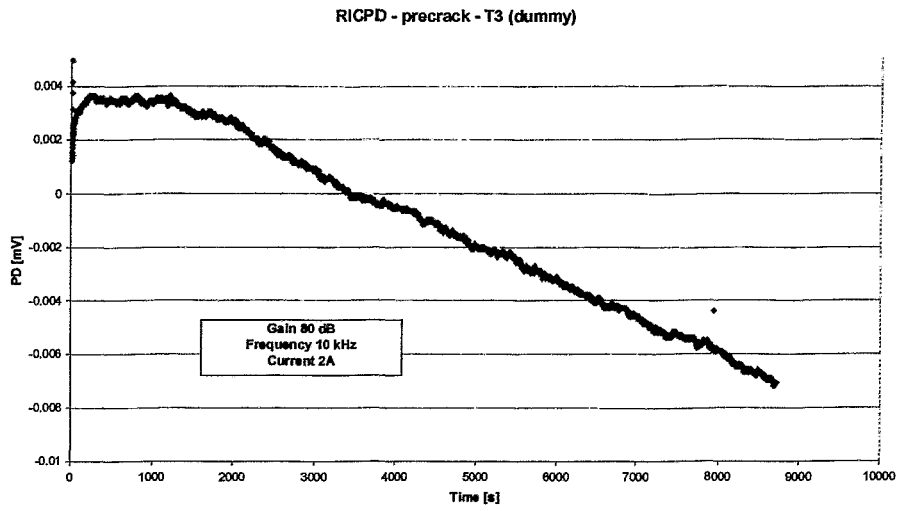

Fig. 12-23 Pre-crack of dummy specimen with RICPD technique

The influence of a clip gauge on the potential drop measurement was also considered, but the signal disturbances were not noticed, Figs. 12-23 and 12-24, so clip gauge was further used. The clip gauge was applied in order to enable the use of the unloading compliance technique for the crack length monitoring as well as to provide further data for additional methods of evaluation like DDR and CCR

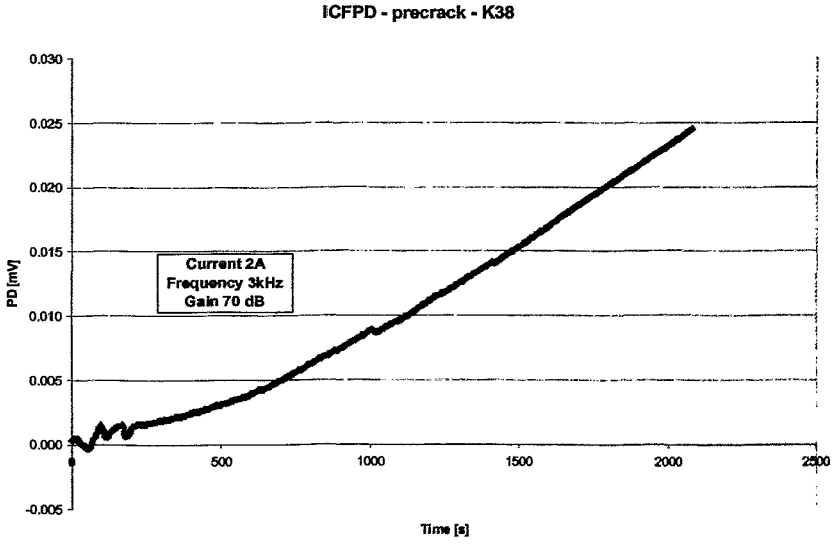

Fig. 12-24 Pre-cracking with ICFPD method without clip gauge

During the tests problems in compliance measurements appeared due to originally used electric insulation plastic-shims. These shims brought parasitic compliances into the loading chain resulting in unrealistic crack lengths. Zircon coated metal sheets were successively used and the test were also carried out without any electric insulation. Almost identical results were obtained for the tests with the metal sheets and without any insulation, thus simplified procedure without electric insulation was applied.

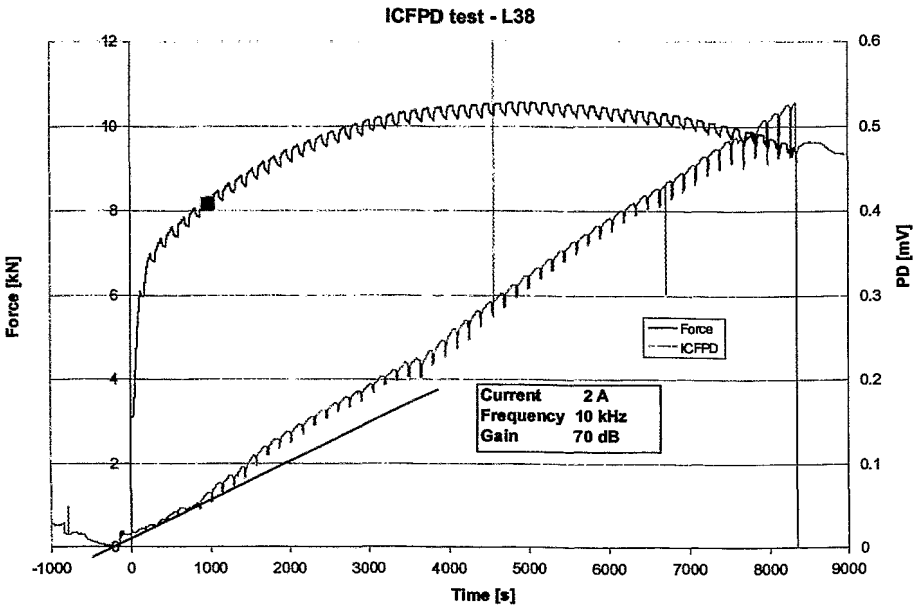

Fig. 12-25 Test of SFA-L specimen with original ICFPD probe

Several specimens were tested with use one of PD techniques together with unloading compliance, example records can be found in Figs. 12-25 and 12-26. One test was also performed with ICFPD without unloading compliance and to one specimen only monotonic loading was applied without any additional technique. After running the tests on the first batch of SFA specimens the design of the probes was modified in order to improve performance. The "bridge wire" connection was changed for both types of the probes. Re-designed RICPD probes were equipped with two identical coils in serial connection. New specimens made of the material A533B Cl.2 with higher fracture toughness, where a bigger change in PD trace was expected, were also machined. Examples of the records obtained with redesigned probes are in Figs. 12-27 and 12-28.

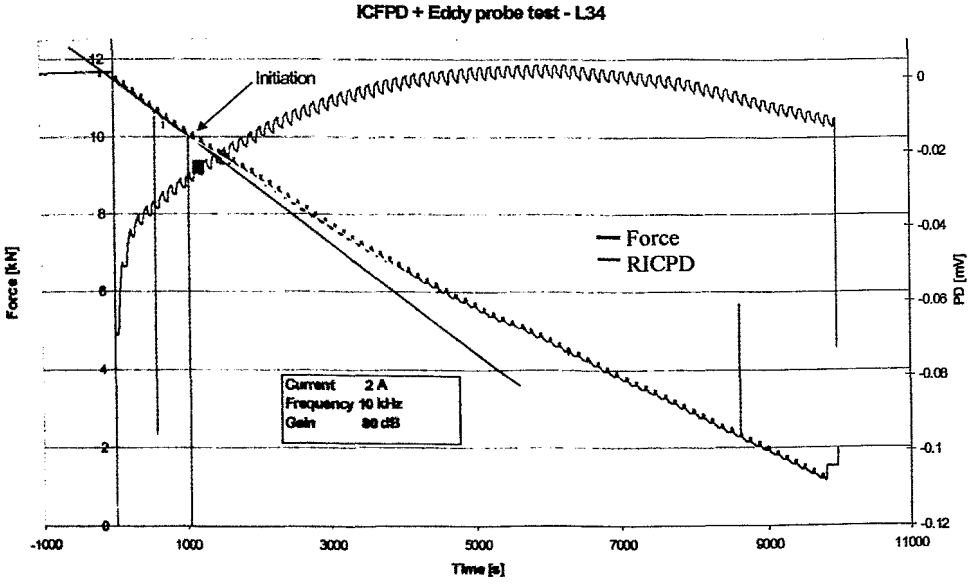

Fig. 12-26 Test of SFA-L specimen with original RICPD probe

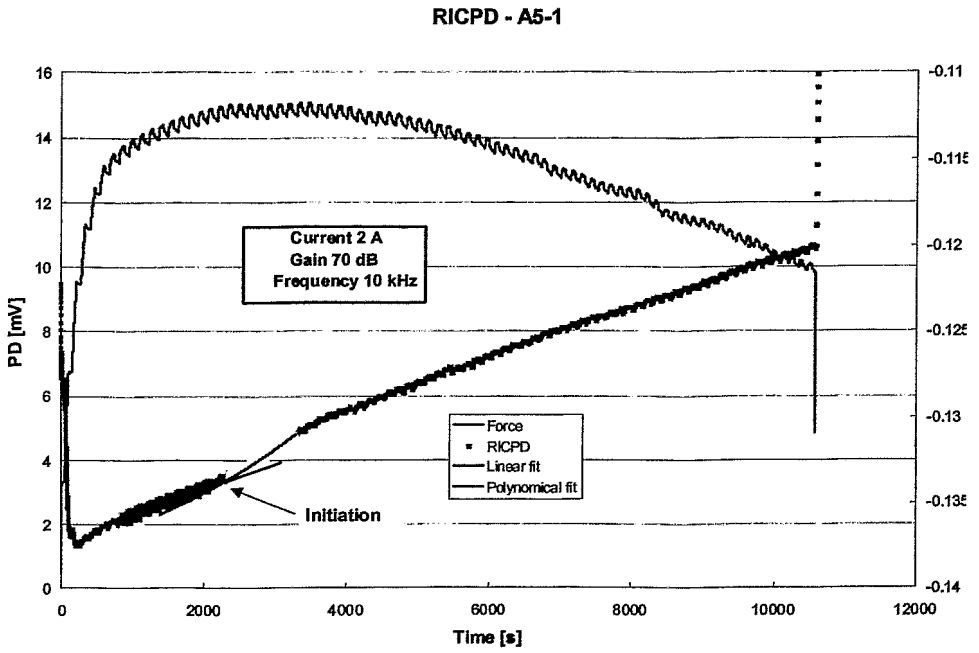

Fig. 12-27 Test of A533B Cl. 2 specimen with re-designed RICPD probes

Additionally, paramagnetic austenitic steel SUS 316L was also used to provide some information on the method performance with such a kind of materials.

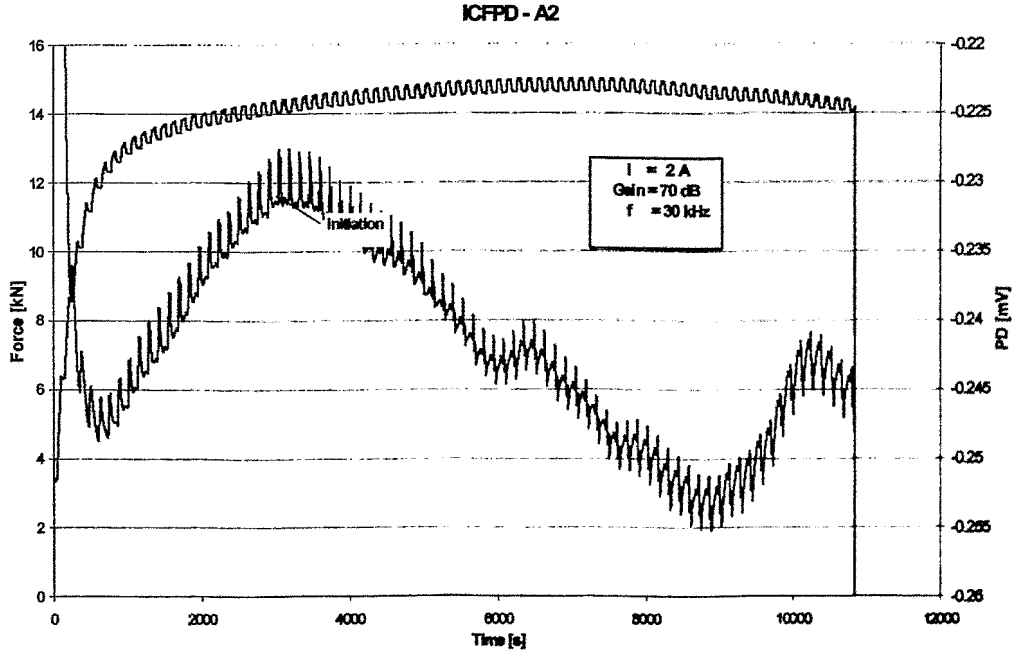

Fig. 12-28 Test of SUS 316L specimen with re-designed ICFPD probes

12.2.4 Evaluation of the tests

Test performed with use of Potential Drop methods were evaluated not only with use of this method, but also with some additional methods as discussed in theoretical part of this report were applied. In all cases as many evaluation methods as possible, in dependence on available experimental data, were applied in order to compare the results obtained by them. Following methods were applied for the crack initiation determination: ICFPD, RICPD or DCPD, DDR, CCR, Δa-CMOD relation was used as well as $J_{0,2BI}$ were evaluated and with use of Δa-CMOD relation. Also $J_{0,2BI}$ values, using actually measured blunting line, were calculated for comparison with the results of the other methods.

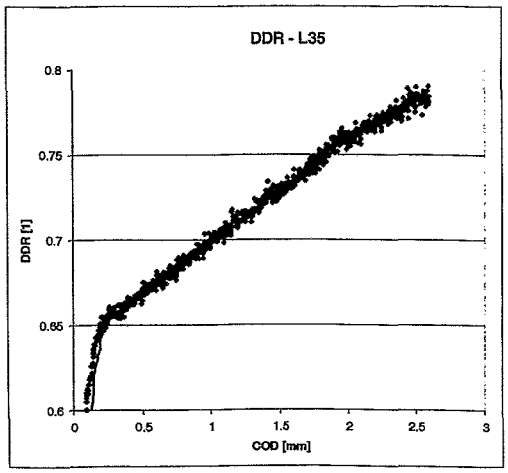

Fig. 12-29a) DDR Method, not distinguishable break point

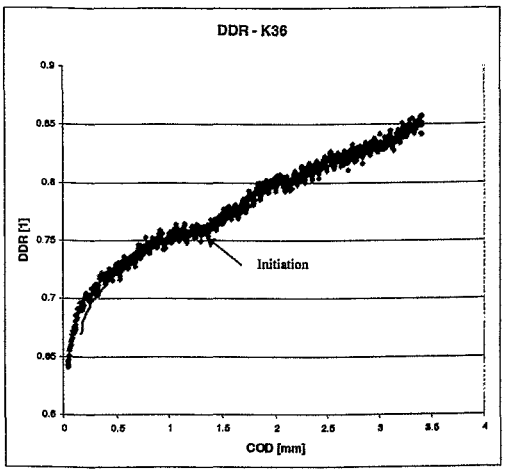

Fig. 12-29b) DDR Method, visible inflection point

Crack initiation according to DCPD method was determined at the break point between initial linear part and subsequent polynomical curve. When RICPD or ICFPD methods were applied, the first change in slope or the first local peak was considered as a crack initiation point, Figs. 12-25 to 12-28. DDR evaluation was done according to method described in Chapter 4.2, Figs. 12-29. In case of CCR two ways of calculation were carried out. Basic calculation was done according to Kobayashi's method described in Chapter 6, but two differently obtained compliances were used. The first one is in accordance with Kobayashi's method, depicted as $CCR_{Kobayashi}$ - Figs. 12-30, and the second one, CCR_{MTS} - Figs. 12-31, was using actually measured crack mouth opening displacement based specimen compliance. The crack initiation was defined as a break point between the initial linear and the following polynomical part. The break point between linear and polynomical part was evaluated as an intersection or in some cases tangent point between the fitted line and polynom of the second order. The fits were done in the region near to the expected initiation point.

On the basis of determined crack initiation points J_i was calculated according to Eq. 11-1. Crack extension at the initiation was considered as negligible and thus no crack extension correction was used. The plastic energy was calculated by the integration of total area under the force-load line displacement trace up to the initiation point from which elastic energy obtained on the basis of the initial elastic slope was subtracted.

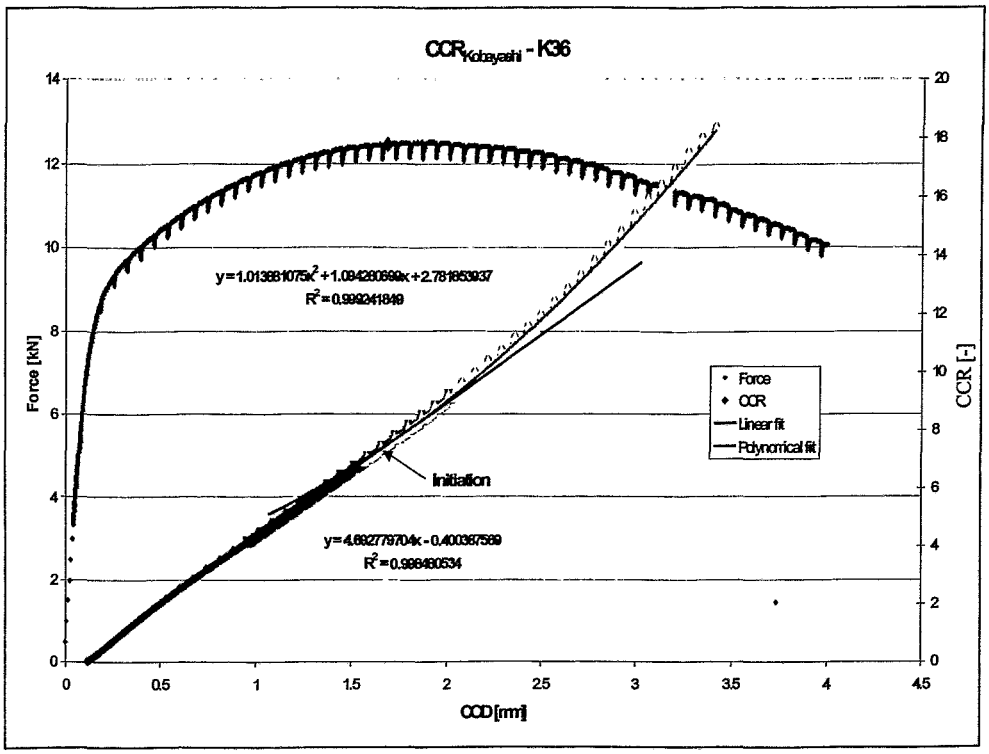

Fig. 12-30 Crack initiation evaluated according to $CCR_{Kobayashi}$

Results of the tests with PD methods are summarized in are summarized in Tabs. 12-9 to 12-11. Example of evaluated J_i values plotted into J-R curve can be found in Fig. 12-32.

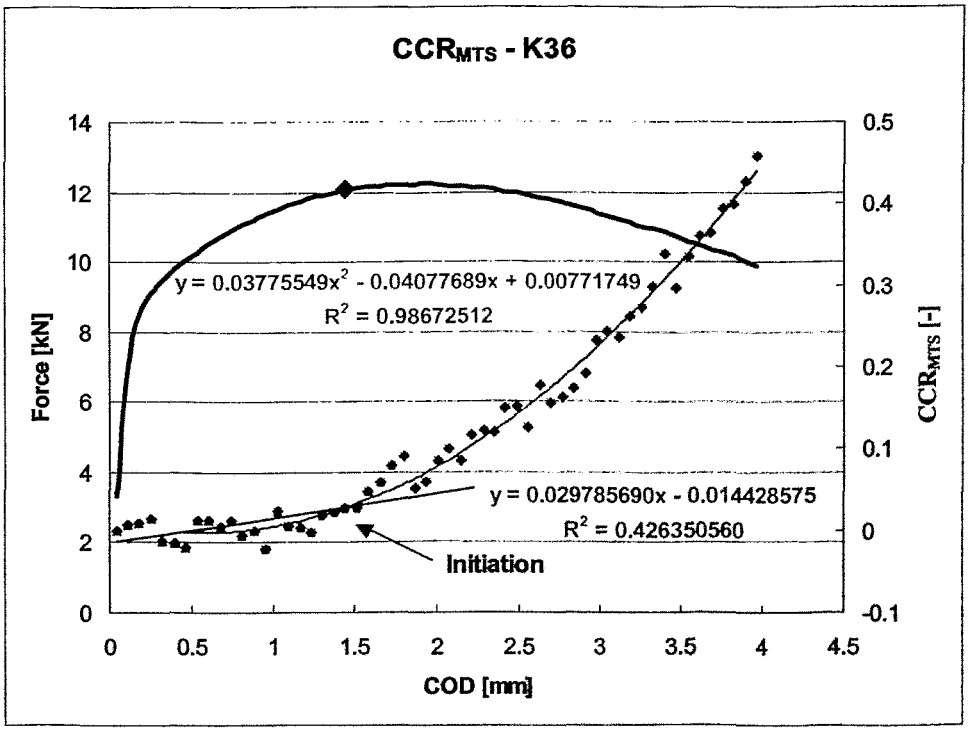

Fig. 12-31 Crack initiation evaluated according to CCR_{MTS}

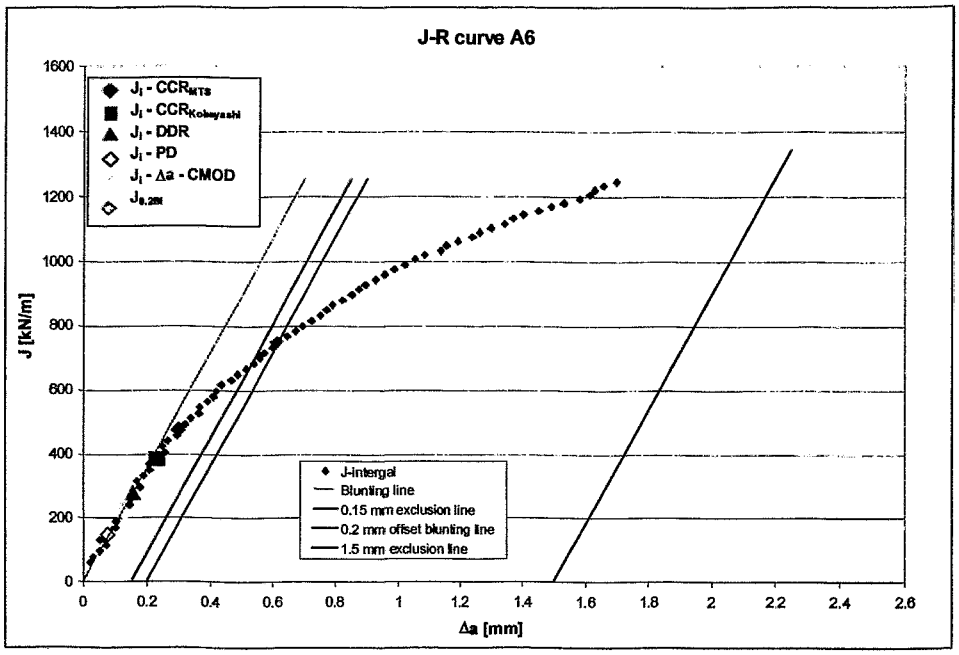

Fig. 12-32 J-R curve of SUS 3160L specimen with depicted J_i values evaluated according to all applied methods

Tab. 12-9 Results of DCPD tests

Specimen	Material	PD Method	B [mm]	B_N [mm]	W [mm]	a [mm]	J_i^{PD} [kN/m]	J_i^{CCR} Kobayashi [kN/m]
A5_3	A533B Cl.II	DCPD	9.99	8.01	9.99	4.67	64.16	55.76
A5_5	A533B Cl.II	DCPD	9.98	8.13	9.99	3.53	57.92	85.02
K7	SFA	DCPD	9.97	8.24	10.00	3.94	60.80	144.82
K8	SFA	DCPD	9.97	8.06	10.00	5.65	54.12	92.64

Tab. 12-10 Results of ICFPD and RICPD tests with original probes

Specimen	Material	PD Method	J_i^{PD} [kN/m]	J_i^{DDR} [kN/m]	J_i^{CCR} Kobayashi [kN/m]	J_i^{CCR} MTS [kN/m]	$J_{0.2BI}$ [kN/m]	$J_i^{\Delta a\text{-}CMOD}$ [kN/m]	Blunting line coefficients ASTM [--]	Blunting line coefficients ESIS [--]	Blunting line slope [MPa]
K35	SFA	RICPD	58.97	226.17	314.51	300.19	512.00	181.83	1.12	0.89	542
K36	SFA	ICFPD	63.42	247.32	310.52	268.44	507.00	205.90	1.37	1.09	664
K37	SFA	ICFPD	63.48	282.67	320.68	---	---	---	---	---	
K38	SFA	ICFPD	54.98	---	317.99	---	---	---	---	---	
L33	SFA	RICPD	286.06	306.06	308.64	394.71	---	---	---	---	
L34	SFA	RICPD	63.99	271.01	286.64	287.06	---	134.04	---	---	
L35	SFA	RICPD	85.90	---	267.04	374.12	465.00	169.51	2.69	2.15	1307
L36	SFA	ICFPD	157.17	---	315.51	---	---	---	---	---	
L37	SFA	Not used	---	200.57	277.89	214.78	458.00	132.77	1.46	1.16	707
L38	SFA	ICFPD	56.48	198.92	280.23	263.11	480.00	147.07	1.44	1.15	701

Tab. 12-11 Results of ICFPD and RICPD tests with re-designed probes

Specimen	Material	PD method	J_i^{PD} [kN/m]	J_i^{DDR} [kN/m]	J_i^{CCR} Kobayashi [kN/m]	J_i^{CCR} MTS [kN/m]	$J_{0.2BI}$ [kN/m]	$J_i^{\Delta a\text{-}CMOD}$ [kN/m]	Blunting line coefficients ASTM [--]	Blunting line coefficients ESIS [--]	Blunting line slope [MPa]
A5_1	A533B Cl.II	RICPD	186.33	255.80	294.21	234.26	417.00	179.00	1.63	1.38	842
A5_2	A533B Cl.II	ICFPD	129.31	---	315.76	226.86	497.00	157.13	1.57	1.33	810
A5_3	A533B Cl.II	RICPD	192.96	268.77	307.59	181.74	406.00	164.92	1.48	1.25	760
A5_4	A533B Cl.II	ICFPD	198.68	255.08	251.89	213.75	422.00	225.25	1.45	1.23	746
A5_5	A533B Cl.II	ICFPD	114.63	---	285.31	283.62	470.00	126.25	1.51	1.28	779
A5_6	A533B Cl.II	RICPD	100.51	---	304.56	290.85	515.00	165.26	1.48	1.25	761
A1	SUS 316L	RICPD	313.79	336.95	226.82	451.60	860.00	191.60	4.83	3.49	1789
A2	SUS 316L	ICFPD	255.01	341.67	---	499.97	947.00	192.08	5.30	3.84	1965
A3	SUS 316L	RICPD	160.96	326.88	---	501.67	943.00	194.73	5.34	3.87	1980
A4	SUS 316L	ICFPD	148.96	364.89	---	458.46	920.00	252.50	5.18	3.75	1921
A5	SUS 316L	ICFPD	111.22	---	---	468.24	917.00	287.17	5.03	3.64	1863
A6	SUS 316L	RICPD	144.44	393.26	277.41	468.88	765.00	220.08	4.83	3.49	1789

12.3 Results discussion

Wide range of the points of interests was investigated in this study and so the discussion of the results firstly deals with each topic separately. Subsequently, the methods are compared together and their performance is discussed.

12.3.1 Blunting line derived crack initiation

ASTM and ESIS procedures recommend some 'generally' valid constants for the blunting line slope using slightly different expression for description of the blunting line. The J-integral corresponding with engineering crack initiation was evaluated according to ASTM and ESIS recommendations. The results could be seen in Fig. 12-16 and 12-17. It is evident, if an inappropriate blunting line coefficients are used, misleading values could be obtained representing unrealistic high or low fracture toughness values. The difference between the recommended blunting line coefficients the real ones is clearly visible in the figures. When commonly used multi specimen testing method is applied the data within blunting region are not available and thus error of about 25 % in the critical J-integral value can be easily attained if recommended blunting line slope is used without further verification.

The blunting line slopes evaluated for 10CrMo9-10, SFA, SUS 316L and A533B Cl. 2 steels are summarized in Tab. 12-6, 12-10 and 12-11. The values are ranging from 1,12 to 6,26 for ASTM blunting line coefficients and 0,89 to 3,87 for ESIS blunting line. The ASTM blunting line coefficients for 10CrMo9-10 steel are ranging from 1,88 to 6,26 in dependence on the material heat treatment. The coefficients for SFA and A533B Cl. 2 steel are well below recommended 2 according to ASTM, resp. 3,75 according to ESIS procedure. ESIS blunting line slope is in very good agreement with measured value for the austenitic steel SUS316L. So determination of the blunting line slope for each tested material seems to be essential.

ESIS procedure also proposes to determine engineering J-integral initiation value with use of perpendicular line at the crack extension 0,2mm. When the critical J-integral obtained according to this method is compared with J-integrals determined on the basis of parallel lines to initial blunting line the difference can reach 60 %. Although these values have to be clearly designed, they should represent the same event – limit of the structure service life and thus their confusion might lead to catastrophic results. There is visible that for both ASTM and ESIS blunting line based procedures the values beyond maximum force were obtained, Fig. 12-18, while ESIS 0,2 perpendicular line derived J integral values yields forces near to F_{max} for Charpy size specimens. In reality the material properties assessed on the basis of such an evaluation would underestimate the real structure state and thus not assure safe further operation.

According to the present results it seems there is not generally valid blunting line coefficient and for the evaluation of considered material behaviour the blunting line slope has to be directly determined. Attained results also stress the need for clearly defined critical value for J-integral for safety assessment, discussed procedures do not assure unambiguous results.

12.3.2 Multiple gauge methods

Three multiple gauge testing methods were applied in this study: Double Clip Gauge (DCG), Double Displacement Ratio (DDR) and Strain Gauge Near to Crack Tip (SGNCT).

DCG and DDR are very similar so they are going to be discussed together. The results obtained with these methods can be seen in Figs. 12-2 to 12-5, 12-14, 12-15 and 12-29. There it could be observed the regions described by the authors of this method, initial elastic deformation, the range of crack tip blunting and, finally, subsequent crack growth. This effect is more pronounced on the specimen with the laser scanner located at the crack tip, which could be probably due to bigger distance between measured points and so higher proportional sensitivity to small changes, but large data scatter was obtained for both methods. For none of specimens clearly flat horizontal plateau, as reported by Kagawa [**24**], was attained. There was always some slope upwards, but the change between the slopes of the plastic deformation and crack growth was usually detectable. There were also some specimens where no clear 'break point' can be defined. This effect can be observed for all used materials so it cannot be directly attributed to the material, but rather to the evaluation. When the data with high scatter are processed smoothing has to be applied and the resulting 'initiation' point can be strongly influenced by the smoothing procedure, so the 'break point' might be in some case suppressed during the smoothing.

When the Strain Gauge Near to Crack Tip method was applied Fig. 12-3 and 12-5, there was not observed sudden strain growth as it was reported in [**33**], especially for the specimen D2. However the curves had similar trend pointing out that some process, probably the crack initiation occurred at time of approx. 150 s, Fig. 12-3. In case of D2, Fig. 12-5, there is clearly the same trend of all curves, except of the one measured between the strips closest to the crack plane but on opposite sides of the crack plane. There is clear change of slope in the point where the crack initiation probably takes place. Final comparison of the crack initiation points determined by different method is shown in Fig. 12-6. For specimens D1 and D2, stretch zone width was not measured, so there is not available direct comparison between physical initiation point and determined initiation points.

DCG and SGNCT methods provided very good results with the dummy specimens D1 and D2. On contrary, rather poor records were obtained in case of the specimens made of 10CrMo9-10 steel, heats E, F and G. The reason why the method seeming promising when specimens D1 and D2 were tested, totally failed in further tests on specimens made of material of heats E, F and G could be in different plastic properties of the materials. Specimens D1 and D2 exhibited stable crack growth with small amount of deflection prior to the crack initiation, while the specimens E, F and G are made of very tough material, where prior to the crack initiation large plastic deformation is necessary. This is probably cause of the problems with the application of this methods with the laser scanner as second gauge. This is confirmed by the study of Böhmert at. al. [98]. The study observed the laser scanner measurement performance as a crack mouth opening gauge for the three point bend specimens. It was found that due to the specimen movement in relation to the laser scanner, large systematic error is attained. The error is bigger with bigger deflection.

Results of the crack initiation toughness J_i evaluation determined for 10CrMo9-10 steel on the basis of multiple gauges measurement in comparison with SZW measurement are summarised in Tab. 12-3. There is visible not very good agreement between J_i^{DCG} and J_i^{SZW}. Reasonable agreement was only found for the specimens made of heat F. This rather poor result can be probably linked to the inaccuracies of Laser scanner measurement and thus if directly attached clip gauge would be used, better results might be attained.

On contrary with previous, rather complicated set up, DDR method uses only commonly measured values. This method provided results very consistent results for A533B specimens, but for the other materials large scatter was observed. DDR method did not prove sensitivity to distinguish between the materials with similar fracture behaviour, materials SFA- K and L. Because of the big scatter the data seem to belong to the same population. 17% results scatter was attained for SUS 316L steel, Tab. 12-10 and 12-11. For these materials no SZW values were available and thus direct comparison is not made.

12.3.3 Potential drop based methods

The records obtained with Potential drop methods were used for J_i evaluation. DCPD method provided relatively clear information on the initiation point for both tested materials, Fig. 12-20. The results are homogeneous with a small scatter, for considered specimens, Tab. 12-9. Calculated J_i values are for both materials almost the same app. 60 kN/m. The same crack initiation value hints on the similar fracture behaviour of these materials which is partly confirmed by evaluated $J_{0,2Bl}$, Tab. 12-10 and 12-11. From this point of view it can be concluded that the method is acceptable sensitive, but the value of 60 kN/m is very low for considered materials. Measurement of SZW was not performed for these specimens and thus no direct confrontation with 'real' initiation values can be made

ICFPD and RICPD methods were used with two modifications of the probes: original and re-designed ones. Also the results can be divided into these two groups. Original probes provided records with the shape similar to DCPD method with distiguishable transition between initial linear and polynomical part, Figs. 12-23 to 12-26. Evaluation of these tests provided generally the results in agreement with DCPD results, Tab. 12-10.

The records obtained with the re-designed probes were not as clear as the previous ones. In case of these records, Figs. 12-27 and 12-28, it was rather complicated to distinguish the point where the initiation might take place that resulted in relatively big results scatter, Tab. 12-11. There are not available specimens for direct comparison between original and re-designed probes, because different materials were tested. From the results obtained with DCPD method and original probes it can be inferred that the J_i values yielded on the basis of re-designed probes are about three times higher. Missing some reference value of J_i no clear statement can be made which value is 'correct'. What is clear for these new probes is that the obtained records are not as clear as in case of original ones and more peaks can be observed. It points out that there are probably some other effects included in measured signal that have no relation to the crack initiation/propagation. The most probable cause of these disturbances is the `bridging wire'.

Present experiences with PD testing and evaluation for the crack initiation determination pointed out two tender spots. The first one is high sensitivity of the

measured signal to the current terminals positioning. Uncorrectly placed terminals could overshadow the change of the specimen electrical properties due to the crack growth. The secont one is that PD records with only slight change of the voltage with the crack extension open the space for subjective interpretation of the traces and thus subjective crack initiation values can be obtained.

12.3.4 Compliance changing rate

Compliance Changing Rate is relatively simple method for J_i evaluation. Two modifications of this method CCR_{MTS}, Figs.12-11 and 12-31, and $CCR_{Kobayashi}$, Fig. 12-30, were applied to most of the specimens, except of those where CMOD was not measured and thus actual specimen compliance was not evaluated. The results of these methods can be seen in Tabs. 12-3, 12-9 to 12-11.

The results of both CCR method modifications are similar. CCR_{MTS} exhibits a little bit bigger scatter in comparison with $CCR_{Kobayashi}$. The results do not have a clear trend which method provides bigger or lower value. It is different for different materials. Both methods demonstrated good sensitivity to detect small material behaviour changes. This can be well seen on the example of SFA material. This material was available in two modifications with just slightly different fracture behaviour, Tab. 12-10, which was detected by these methods. Good repeatability of this method was observed also for A533B steel. The only visible large discrepancy between resulting values can be seen in case of specimens made of SUS 316L austenitic steel. $CCR_{Kobayashi}$ method encountered in this case higher scatter in comparison with previous results obtained with this method. For SUS 316L it was very difficult to find the knee point because of almost linear trend, so for most of the specimens the J_i was not evaluated. On contrary to $CCR_{Kobayashi}$, CCR_{MTS} provided good results even for this material.

On the basis of previous results obtained with other materials it can be inferred that Kobayashi's method is not applicable to all kinds of materials. On contrary, the method using actually measured specimen compliance provided traces with clearly detectable break points yielding homogeneous results for all investigated materials. Present experiences with Kobayashis's method are in contradiction with the experiences of Tosal [51] and Zhang [5] who reported large scatter associated with this method application.

12.3.5 Other Methods

Further evaluation procedures were applied to 10CrMo9-10 - E, F and G specimens. Different relations CMOD-CTOD-DISPLACEMENT-FORCE and their derivations, according to references in literature, were observed. Examples of these relations could be seen in Fig. 12-7, 12-8, 12-12 and 12-13. Generally it can be stated the curves are smooth without any visible inflection point hinting Displacement, Fig. 12-12, which exhibit two breakpoints, but both are early in comparison with stretch zone width measurement. Relatively good results were attained when the relations crack extension versus CMOD were used for the initiation point determination, Fig. 12-10. Initiation values obtained with this method were in very good agreement with results of SZW evaluation, Tab. 12-3. Also the sensitivity to detect even small material behaviour changes was proved on SFA material, Tab. 12-10. The method provided higher scatter for the austenitic steel, Tab. 12-11.

12.3.6 J-Integral Calculation

The assessment of J-integral calculation methods was carried out in order to evaluate the relation of the values obtained according to different presently used procedures. ASTM basic and J-R curve method and ESIS procedure were investigated. For ASTM method also the influence of the plastic energy calculation on the results was evaluated. Plastic energy on the basis of original slope and actual compliance slope was calculated. For the results see Fig. 11-2.

The plastic energy calculation influence on the resulting J-R curve was almost negligible. The curves were almost identical therefore the J-Integrals calculated with use of both plastic energies can be easily comparable.

The effect of the crack extension correction when a single specimen evaluation procedure was used pointed out only small difference in the J-integral values. When crack extension correction is not applied, a little bit higher values can be obtained at higher crack extension values. Within the region of interest for the safety assessment with use of J-R curves, both formulas provide almost identical results. In comparison with single specimen method, the multiple specimen method yields a little higher values. In this case it can be also stated that in the initial part of the J-R curve are values the same.

ESIS procedure results compared with previously obtained results show slightly higher values at small crack extensions and at bigger Δa, ESIS curve follows ASTM curve for multiple specimen method. With the ESIS method can be thus obtained a little bigger values in the initial part of J-R curve where J_i is determined. Anyway the difference in the values might be in order of 2-3% which is within the range of the accuracy of the J-integral calculation in dependence on the accuracy of the specimen dimensions measurement, crack growth measurement and so on. Moreover, the inaccuracy of the crack initiation determination is so high that this error can be neglected.

12.3.7 Comparison of J_i values obtained with all considered methods

Summarization of the crack initiation values measured on Cr-Mo reactor pressure vessel steels, Tab. 12.2, showed various values in dependence on the applied evaluation technique. All the methods are going to be compared with stretch width zone based initiation considered as 'true' physical initiation point. The relationship crack extension vs. CMOD based crack initiation exhibited very good agreement with SZW based values. DCG method provided results with opposite trend in comparison with previous two methods. The highest J_i^{DCG} was attained for the specimen with the lowest J_i^{SZW}. Also the consistency of the results for separate material heats was rather poor having a large scatter of the values. DDR method results and results of dF/dDisplacement evaluation are relatively consistent, but there is disagreement with J_i^{SZW} results and no common data trend can be seen. Compliance Changing Rate method with measured specimen compliance, CCR_{MTS}, had opposite trend to SZW based method and so disagreement was found. $CCR_{Kobayashi}$ provided results following the trend of J_i^{SZW} very well. There was no constant difference between these methods for separate materials. For the materials with lowest crack resistance were results of $CCR_{Kobayashi}$ higher while for the materials with the highest toughness, within tested materials, lower values were obtained. Among all of applied methods the best

agreement with J_i^{SZW} was found for $J_i^{\Delta a - CMOD}$. Moreover Δa – CMOD based evaluation yielded more consistent results than SZW measurements.

When the J_i values obtained according to considered methods are plotted into J-R curve, the initiation values based on the SZW measurement and Δa – CMOD evaluation agreed very well with the region where the curve starts to bend, Figs. 12-16 and 12-17. The other values are oscillating around this region without clear trend.

Crack initiation determination results attained with SFA, A533B and SUS316L steels summarized in Tabs., 12-9 to 12-11 are similar to previous one. For these materials SZW was not measured and thus there were no reference values.

Generally, all of the methods were following the same trend and qualitatively detected the material with higher or lower fracture toughness correctly. When the values itself are considered wide range of values were attained for each specimen. The closest values yielded both CCR methods, which is probably coming from the fact that they have common base. Otherwise values exceeding 100% difference with reference values were attained. With use of DCPD and original ICFPD and RICPD probes similar values were obtained. This is an interesting result, because Charpy specimens were tested with DCPD method while specimens of cross section 12,5 X 25mm were tested with ICFPD and RICPD methods. This might confirm that size independent crack initiation values were evaluated. J_i for these methods were the smallest of all other methods. Re-designed ICFPD and RICPD probes provided ambiguous records and the evaluated J_i values were approximately three times higher in comparison with previous results.

Evaluated initiation J-integrals plotted into J-R curve are summarized in Fig. 12-32. It is visible that PD based initiation values are in the beginning of the blunting line. Δa – CMOD and DDR based integrals are also rather low and the best agreement with expected crack initiation position at the end of blunting line exhibits $CCR_{Kobayashi}$ evaluation for investigated materials. The same behaviour was observed for most of the specimens.

13 Conclusion

An extensive study of methods for ductile crack initiation determination was performed on three point bend specimens made of Cr-Mo 9-10, SFA, A533B Cl.2 and SUS 316L steels. With use of broad literature survey, various method for crack initiation determination ranging from double clip gauge ratio method to critical plastic theory were studied. The most promising methods for which experimental equipment was available were investigated. Multiple gauge methods and potential drop based methods were applied together with various evaluation procedures. Blunting line problems as well as problems of J-integral calculation according to ASTM and ESIS recommendation was also taken into account.

The analysis of J integral calculation formulas demonstrated that all recommended formulas yield very similar values. ESIS formula provides slightly higher values than ASTM procedure in the blunting region of the J-R curve, but the difference is within a few percents and bigger error associated with the crack initiation J-integral determination can be expected from the crack initiation point detection.

The investigation of the blunting line influence on the resulting engineering initiation integrals pointed out that there is probably not any constant blunting line slope, at least for blunting line expressions used in ASTM or ESIS procedures, generally valid for all materials. Thus actual blunting line slope is necessary to determine for considered material in order to avoid of overestimation or underestimation of the material fracture resistance in case when inappropriate coefficients are used.

Applied procedures for the crack initiation determination provided results and performance in the wide range. Strong dependence on tested material was noticed for most of the methods. For example crack extension versus crack mouth opening displacement, Δa – CMOD, related method provided results with very good agreement with stretch zone width based values for the first series of specimens. Later, higher scatter was observed and not persuading results were obtained. Originally preferred multiple gauge based methods also did not provide satisfying results. In this case the high scatters might be caused by the error of laser measurement on three point bend specimen. Compliance changing rate according to Kobayashi's method provided consistent results, but the values were in some cases strongly deviating from reference stretch zone width derived data.

Three modifications of potential drop methods were utilised, DCPD, ICFPD and RICPD These tests provided relatively very consistent results, but very low initiation values were obtained, about 60 kN/m. Agreement for the crack initiation values for specimens of different dimensions was attained. Use of newly designated probes used for some of the tests pointed out issues that have to be considered for further tests, the probes optimal design of wiring.

Generally spoken it was not found one method applicable to all materials providing satisfying results. At present level the method used for crack initiation detection for the material of interest has to be experimentally verified with stretch zone width measurement firstly and then it can be applied to further tests.

Further investigations should be performed in order to establish reliable and accurate technique for the crack initiation determination. More crack initiation data evaluated according to various methods have to be confronted with stretch zone width based values. Multiple gauge method has to be verified with use of clip gauges instead of Laser scanner for considered implementation, three point bend testing of Charpy size specimens.

Acknowledgements

Potential drop based measurements were perfomed thanks to kind support of Prof. Tetsuo Shoji at Fracture Research Institute of Tohoku University, Sendai, Japan.

References

1. ASTM E1921-02 Standard test method for determination of reference temperature, T_o, for ferritic steels in transition range.
2. Schwalbe, K.-H., Neale, B.K., Heerens, J. : The GKSS test procedure for determining the fracture behaviour of materials, Report GKSS 94/E/60, 1994.
3. ASTM E399-90 Standard test method for plane-strain fracture toughness of metallic materials.
4. ASTM E1820-01 Standard test method for measurement of fracture toughness.
5. Zhang, X.P., Shi, Y.W.: Comparative studies of several methods to determine the dynamic fracture toughness of nuclear pressure vessel steel A 508 CL3 with Charpy-size specimen, International Journal of Fracture 81, pp. 195-204, 1996.
6. Roos, E., Eisele, U.: Determination of material characteristic values in elastic-plastic fracture mechanics by means of J-integral crack resistance curves, Journal of Testing and Evaluation, Vol. 16, No. 1, pp. 1-11, 1988.
7. Schwalbe, K.H., Hayes, B., Bastian, K., Cornec, A.: Validation of the Fracture Mechanics Test Method EGF P1-87D (ESIS P1-90/ESIS P1-92) – Analysis of an Experimental Round Robin, Fatigue Fracture Engineering Materials and Structures, Vol. 16, No. 11, pp. 1231-1284, 1993.
8. Heerens, J., Cornec, A., Schwalbe, K.H.: Results of a round robin on stretch zone width determination, Fatigue and Fracture of Engineering Materials and Structures, Vol. 11, No. 1, pp. 19-29, 1988.
9. Rintamaa, R.: Single specimen fracture toughness determination procedure using instrumented impact test, Evaluating material properties by dynamic testing, ESIS 20, Mechanical Engineering Publications, London, UK, pp. 97- 123, 1996.
10. Krasowsky, A.J.: Stretch zone stereoscopic measurements as an independent control of material fracture toughness, Proceedings of the 7th European Conference on Fracture, Budapest, Hungary, pp. 758-760, 1988.
11. Pluvinage, G.: Dynamic fracture toughness at crack initiation, propagation and arrest for two pipe-line steels, Eng. Fracture Mechanics, Vol. 43, No. 6, pp. 1063-1084, 1992.
12. Zhang, X.P., Shi, Y.W.: Constraint of side-groove and its influence on fracture toughness parameter in Charpy-size specimen, Engineering Fracture Mechanics, Vol. 43, No. 5, pp. 863-867, 1992.
13. Kobayashi, H., Nakamura, H., Nakazawa, H.: Evaluation of blunting line and elastic-plastic fracture toughness, Elastic-plastic fracture: 2nd Symposium-Fracture Resistance Curves and Engineering Applications Test Methods: Users Experience, ASTM STP 803, C.F. Shih, J.P. Gudas, Eds., ASTM, pp. II420-II438, 1983.
14. Kobayashi, H., Nakamura, H., Nakazawa, H.: Comparison of J_{IC} test methods resommended by ASTM and JSME, Elastic-Plastic Fracture Test Methods: Users Experience, ASTM STP 856, E.T. Wesse, F.J. Loss, Eds., ASTM, pp. 3-22, 1985.
15. ISO/TC/164/SC4-N140(Rev): Metallic materials-unified method of test for the determination of quasistatic fracture toughness.

16. Chen, B.Y., Shi, Y.W.: A comparison of various dynamic elastoplastic fracture toughness evaluating procedure by instrumented impact test, Engineering Fracture Mechanics, Vol. 36, No. 1, pp. 17-26, 1990.

17. Davies, P.H.: An Elastic-Plastic Fracture Mechanics Study of Crack Initiation in 316 Stainless Steel, Elastic-Plastic Fracture: Second Symposium, Volume II--Fracture Resistance Curves and Engineering Applications, ASTM STP 803, C. F. Shih and J.P. Gudas, Eds., American Society for Testing and Materials, pp. II-611-11-631, 1983.

18. Gibson, G.P., Druce, S.G.: Some observations on J-R curves, Elastic-Plastic Fracture Test Methods: Users Experience, ASTM STP 856, E.T. Wesse., F.J. Loss Eds., ASTM, pp. 166-182, 1985.

19. Ingham, T.: The interpretation and the analysis of upper shelf toughness data, Elastic-Plastic Fracture Test Methods: Users Experience, ASTM STP 856, E.T. Wesse and F.J. Loss, Eds., ASTM, pp. 47-67, 1985.

20. Landes, J.D.: The blunting line in elastic-plastic fracture, Fatigue Fract. Engng. Mater. Struct., Vol. 18., No. 11, pp. 1289-1297, 1995.

21. De Vries, M.I., Schaap, B.: Experimental observations of ductile crack growth in type 304 stainless steel, Elastic-Plastic Fracture Test Methods: Users Experience, ASTM STP 856, E.T. Wesse., F.J. Loss, Eds., ASTM, pp. 183-195, 1985.

22. Yagawa, G., Yoshimura, S.: Dynamic fracture mechanics with electromagnetic force and its application to fracture toughness testing, Engineering Fracture Mechanics, Vol. 23, No. 1, pp. 265-285, 1986.

23. Schwalbe, K.H., Heerens, J., Knaack, J.: Suggestions for a modification of ASTM E 813, Elastic-plastic Fracture Test Methods: Users Experience, ASTM STP 856, E.T. Wesse, F.J. Loss Eds., ASTM, pp. 411-416, 1985.

24. Kagawa, H., Fujita, T., Akiyania, T., and Urabe, N: Determination of J_i Values by the Double Clip-on Gage Compliance Method, Elastic-Plastic Fracture Test Methods: The User's Experience, ASTM STP 856, E.T. Wesse. and F.J. Loss, Eds., American Society for Testing and Materials, pp. 294-307, 1985.

25. Joyce, J.A., Hackett, E.M.: An advanced procedure for J-R curve testing using a drop tower, Nonlinear Fracture Mechanics: Volume I: Time Dependent Fracture, ASTM STP 995, A. Saxena, J.L. Bassani, Eds., ASTM, pp. 298-317, 1989.

26. El-Soudani, S. M., Knott, J.F.: Quantitative Fractographic Definition and Detection of Fracture Initiation in COD/K_{Ic} Test Specimens, Elastic-Plastic Fracture: Second Symposium, Volume 11-Fracture Resistance Curves and Engineering Applications, ASTM STP 803, C. F. Shih and J. P. Gudas, Eds., American Society for Testing and Materials, pp. II-483-II-507, 1983.

27. Anderson, T.L., McHenry, H.I., Dawes, M.G.: Elastic-plastic fracture toughness tests with single-egde notched bend specimens, Elastic-Plastic Fracture Test Methods: Users Experience, ASTM STP 856, E.T. Wesse., F.J. Loss, Eds., ASTM, pp. 210-229, 1985.

28. Rintamaa, R., Zimmermann, C.: Advanced instrumented impact testing facility for characterization of dynamic fracture behaviour, Nuclear Engineering and Design 96, pp. 159-166, 1986.

29. Guduru, R., Singh, R. P., Ravichandran, G., Rosakis, A. J.: Dynamic crack initiation in ductile steels, J.Mech. Phys Solids, Vol. 46, No.10, pp.1997-2016, 1998.

30. Zimmermann, C.: On the determination of fracture mechanics data using the near-field at the crack tip of dynamically loaded cracks, Nuclear Engineering and Design 76, pp. 359-363, 1983.

31. Lin Yunhsan, YAN Wenbin, Tu Mingjing: Crack initiation point determination and dynamic fracture toughness for Charpy pre-cracked specimen, Acta Metallurgica Sinica, Series A. Vol. 5, No. 5, pp. 379-384, 1992.

32. Kussmaul, K., Klenk, A., Link, T., Schüle, M.: Dynamic material properties and their application to components, Nuclear Engineering and Design 174, pp. 219-235, 1997.

33. Bernard, J., Verzeletti, G.: Elastic-plastic fracture toughness characteristics of irradiated 316H stainless steel, Elastic-Plastic Fracture Test Methods: Users Experience, ASTM STP 856, E.T. Wesse and F.J. Loss, Eds., ASTM, pp. 131-149, 1985.

34. Yagawa, G., Yoshimura, S.: On the dynamic fracture toughness and crack tip strain behaviour of nuclear pressure vessel steel: application of electromagnetic force, Nuclear Engineering and Design 97, pp. 195-209, 1986.

35. Grabulov, V., MacGillivray, H.J., Tomic, D., Jovanovic, P.: Evaluation of static and dynamic R-curve using DC potential drop single specimen method, Proceedings of the 9th European Conference on Fracture, Varna, Bulgaria, pp. 315-320, 1992.

36. MacGillivray, H.J., Turner, C.E.: A comparison of dynamic R-curve methods, International Phys. Conf. Ser. No. 102, session 1, paper presented at International Conference of Mechanical Properties of Materials at High Rates of Strain, Oxford, UK, 1989.

37. Miya, K., Yanagi, H., Someya, K.: A new technique for detection of dynamic crack initiation, Nuclear Engineering and Design 94, pp. 281-289, 1986.

38. Nguyen-Duy, P., Phelippeau, G.: Determination of the fracture-energy criterion J_{IC} of two steels by static and dynamic testing, Journal of Testing and Evaluation, Vol. 7, No. 6, pp. 310-316, 1979.

39. Bakker, A., A DC potential drop procedure for crack initiation and R-curve measurement during ductile fracture tests, Elastic-Plastic Fracture Test Methods: Users Experience, ASTM STP 856, E.T. Wesse., F.J. Loss, Eds., ASTM, pp. 394-410, 1985.

40. Thaulow, C., Hauge, M., Gunleiksrud, A., Paauw, A.J.: Single specimen test measurement of J_i and J-da with pulsed D-C potential-drop technique, Fracture Mechanics: 18^{th} symposium, ASTM STP 945, D. T. Read, R.P. Reed, Eds., ASTM, Philadelphia, pp. 333-346, 1988.

41. Hollstein, T., Blauel, J.G., Voss, B.: On the determination of plastic fracture material parameters: A comparison of different test methods, Elastic-Plastic Fracture Test Methods: Users Experience, ASTM STP 856, E.T. Wesse., F.J. Loss, Eds., ASTM, pp. 104-116, 1984.

42. Huang, F.H.: Fracture Toughness evaluation for Zircaloy-2 pressure tubes with the Electric-potential method, Small Specimen Test Techniques Applied to Nuclear Reactor Vessel Thermal Annealing and Plant Life Extension. ASTM STP 1204, Philadelphia, USA, pp. 182-198, 1993.

43. Schwalbe, K.H., Hellmann, D., Heerens, J., Knaack, J., Müller-Roos, J.: Measurement of stable crack growth including detection of initiation of growth using the DC potential drop and the partial unloading methods, Elastic-Plastic Fracture Test Methods: Users Experience, ASTM STP 856, E.T. Wesse., F.J. Loss, Eds., ASTM, pp. 338-362, 1985.

44. De Roo, P., Marandet, B.: Application of A.C. potential drop method to the detection of initiation in static and dynamic testing, CSNI Workshop "Ductile Fracture Test Methods", Paris, France, pp.75-83, 1982.

45. Wallin, K., Saario, T., Auerkari, P., Saarelma, H., Torrönen, K.: Comparison of potential drop and unloading compliance methods in determining ductile crack extension, Elastic-Plastic Fracture Test Methods: Users Experience, ASTM STP 856, E.T. Wesse., F.J. Loss, Eds., ASTM, pp. 363-374, 1985.

46. Satoh, M., Funada, T., Urabe, Y., Hojo, K.: Measurement of rapid loading fracture toughness J_{Id}, Factors that affect the precision of mechanical tests, ASTM STP 1025, R. Papirno, H.C. Weiss, Eds., American Society for Testing and Materials, pp. 63-76, 1989.

47. Reiff, K., Ernst, P.: CTOD measured by means of a modified Charpy-V specimen, Fatigue Fract. Engng. Mater. Struct. Vol. 20, No 1., pp. 29 –39, 1997.

48. Shoji, T., Kim, H., Maeda, T., Sato, Y., Watanabe, Y.: A novel nondestructive inspection and monitoring technique for plant life management – Induced Current Focussing Potential Drop Technique., Proceedings of International Symposium on Plant Ageing and Life Predictions of Corrodible Structures, Sapporo, Japan, pp. 371-376, 1995.

49. Sato, Y., Shoji, T.: High Sensitivity Inspection of Defects in Welds by Remotely Induced Current Potential Drop Technique, Nondestructive Characterization of Materials IX, R.E. Green Jr., Ed., American Institute of Physics, pp. 107-112, 1999.

50. Kobayashi, T., Yamamoto, I., Niinomi, M.: Evaluation of dynamic fracture toughness parameters by instrumented Charpy impact test, Engineering Fracture Mechanics, Vol. 24, No. 5., pp. 773-782, 1986.

51. Tosal, L., Rodriguez, C., Belzunce, F.J., Betegon, C.: Comparison of the static and dynamic fracture behaviour of an AE-460 structural steel, Engineering Fracture Mechanics 66, pp. 537-549, 2000.

52. Shanmugam, P., Jana, B., Pathak, S.D.: Dynamic fracture toughness of banded HSLA steel, Journal of Testing and Evaluation, Vol. 23, No. 1, pp. 11-18, 1995.

53. Tseng, M.K., Marcus, H.L.: A single specimen determination of J_{IC} for aluminium alloys, Engineering Fracture Mechanics, Vol. 16, No. 6., pp. 895-903, 1982.

54. Kobayashi, T., Niinomi, M., Yamamoto, I., Kamimura, M.: Evaluation of dynamic elastic-plastic fracture toughness parameters by instrumented test,Impact loading and dynamic behaviour of materials, Ed. Chiem, C.Y., Kunze, H.D., Meyer, L.W., DGM, Vol. 1, pp. 197-204, 1988.

55. Crostac, H.A., Engelhardt, A.H.: Acoustic emission measurement during instrumented impact tests, "Quantitative NDE in the Nuclear Industry", Proc. of the 5th Int. Conference, San Diego, California, pp. 335-338, 1982.

56. Richter, H.: Ermittlung zähbruchmechanischer Kennwerte unter schlagartiger Belastung mittels Schallemission, Report FZR-299, ISSN 1437-322X, Forschungszentrum Rossendorf, 2000.

57. Petrisic, J., Grabec, I.: Acoustic emission generated by the crack propagation, Proceedings of the 7th European Conference on Fracture, Budapest, Hungary, pp. 758-760, 1988.

58. Richter, H., Viehrig, H.W., Boehmert, J.: The use of acoustic emission to determine characteristic dynamic strength and toughness properties of steel, Nuclear Engineering and Design 188, pp.241 – 254, 1999.

59. Viehrig, H.W., Boehmert, J., Richter, H., Valo, M.: Use of instrumented Charpy tests for determination of crack initiation toughness, Pendulum Impact testing: A Century of Progress, ASTM STP 1380, ASTM, West Conshohocken, PA, pp. 354-365, 1999.

60. Viehrig, H.W., Popp, K.: Measurement of dynamic elastic-plastic fracture toughness parameters using various methods, Int. J. of Pressure Vessels and Piping 55, pp. 233-241, 1993.

61. Williams, R. V.: Acoustic Emission, Adam Hilger Ltd., ISBN 0-85274-359-9, 1980.

62. Steffens, H.D., Crostack, H.A., Engelhardt, A.H.: The application of acoustic emission to the determination of material behaviour under dynamic loading, Acoustic Emission, DGM, ISBN 3-88355-030-2, 1980.

63. Yasunaka, T., Iwao, N., Furuya, N., Kimura, K., Yamawaki, H.: Measurement of J_{IC} and its evaluation for high strength steels using both ultrasonic though transition and angle beam methods, Transactions of National Research Institute for Metals, Vol. 28, No. 3, pp. 241-247, 1986.

64. Loibnegger, F., Salzmann, F., Varga, T: Detection of crack initiation in fatigue precracked Charpy-type specimens, Nuclear Engineering and Design 96, p. 139-148, 1986.

65. Kalkhof, D., Görner, W.: Measurement of crack growth by means of continuous sound during instrumental Charpy-test, Proceedings of the 7th European Conference on Fracture, Budapest, Hungary, pp. 755-757, 1988.

66. Hirano, K., Kobayashi, H., Nakazawa, H.: A single specimen determination of elastic-plastic fracture resistance by Ultrasonic Method, Fracture mechanics: 17th Volume, ASTM STP 905, J.H. Underwood, R. Chait, C.W. Smith, D.P. Wilhelm, W.A. Andrews, J.C. Newman Eds., ASTM, pp. 415-434, 1986.

67. Yasunaka, T., Iwao, N., Furuya, N., Kimura, K., Hoshimoto, K.I., Muto, I., Fukuhara, S., Yoshida, H.: Ultrasonic detection of onset of crack extension in fracture toughness specimen of a HT60 steel, Transactions of National Research Institute for Metals, Vol. 25, No. 4, pp. 227-234, 1983.

68. Bergmann, U.: Ultraschallverfahren zur Rissfortschrittsmessung bei der Ermittlung vor Risswiderstandskurven, Forschungszentrum Rossendorf, Wissenschaftlich-Technische Berichte, FZR-330, ISSN 1437-322X, Sept. 2001.

69. Marsch, K.J., Smith, R.A., Rithcie, R.O.: Fatigue crack measurement: Techniques and applications, ISBN 0 947817 46 8, EMAS, 1991.

70. Winkler, S.R.: Magnetic emission detection of crack initiation, Fracture Mechanics: 21st Symposium, ASTM STP 1074, J.P. Gudas, J.A. Joyce, E.M. Hackett, Eds., ASTM, pp. 178-192, 1990.

71. Ortmann, R., Blumenauer, H., Eichler, B.: Ergebnisse der Anwendung des instrumentierten Kerbschlagbiegeversuchs zur Bestimmung der bruchmechanischen Kenngrössen K_{Id} und J_{di}, Tagung Werkstoffprüfung 1991, Bad Nauheim, pp. 65-72, 1991.

72. Winkler, S.: Magnetische Emission: Ein neues Brucherkennungsverfahren, Report T3/88, Fraunhofer Institut, Freiburg, 1988.

73. Michael, A., Pusch, G., Winkler, S., Schuler, J.: Prüfmethodische Aspekte zur dynamischen Beanspruchung von GGG-40-Werkstoffen, Report 1/93, Bergakademie Freiberg, 1993.

74. Lenkey, G. B.: On the determination of dynamic fracture toughness properties by instrumented impact testing, Pendulum Impact Testing: a Century Progress, ASTM STP 1380, ISBN 0-8031-2864-9, Baltimore, pp. 366-381, 2000.

75. Lenkey, G. B.: On the Applicability of Magnetic Emission Measurement Technique for Dynamic Fracture Toughness Determination of Large Specimens, ECF 14: Fracture Mechanics Beyond 2000, A. Neimitz, I.V. Rokach, D. Kocanda, K. Golos, Eds., pp. 357-364, 2000.

76. Joyce, J.A., Hackett, E.M.: Dynamic J-R curve testing of a high strength steel using the Key-curve and multispecimen techniques, Fracture Mechanics: 17th Volume, ASTM STP 905, J.H. Underwood, R. Chait, C.W. Smith, D.P. Wilhelm, W.A Andrews, J.C Newman, Eds., ASTM, pp. 741-774, 1986.

77. Ernst, H.A., Paris, P.C., Rossow, M., Hutchinson, J.W.: Analysis of load-displacement relationship to determine J-R curve and tearing instability material properties, Fracture Mechanics, ASTM STP 677, C.W. Smith, Ed., ASTM, pp. 581-599, 1979.

78. Jones, R.L., Davies, P.C.: Experimental characterization of dynamic tensile and fracture toughness properties, Fatigue and Fracture of Engineering Materials and Structures, Vol. 12, No. 5, pp. 423-437, 1989.

79. Joyce, J.A.: Static and dynamic J-R curve testing of A533B steel using the Key-curve analysis technique, Fracture Mechanics: 14th symposium, Volume I: Theory and Analysis, ASTM STP 791, J.C.Lewis and G. Sines, Eds., ASTM, pp. I-543-I560, 1983.

80. Andrews, W. R.: Determination crack extension using a displacement based Key-curve method, Elastic-Plastic Fracture Test Methods: Users Experience, ASTM STP 856, E.T. Wesse., F.J. Loss, Eds., ASTM, pp. 308-321, 1985.

81. Wallin, K.: A simplified key-kurve approach for J-R-curve testing of CT-specimens, VTT Research Report 503, Espoo, Finland, 1987.

82. Ernst, H.A., Paris, P.C., Landes, J.D.: Estimations on J-integral and tearing modulus T from a single specimen test record, Fracture Mechanics: 13th Conference, ASTM STP 743, Richard Roberts ed., ASTM, pp. 476-502, 1981.

83. Bacon, C., Färm, J., Lataillade, J.L.: Dynamic fracture toughness determined from load point displacement, Experimental Mechanics, pp. 217-223, 1994.

84. Kapp, J.A., Underwood, J.H.: Single specimen J-based fracture toughness test for high-strength steels, Fracture Mechanics: 14th Symposium-Volume II: Testing and Applications, ASTM STP 791, J.C. Lewis., G. Sines, Eds., ASTM, pp. 402-414, 1983.

85. Yin, X.C.: A simple iterative Key-curve method for determining J-R curves, International Journal of Pressure Vessel and Piping 53, pp. 143-157, 1993.

86. Etemad, M.R., Turner, C.E: Further evidence on the normalization of J-R curves, Proceedings of the 7th European Conference on Fracture, Budapest, Hungary, p. 684-686, 1988.

87. Fortes, C.J.F.O., Bastian, F.L.: A normalization method for developing J-R and CTOD-R curves with the LMN functions, Journal of Testing and Evaluation, Vol. 25, No. 3, pp. 302-307, 1997.

88. Herrera, R., Carcagno, G., deVedia, L.: Evaluation of dynamic fracture toughness using the normalization method, Fracture Mechanics: 23th Symposium, ASTM STP 1189, Ravinder Chona, Ed., ASTM, pp. 168-184, 1993.

89. Hu, J.M., Albrecht, P., Joyce, J.A.: Load ratio method for estimating crack extension, Fracture Mechanics: 22nd Symposium, ASTM STP 1131, A. Ernst, A. Saxena, D.L. Mcdowell, Eds., ASTM, pp. 880-903, 1992.

90. Reese, E.D., Schwalbe, K.H.: The linear normalization technique - an alternative procedure for determining J-R curves from a single specimen test record based on Landes' normalization method, Fatigue and Fracture of Engineering Materials and Structures Vol. 16, No. 3, pp. 271-280, 1993.

91. Byun, T.S., Lee, B.S., Yoon, J.H., Hong J.H.: An iteration method for directly determining J-resistance curves of nuclear structural steels, Journal of Material Science 34, pp. 2039-2047, 1999.

92. Karisallen, K.J., Morisson, J.: A simple load-drop method for estimating crack extension during fracture toughness tests, Engineering Fracture Mechanics Vol. 47, No. 4., pp. 583-5892, 1994.

93. Kobayashi, T., Niinomi, M.: Evaluation of dynamic crack initiation and growth toughness by computer aided Charpy impact testing system, Nuclear Engineering and Design 111, pp. 27-33, 1989.

94. Lai, Z.H., Chen, L.J., Chang, C.M., Chao, C.S.M., Chao, C.S.: A new method of determining J_{IC} of steel by means of single specimen, Engineering Fracture Mechanics Vol. 17, No. 5., pp. 395-403, 1983.

95. Martinelli, A., Venzi, S.: Tearing modulus, J-integral, CTOA and crack profile shape obtained from the load-displacement curve only, Engineering Fracture Mechanics Vol. 53, No. 2., pp. 263-277, 1996.

96. Anderson, T.L.: Fracture Mechanics – Fundamentals and Applications, ISBN 0-8493-4277-5, 1991.

97. Wallin, K., Laukkanen, A.: Comparison of ASTM and ESIS Crack Growth Corrections for J-R Curve Testing – possibility for a Unified Procedure?, ECF 14: Fracture Mechanics Beyond 2000, A. Neimitz, I.V. Rokach, D. Kocanda, K. Golos, Eds., pp. 537-544, 2000.

98. Böhmert, J., Weiss, R., Webersinke, W.: Anwendung eines Laserextensometer zur Ermittlung von Risswiderstandskurven, Deformation und Bruchverhalten von Kunststoffen, 8. Problemseminar, Halle, Germany, 20-22. June 2001.